



THE HONG KONG
POLYTECHNIC UNIVERSITY

香港理工大學

Pao Yue-kong Library

包玉剛圖書館

Copyright Undertaking

This thesis is protected by copyright, with all rights reserved.

By reading and using the thesis, the reader understands and agrees to the following terms:

1. The reader will abide by the rules and legal ordinances governing copyright regarding the use of the thesis.
2. The reader will use the thesis for the purpose of research or private study only and not for distribution or further reproduction or any other purpose.
3. The reader agrees to indemnify and hold the University harmless from and against any loss, damage, cost, liability or expenses arising from copyright infringement or unauthorized usage.

IMPORTANT

If you have reasons to believe that any materials in this thesis are deemed not suitable to be distributed in this form, or a copyright owner having difficulty with the material being included in our database, please contact lbsys@polyu.edu.hk providing details. The Library will look into your claim and consider taking remedial action upon receipt of the written requests.

The Hong Kong Polytechnic University

Department of Building Services Engineering

**Control and Optimization of Dedicated Outdoor
Air-Chilled Ceiling Systems Using Liquid Desiccant
Dehumidification**

Ge Gaoming

**A thesis submitted in partial fulfillment of the requirements
for the Degree of Doctor of Philosophy**

March, 2011

CERTIFICATE OF ORIGINALITY

I hereby declare that this thesis is my own work and that, to the best of my knowledge and belief, it reproduces no material previously published or written, nor material that has been accepted for the award of any other degree or diploma, except where due acknowledgement has been made in the text.

I also declare that the intellectual content of this thesis is the product of my own work, except to the extent that assistance from others in the project's design and conception or in style, presentation and linguistic expression is acknowledged.

_____ (Signed)

_____ Ge Gaoming _____ (Name of student)

Department of Building Services Engineering

The Hong Kong Polytechnic University

Hong Kong, P.R. China

March, 2011

ABSTRACT

Abstract of thesis entitled: Control and Optimization of Dedicated Outdoor Air-Chilled Ceiling Systems Using Liquid Desiccant Dehumidification

Submitted by : Ge Gaoming

For the degree of : Doctor of Philosophy

at The Hong Kong Polytechnic University in March, 2011.

Dedicated outdoor air-chilled ceiling (DOAS-CC) system, as an alternative air conditioning manner, has attracted world-wide interests in recent years. It can achieve independent control of indoor temperature and humidity, provide more effective ventilation, prevent virus and bacteria transmission among different zones, etc; therefore it can improve indoor thermal comfort and indoor air quality. Considering the huge energy consumption for treating outdoor air in hot and humid regions like Hong Kong, total heat recovery and independent dehumidification technologies are desirable for energy saving in air conditioning. A DOAS-CC system adopting a novel membrane-based total heat exchanger and liquid desiccant dehumidification is proposed and studied in the research.

Robust control is prerequisite for reliable operation of air-conditioning systems besides proper designs and maintenance. It also has significant impacts on energy use as well as occupants' comfort, healthy and productivity. However, control issues in the DOAS-CC system and the liquid desiccant dehumidification process have been rarely concerned. Therefore, the aim of this research is to develop robust local control methods

and optimal control strategies for the DOAS-CC integrated system to achieve the desired indoor thermal comfort and indoor air quality with minimum energy consumption. The aim is reached through addressing the following scientific issues: (1) performance study of the membrane-based total heat exchanger; (2) control characteristics of the liquid desiccant dehumidification system; (3) system approach based global optimization of air-conditioning systems considering multiple objectives and multiple variables. In addition, control strategy for preventing condensation on the surface of chilled ceiling is also developed.

The main works of this research are shown as follows. Firstly, a comprehensive mathematical simulator for the whole DOAS-CC system has been developed on the TRNSYS platform. Mathematical models of major components including the membrane-based total heat exchanger, the liquid desiccant dehumidifier and regenerator are developed based on the simplified heat and mass transfer analysis method and the principle of mass and energy conservation. Main components of the system are validated by experimental data. Performance of the system can be studied by the simulator.

Secondly, control strategies for the liquid desiccant dehumidification system are developed to achieve independent control of the supply air temperature and humidity. Control methods for the air dehumidification and cooling process in the dehumidifier side as well as desiccant solution regeneration process in the regenerator side are proposed and evaluated. Control characteristics of the liquid desiccant dehumidification system are also investigated.

Thirdly, control methods for the multi-zone dedicated outdoor air system are

developed to decouple the indoor air temperature, humidity and ventilation controls. The performance of optimization control methods, such as supply air humidity ratio reset and demand controlled ventilation strategy, are evaluated by simulation tests in the system.

Fourthly, a model-based global optimal control strategy is developed to reduce the energy consumption of the DOAS-CC system and provide comfort indoor environment. The indoor air temperature, indoor air humidity and total energy consumption are considered simultaneously. The supply air temperature and humidity of the DOAS and the supply water temperature in the system are optimized using the Genetic Algorithm (GA) based on the trade-off among the indoor air temperature, indoor air humidity and total system energy consumption in the format of a system response-based cost function.

Finally, a predictive condensation control strategy is developed for the DOAS-CC system to prevent condensation occurring at the start-up moment of chilled ceiling system. Neural network (NN) based models are developed to predict the temperature on the surface of chilled ceiling and the indoor air dew-point temperature at the start-up period, hence to predict whether condensation will occur or not. Another model is developed to predict the optimal prior operation time for DOAS to prevent condensation. The performance of this predictive condensation strategy is evaluated.

PUBLICATIONS ARISING FROM THIS THESIS

Journal papers

Niu, X.F., F. Xiao, and G.M. Ge. 2010. Performance analysis of liquid desiccant based air conditioning system under variable fresh air ratios. *Energy and Buildings* 42(12): 2457-2464.

Xiao, F., G.M. Ge, and X.F. Niu. 2011. Control performance of a dedicated outdoor air system adopting liquid desiccant dehumidification. *Applied Energy* 88(1):143-149.

Ge, G.M., F. Xiao, and X.F. Niu. 2011. Control strategies for a liquid desiccant air-conditioning system. *Energy and Buildings* 43(6):1499-1507.

Ge, G.M., F. Xiao, and X.H. Xu. 2011. Model-based optimal control of a dedicated outdoor air-chilled ceiling system using liquid desiccant and membrane-based total heat recovery. *Applied Energy*. doi: 10.1016/j.apenergy.2011.04.045.

Ge, G.M., F. Xiao, and S.W. Wang. Neural network-based predictive condensation control for dedicated outdoor air-chilled ceiling systems. Submitted to *Energy and Buildings*.

Conference papers

Ge, G.M., F. Xiao, and S.W. Wang. 2009. Indoor thermal comfort and energy efficiency of various air-conditioning schemes for museum buildings. *Proceeding of the 11th International IBPSA Conference*, Glasgow, Scotland, July 27-30: 2236-2242.

Ge, G.M., F. Xiao, and L.Z. Zhang. 2009. A comparative study on energy efficiency and indoor thermal comfort of DOAS applied to multi-zone air-conditioning systems. *Proceeding of the 6th International Symposium on Heating, Ventilating and Air*

Conditioning, Nanjing, China, Nov. 6-9: 405-412.

Ge, G.M., F. Xiao, and S.W. Wang. 2010. Optimization of a liquid desiccant based dedicated outdoor air-chilled ceiling system serving multi-zone spaces. *Proceeding of the 8th International Conference on System Simulation in Buildings*, Liege, Belgium, Dec. 13-15, 2010.

ACKNOWLEDGEMENTS

I wish to express my greatest gratitude and appreciation to my Chief Supervisor, Dr. Linda Fu Xiao. Without her continuous guidance, encouragements and supports during the entire course of my research work, the thesis would not be finished.

I would like to express my sincerest appreciations to my Co-Supervisors, Chair Professor Shengwei Wang from the Department of Building Services Engineering, The Hong Kong Polytechnic University, and Professor Lizhi Zhang from the Key Laboratory of Enhanced Heat Transfer and Energy Conservation of Education Ministry, South China University of Technology, for their valuable assistance and guidance.

Special thanks are due to my colleagues in the Building Automation and Energy Management research group for their company and support throughout the PhD study.

Lastly, I would like to express my deepest appreciation to my family members: my parents, especially my wife Wen Zhang for their unconditional trust and support in my life. This thesis is to them.

TABLE OF CONTENTS

CERTIFICATE OF ORIGINALITY	i
ABSTRACT	ii
PUBLICATIONS ARISING FROM THIS STUDY	v
ACKNOWLEDGEMENTS	vii
TABLE OF CONTENTS	viii
LIST OF FIGURES	xii
LIST OF TABLES	xvi
NOMENCLATURE.....	xviii
CHAPTER 1 INTRODUCTION	1
1.1 Motivation.....	1
1.2 Aim and Objectives.....	6
1.3 Organization of This Thesis.....	7
CHAPTER 2 LITERATURE REVIEW	10
2.1 Conventional Air-conditioning Systems and Their Problems	10
2.1.1 Conventional Air-conditioning Systems.....	10
2.1.2 Problems of Conventional Air-conditioning Systems	12
2.2 Dedicate Outdoor Air-chilled Ceiling Systems	13
2.2.1 Dedicated Outdoor Air System.....	14
2.2.2 Chilled Ceiling System	16
2.2.3 Total Heat Recovery	19
2.2.4 Liquid Desiccant Dehumidification.....	22

2.3 Control and Optimization of HVAC Systems.....	26
2.3.1 Control and Optimization of Conventional HVAC Systems	26
2.3.2 Control and Optimization of DOAS-CC Systems	34
2.4 Summary	37
CHAPTER 3 BUILDING SYSTEM AND SIMULATION PLATFORM	38
3.1 Building and System Descriptions	38
3.2 Development of the System Simulation Platform.....	42
3.2.1 Introduction of the Simulation Platform	42
3.2.2 Mathematic Models of Major Components	43
3.2.3 Validations of the Component Models	51
3.3 Tests of the System Simulation Platform.....	58
3.3.1 System Response Tests	59
3.3.2 Effect of Total Heat Exchanger on System Energy Performance.....	63
3.4 Summary	65
CHAPTER 4 CONTROL OF THE LIQUID DESICCANT SYSTEM.....	66
4.1 Control Strategies of the Liquid Desiccant System	66
4.1.1 Control Methods of Air Dehumidification Process	69
4.1.2 Control Methods of Solution Regeneration Process	69
4.1.3 Effectiveness of Control Methods.....	69
4.2 Control Performance of the Liquid Desiccant System.....	75
4.3 Outdoor Air Ventilation Strategy in Liquid Desiccant Based Air-conditioning Systems	85
4.3.1 Test Condition.....	87

4.3.2 Results Analysis.....	88
4.4 Summary	96
CHAPTER 5 INDEPENDENT TEMPERATURE AND HUMIDITY CONTROL IN MULTI-ZONE DEDICATED OUTDOOR AIR SYSTEMS.....	98
5.1 Brief of Independent Temperature and Humidity Control System.....	98
5.2 Control Strategies of the Dedicated Outdoor Air System.....	100
5.2.1 Basic Strategy.....	101
5.2.2 Supply Air Humidity Ratio Set-point Reset	102
5.2.3 Demand-controlled Ventilation Based Supply Air Humidity Reset.....	103
5.3 Performance of Various Control Strategies	104
5.4 Summary	109
CHAPTER 6 SIMPLIFIED MODELS OF MAJOR COMPONENTS FOR ONLINE APPLICATIONS	111
6.1 Importance of Simplified Model.....	111
6.2 Simplified Model of Major Components	112
6.2.1 Simplified Membrane-based Total Heat Exchanger Model.....	113
6.2.2 Simplified Dehumidifier Model.....	113
6.2.3 Simplified Regenerator Model.....	115
6.2.4 Simplified Cooling Coil Model.....	116
6.2.5 Simplified Fan/pump Model	117
6.2.6 Simplified Chilled Ceiling Model.....	117
6.2.7 Simplified Building Model	118
6.2.8 System Performance Prediction Model.....	119
6.3 Validation of Simplified Models.....	122

6.4 Summary	127
CHAPTER 7 MODEL-BASED ONLINE OPTIMAL CONTROL OF DEDICATED	
OUTDOOR AIR-CHILLED CEILING SYSTEMS.....	
7.1 Development of the Optimal Control Strategy	129
7.1.1 Outline of the Optimal Control Strategy	130
7.1.2 Formulation of the Cost Function	132
7.2 Performance Analysis of the Optimal Control Strategy	133
7.2.1 Performance of the Optimal Control Strategy	135
7.2.2 Impacts of the Weighting Factors	140
7.3 Summary	141
CHAPTER 8 CONDENSATION CONTROL OF DEDICATED OUTDOOR	
AIR-CHILLED CEILING SYSTEMS	
8.1 Introduction of Condensation Risks.....	144
8.2 Brief of Artificial Neural Network (NN)	146
8.3 NN-based Predictive Condensation Control for DOAS-CC System	152
8.3.1 NN Models for Condensation Control.....	155
8.3.2 Training and Validation of the NN Models	158
8.3.3 Condensation Control Performance	164
8.4 Summary	167
CHAPTER 9 CONCLUSIONS AND RECOMMENDATIONS	
REFERENCES.....	176

LIST OF FIGURES

Figure 1.1	Estimated technical energy savings potential and simple payback periods for the 15 options.....	4
Figure 2.1	Schematic of a dedicated outdoor air system.....	14
Figure 2.2	Principles of radiant ceiling panel cooling.....	17
Figure 2.3	Schematic of an energy wheel.....	21
Figure 2.4	Schematic of cross-flow and counter-flow membrane HRVs.....	22
Figure 2.5	Basic configuration of a liquid desiccant dehumidification system.....	24
Figure 2.6	Classification of optimal control methods in HVAC systems	28
Figure 3.1	Layout of half a typical floor	39
Figure 3.2	Schematic of the DOAS-CC system and its control system: (a) the whole DOAS-CC system; (b) liquid desiccant cooling module	41
Figure 3.3	Heat balance on the zone air node.....	44
Figure 3.4	Schematic of a membrane-based parallel-plates enthalpy exchanger.....	46
Figure 3.5	Schematic of chilled ceiling panel	49
Figure 3.6	Experimental rig of the membrane-based enthalpy exchanger	52
Figure 3.7	Comparison of experimental and simulation results: (a) sensible effectiveness; (b) latent effectiveness	54
Figure 3.8	Outdoor air temperature and humidity on the summer test day	59
Figure 3.9	Occupancy profiles of individual zones and the total occupancy profile ..	59
Figure 3.10	Supply air humidity responses	60
Figure 3.11	Supply air temperature responses.....	61
Figure 3.12	Indoor air temperature and humidity responses	62

Figure 3.13	Indoor CO ₂ concentration response	62
Figure 3.14	Chilled ceiling responses	63
Figure 4.1	Schematic of the proposed liquid desiccant-based dedicated outdoor air system.....	67
Figure 4.2	Control performance in the air dehumidification process: (a) variable strong solution inlet temperature method; (b) variable strong solution flow rate method.....	71
Figure 4.3	Control performance in the solution regeneration process: (a) variable diluted solution inlet temperature method; (b) variable regeneration air flow rate method	73
Figure 4.4	Effect of strong solution concentration on ECOP and COP	77
Figure 4.5	Effect of solution flow rate on ECOP and COP	78
Figure 4.6	Effect of ambient air temperature on ECOP and COP.....	79
Figure 4.7	Effect of ambient air humidity ratio on ECOP and COP	80
Figure 4.8	Effect of supply air flow rate on ECOP and COP.....	81
Figure 4.9	Effect of supply air humidity ratio on ECOP and COP	82
Figure 4.10	Effect of regeneration air volume on COP.....	83
Figure 4.11	Effect of regeneration solution inlet temperature on COP.....	83
Figure 4.12	Energy consumption of the proposed system using different control strategies	84
Figure 4.13	Air handling processes of the two systems	86
Figure 4.14	Latent load and sensible load distribution under different fresh air ratios	90
Figure 4.15	Desiccant solution mass flow rate under different fresh air ratios.....	91
Figure 4.16	Heating load for solution regeneration and air cooling load variations under different fresh air ratios.....	91
Figure 4.17	COP of the liquid desiccant based system under different fresh air ratios	94

Figure 4.18	Total power consumption of the two systems compared	95
Figure 5.1	Flowchart of supply air humidity ratio set point reset strategy	103
Figure 5.2	Indoor air temperature and humidity responses when adopting basic control strategy	104
Figure 5.3	CO ₂ concentration response when adopting basic control strategy	105
Figure 5.4	Supply air humidity ratio and maximum RH when adopting the supply air humidity ratio set point reset	106
Figure 5.5	Comparison between actual occupancy and detected occupancy	107
Figure 5.6	Indoor air CO ₂ concentration response when adopting DCV strategy ...	108
Figure 6.1	Outdoor air temperature and humidity on the summer day	122
Figure 6.2	Validation of the simplified dehumidifier model	123
Figure 6.3	Validation of the simplified regenerator model	124
Figure 6.4	Validation of the simplified chilled ceiling model	125
Figure 6.5	Comparison of measured and predicted CO ₂ generation rates of zone 5	126
Figure 6.6	Comparison of measured and predicted air temperature of zone 5	127
Figure 7.1	Illustration of the optimal control strategy	130
Figure 7.2	Temperature and humidity profiles of test days	134
Figure 7.3	Set-points under optimal control strategy on the summer day (Setting I)	136
Figure 7.4	Temperature and RH of zone 5 using the optimal strategy (Setting I) and the conventional strategy	137
Figure 8.1	Schematic diagram of a multilayer feed forward neural network	148
Figure 8.2	Information processing in a neural network unit	149
Figure 8.3	Schematic of DOAS-CC systems and its control system	153
Figure 8.4	The flowchart of condensation prediction at startup moment	154

Figure 8.5	The structure of neural network for T_{panel} prediction.....	156
Figure 8.6	The structure of neural network for indoor air DPT prediction.....	157
Figure 8.7	The structure of neural network for prior time prediction of DOAS.....	158
Figure 8.8	The validation result for NN-based T_{panel} prediction	160
Figure 8.9	The validation result for NN-based indoor air DPT prediction	162
Figure 8.10	The validation result for NN-based optimal prior time prediction	163
Figure 8.11	The needed prior time of DOAS at different infiltration rates.....	166

LIST OF TABLES

Table 1.1	Summary of the 15 technology options selected for refined study	3
Table 3.1	Basic data of the multi-zone space	39
Table 3.2	Structural parameters and nominal operating condition of the exchanger .	53
Table 3.3	Experimental results of the total heat exchanger.....	53
Table 3.4	Comparison of experimental data with analytical solutions for the dehumidification process.....	56
Table 3.5	Comparison of experimental data with analytical solutions for the regeneration process	57
Table 3.6	Breakdown of primary energy consumption of the integrated system.....	64
Table 4.1	System design parameters	70
Table 4.2	States of several points of the air handling process.....	88
Table 4.3	States of the mixed air with different fresh air ratios	89
Table 4.4	States of the air after dehumidification by liquid desiccant	92
Table 5.1	Breakdown of energy consumption of the system	109
Table 7.1	Control settings of the cost function of the optimizer	134
Table 7.2	Summary of the costs of the optimal strategy with different control settings on the summer test day	138
Table 7.3	Summary of the environmental and energy performance of different strategies oin the summer test day.....	139
Table 7.4	Summary of the environmental and energy performance of different strategies on the spring test day.....	140
Table 8.1	Training and validation data for T_{panel} prediction in zone 5	159
Table 8.2	Training and validation data for indoor air DPT prediction in zone 5	161

Table 8.3 Training and validation data for prior time prediction 162

Table 8.4 T_{panel} prediction of each day during Aug. 1st-8th..... 164

Table 8.5 Indoor air DPT prediction of each day during Aug. 1st-8th..... 165

Table 8.6 Optimal prior time prediction of each day during Aug. 1st-8th..... 165

NOMENCLATURE

Symbols	Description	Unit
A	cross-sectional area of packing	m^2
C	CO ₂ concentration	ppm
COP	coefficient of performance	ND
C_c	Overall thermal capacity of a coil	kW/k
C_s	solution concentration	%
c_{pa}	Air specific heat	$kJ/kg^\circ C$
c_{pw}	specific heat of water	$kJ/kg^\circ C$
D	moisture load	kg/s
E	electricity energy consumption of the system	kW
$ECOP$	Electric coefficient of performance	ND
E_{ch}	electricity energy consumption of the chiller	kW
E_{fan}	electricity energy consumption of the fans	kW
F_H	heat transfer coefficient	$kW/m^2^\circ C$
F_M	mass transfer coefficient	$kg/m^2 s$
h	enthalpy	kJ/kg
J	cost function	ND
L	length of packing	m
Le	Lewis number	ND
m	mass flow rate	kg/s
M	air mass	kg

NTU	number of transfer units	ND
P	partial pressure of water vapor	Pa
Q	heat transfer rate	kW
Q_C	cooling production of the dehumidification system	kW
Q_{CC}	heat flow extracted by the chilled ceiling panel	kW
Q_{ch}	cooling energy consumption	kW
Q_h	heating energy consumption	kW
Q_{sen}	Sensible heat load	kW
Q_T	thermal energy consumption	kW
R	heat resistance	$^{\circ}\text{C} / \text{kW}$
RH	relative humidity	%
T	temperature	$^{\circ}\text{C}$
S	Pollutant load	$10^{-6}\text{m}^3/\text{s}$
t	time	s
UA	heat transfer coefficient	kW/K
v	transfer surface area per unit volume of packing	m^2/m^3
V	volumetric flow rate	m^3/s
V_s	solution flow rate	L/s
w	air humidity ratio	kg/kg
W	power consumption	kW
Δt_{sim}	Simulation time step	s
Δt_{pred}	Prediction period	s

Greek letters

α weighting factor or mass transfer effectiveness

β	heat transfer effectiveness
ε	effectiveness
η	device effectiveness
λ	model parameter
φ, γ	coefficients
Δ	interval

Subscript	Description
a	air
amb	ambient
c	cooling
deh	dehumidifier
E	energy
e	Air in equilibrium with desiccant
ex	exhaust air
f	fresh air
i	the i th zone
in	inlet
L	latent
max	maximum
min	minimum
out	outlet
rgn	regenerator
s	solution

<i>sup</i>	supply air
<i>S</i>	sensible
<i>tot</i>	Total
<i>w</i>	water
<i>set</i>	Set-point

Supscript	Description
<i>k</i>	current sampling step
<i>k-1</i>	Previous sampling instants
<i>k+1</i>	next sampling instants

Note: ND= No dimensions.

CHAPTER 1 INTRODUCTION

1.1 Motivation

Energy saving and indoor environment quality are two major concerns in building heating, ventilating and air conditioning (HVAC) systems, which draw more and more attentions from designers, operators, occupants and researchers. According to the statistics provided by the International Energy Agency (IEA) in 2010, the building sector currently accounts for about one third of the final energy use worldwide (IEA 2010). Among building energy services, HVAC systems are the largest energy users, which are responsible for 10-20% of final energy use in developed countries (Perez-Lombard 2008). Hong Kong energy end-use data showed that the space air-conditioning is one of the major energy users in buildings, which consumes about 27% of the total electricity in buildings and about 14% of all energy in Hong Kong in 2008 (EMSD 2010). Energy-efficient HVAC systems are therefore essential and expected to reduce energy consumption of buildings and promote environmental sustainability.

The purpose of a ‘comfort’ HVAC system is to provide and maintain a comfortable environment within a building for the occupants. Indoor air quality (IAQ) and indoor thermal comfort are two important aspects of indoor environment. Conventional air conditioning schemes, such as constant air volume (CAV) systems, variable air volume (VAV) systems and fan-coil unit (FCU) systems, face challenges in indoor environment quality and energy efficiency. For instance, wet surfaces of cooling coils, higher relative

humidity (RH) in part load conditions, ineffective outdoor air ventilation in multi-zone applications, etc. Conventional air conditioning systems are widely criticized for Sick Building Syndrome (SBS), which is harmful for occupants' health and productivity. According to the estimation by Lawrence Berkeley National Laboratory in 1996, US companies lost as much as \$48 billion annually in medical expenses due to biological contaminants that lead to sick building illnesses and \$160 billion annually in lost productivity due to inadequate ventilation (Fisk 2002). In Hong Kong, studies of randomly selected office buildings have shown that up to 60% of workers reported at least one work-related symptom and 10-25% reported such symptoms occurring twice weekly or more. The loss of productivity from sick building syndrome was estimated to be \$180 billion in 1998 (HK EPD 2010).

There are increasing interests in developing new technologies and air-conditioning systems which can improve system energy performance and indoor environment. In 2002, Department of Energy (DOE) proposed 15 kinds of technology options for energy savings in commercial building HVAC systems (Roth et al. 2002). Table 1.1 displays the 15 technologies selected, including their technology status and technical energy savings potentials. Technical energy savings potential is the annual energy savings that would occur relative to 'typical new' equipment if the technology option immediately was installed practices in all reasonable applications. It indicates the potential for considerable reduction of the 4.5 quads of primary energy consumed by HVAC systems in commercial buildings.

Table 1.1 Summary of the 15 technology options selected for refined study (Roth et al. 2002)

Technology Option	Technology Status	Technical Energy Savings Potential (quads)
Adaptive/Fuzzy Logic Controls	New	0.23
Dedicated Outdoor Air Systems	Current	0.45
Displacement Ventilation	Current	0.20
Electronically Commutated Permanent Magnet Motors	Current	0.15
Enthalpy Recovery Heat Exchangers for Ventilation	Current	0.55
Heat Pumps for Cold Climates (Zero-Degree Heat Pump)	Advanced	0.1
Improve Duct Sealing	Current/New	0.23
Liquid Desiccant Air Conditioners	Advanced	0.2/0.06 ¹
Microenvironments/Occupancy-Based Control	Current	0.07
Microchannel Heat Exchanger	New	0.11
Novel Cool Storage	Current	0.2/0.03 ²
Radiant Ceiling Cooling/Chilled Beam	Current	0.6
Smaller Centrifugal Compressors	Advanced	0.15
System/Component Diagnostics	New	0.45
Variable Refrigerant Volume/Flow	Current	0.3

¹ Savings for use as DOAS and relative to a conventional DOAS, respectively.

² Savings for all packaged and chiller systems and only water-cooled chiller, respectively.

Many of the 15 options had attractive simple payback periods, as shown in Figure 1.1. It is encouraging for designer and operator to implement these technologies in practical applications. In addition, several of the technologies share common non-energy benefits that can improve the indoor environment of HVAC systems. For instance, dedicated outdoor air systems and energy recovery heat exchanger can improve indoor humidity control, while liquid desiccant systems can enhance indoor air quality. These energy savings technologies can be adopted in HVAC systems to improve the system energy efficiency and indoor environment.

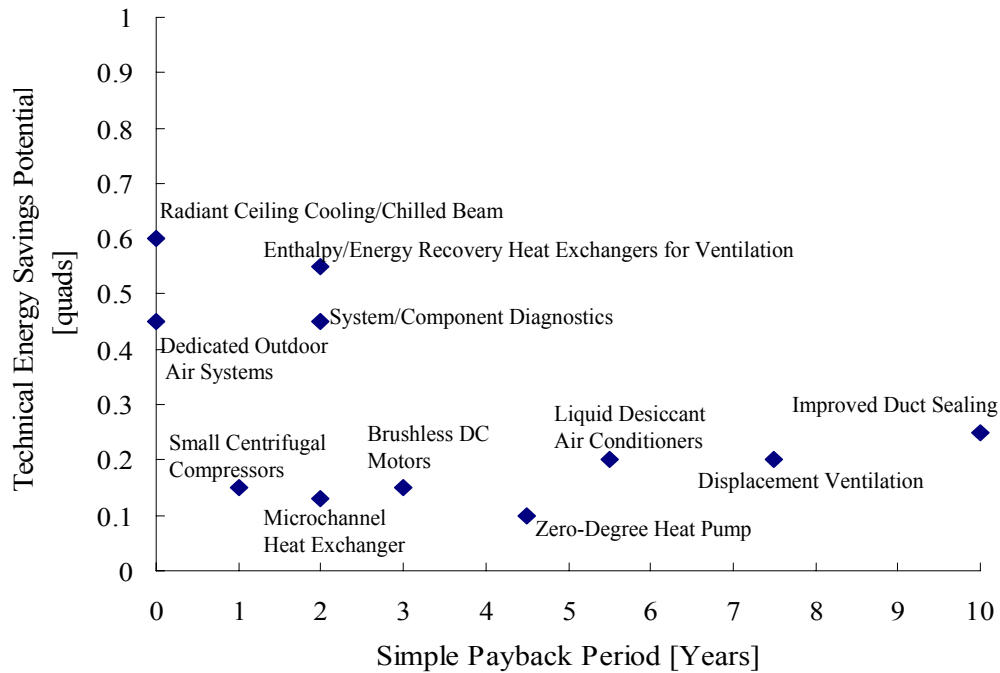


Figure 1.1 Estimated technical energy savings potential and simple payback periods for the 15 options (Roth et al. 2002)

Research on new air-conditioning systems is also very active in recent years. A novel air conditioning system which integrates a dedicated outdoor air system (DOAS) with parallel sensible load treatment equipments, such as chilled ceiling (CC) panels, has been attracting a lot of interests (Mumma 2002). The DOAS and the parallel unit in a DOAS-CC integrated system are two independent subsystems. The dedicated outdoor air system takes charge of removal of the total latent load and a part of sensible load of space, as well as direct delivery of the required amount of outdoor air into conditioned space for ventilation purpose. The parallel terminal is responsible for removing the remainder part of sensible load. The treatment of sensible load (temperature control) and latent load (humidity control) is hence decoupled. In DOAS-integrated systems, the amount of fresh air distributed to each zone is independent and solely determined by the

occupant number in that zone; therefore it can verify the ventilation air distribution required by ASHRAE ventilation standard 62.1-2007 (ASHRAE 2007a). The outdoor air ventilation in this system hence is more effective than that in traditional VAV systems owing to the more straightforward outdoor air delivery mode. The integrated system can provide more healthy and comfortable indoor environment compared with conventional systems, and has higher energy efficiency.

Energy consumption on treating fresh air is extensive. About 20-40% of the overall energy consumption of air conditioning system is consumed in fresh air handling process. The ratio can be even higher in hot and humid regions where latent load from fresh air is as heavy as 50% of the cooling load (Zhang and Xiao 2008). For the DOAS, which is a 100-percent outdoor-air system, energy recovery is required in most cases according to ANSI/ASHRAE/IESNA Standard 90.1-2007, and the energy-recovery system should be with at least 50-percent recovery effectiveness (ASHRAE 2007b). Energy saving in treating fresh air is critical for building energy efficiency. Efficient energy recovery from exhaust air and independent dehumidification are effective ways to reduce energy consumption for treating fresh air. Owing to the rapid progress on the membrane-based enthalpy exchanger and liquid desiccant dehumidification technologies, economical and efficient dedicated outdoor air systems are gradually becoming feasible nowadays. Since the latent load is removed by independent dehumidification, the hybrid system can also prevent the occurrence of wet surface and reduce the electricity peak load caused by air-conditioning systems. In this study, a dedicated outdoor air-chilled ceiling system integrated with membrane-based total heat exchanger and liquid desiccant dehumidification is proposed and investigated.

In order to achieve the desired indoor air quality, indoor thermal comfort and energy performance, reliable control for the integrated system is prerequisite. However, control studies on the novel DOAS-CC integrated system and its major subsystems including the liquid desiccant system are quite few so far, especially in multi-zone applications. In addition, system approach based optimal control of HVAC system can improve the overall performance of air conditioning systems, which has been demonstrated by previous research. But research on the optimal control of the DOAS-CC system is not found yet. In recent years, projects adopting DOAS, chilled ceiling, total heat recovery and liquid desiccant dehumidification increase rapidly. It is the critical time to study control and optimization strategies for such systems during their operations. The aim of this research is to develop reliable local control loops and optimal control strategies for the novel DOAS-CC integrated system to achieve the desired indoor air quality and indoor thermal comfort for multi-zone spaces with minimum energy consumption.

1.2 Aim and Objectives

The dedicated outdoor air-chilled ceiling system adopting total heat recovery and liquid desiccant dehumidification is a novel air-conditioning scheme. Development of basic control methods for the liquid desiccant dehumidification subsystem and the whole DOAS-CC integrated system can ensure normal operation and desired indoor environment. Systematic optimization of the multi-zone DOAS-CC systems can play significant roles in maintaining the satisfactory IAQ and thermal comfort, as well as reducing the overall energy consumption of buildings. However, current studies on these issues are far away from being sufficient. Therefore, performance study and control of

the DOAS-CC integrated system is the main work of this research. The aim is achieved by addressing the following objectives:

1. Investigate the heat and mass transfer performance of a novel membrane-based total heat exchanger by numerical simulation and experimental study.
2. Develop and validate control methods for typical packing type counter-flow liquid desiccant dehumidification system. Compare the performance of the liquid desiccant dehumidification system using different control methods under various operation conditions.
3. Develop and validate local control loops for the multi-zone dedicated outdoor air system to decouple the indoor air temperature, humidity and ventilation controls. In addition, optimization methods that can improve system energy performance are also developed and evaluated.
4. Develop and validate system approach based optimal control strategy for the DOAS-CC system to consider the overall performance of the integrated air-conditioning system, including indoor air temperature, indoor air humidity and total energy consumption simultaneously by optimizing system variables of the supply air temperature, supply air humidity and the supply water temperature in the system.
5. Develop condensation control strategy to prevent the condensation occurring on the surface of chilled ceiling panels at the start-up period of the DOAS-CC system.

1.3 Organization of This Thesis

The thesis is organized into nine chapters as below.

Chapter 1 presents the motivations of this research, the aim and objectives, and the organization of this thesis.

Chapter 2 presents a literature review on the dedicated outdoor air system, chilled ceiling system, total heat recovery and desiccant dehumidification technologies, as well as control and optimization of HVAC systems.

Chapter 3 introduces the investigated building air-conditioning system and basic control loops of the integrated DOAS-CC system. Mathematic models of major components, such as membrane-based total heat exchanger, liquid dehumidifier, liquid desiccant regenerator, etc. are built up and validated, and a comprehensive system simulator for the whole DOAS-CC system is developed and tested on the TRNSYS platform.

Chapter 4 develops control methods for the supply air dehumidification and liquid desiccant regeneration processes in the liquid desiccant system. The characteristics of the liquid desiccant system using various control methods and effects of different parameters on the performance of the system are also studied.

Chapter 5 presents local control methods for the normal operation of the multi-zone DOAS system, and energy-efficient optimization strategies, such as supply air humidity ratio reset strategy and demand controlled ventilation (DCV) strategy for the air-conditioning system. The performances of the DOAS system using these strategies are tested.

Chapter 6 presents the simplified models of major components, such as total heat exchanger, liquid dehumidifier, liquid desiccant regenerator, chilled ceiling, etc. of the DOAS-CC system for online optimal control. The validation results of these simplified models are also presented.

Chapter 7 presents a model-based online optimal control strategy for the DOAS-CC system based on the trade-off among the indoor air temperature, indoor air humidity and total system energy consumption in the format of a system response-based cost function. Set-points of three variables, i.e. the supply air temperature and humidity of the dedicated outdoor air subsystem as well as the supply water temperature, are optimized by genetic algorithm (GA) to minimize the overall cost of the system. The performance of the optimal control strategy is tested and compared with that of a conventional control strategy.

Chapter 8 presents a neural network based predictive condensation control strategy for the DOAS-CC system to predict and prevent the condensation occurrence on the surface of chilled ceiling panels in the system start-up period. The performance of this strategy is tested.

Chapter 9 summarizes the work reported in this thesis, and gives some recommendations for future research and applications.

CHAPTER 2 LITERATURE REVIEW

This chapter mainly presents the features and current research status of dedicated outdoor air-chilled ceiling systems and some new energy savings technologies, as well as a review of the research on control and optimization of HVAC systems. Section 2.1 briefly introduces the deficiencies of conventional air-conditioning systems. Section 2.2 presents the features of dedicated outdoor air-chilled ceiling systems and several energy efficient technologies, such as total energy recovery and liquid desiccant dehumidification, which can be utilized in the integrated system. Section 2.3 presents the current research on control and optimization of conventional HVAC systems as well as control of DOAS-CC system.

2.1 Conventional Air-conditioning Systems and Their Problems

2.1.1 Conventional Air-conditioning Systems

Air-conditioning systems have been widely used in commercial buildings to meet occupants' demand for acceptable indoor environmental quality and thermal comfort. As well known, several conventional air-conditioning systems, including constant air volume (CAV) systems, variable air volume (VAV) systems and fan-coil units (FCU), can be selected and adopted in practical applications. The basic principles of these conventional air-conditioning systems are briefly introduced as follows.

In a CAV system, the supply air flow rate of the system is constant, while the supply air temperature is adjusted to cope with room sensible load changes and control indoor air temperature. The adjustment of the supply air temperature is achieved by regulating the chilled water flow rate through the cooling coil in the air handling equipment. The control is simple in this system.

Variable air volume system is a popular system in use nowadays in large office and commercial buildings. In a VAV system, there are two basic close-loop controls. One is responsible for maintaining a constant supply air temperature and the other for regulating the supply air flow rate to cope with room sensible load changes. The principle of the VAV system is adverse to that of the CAV system. In part load conditions, the actual supply air flow rate in VAV system is lower than that in CAV system, which can reduce the energy consumption of fans and hence improve the energy efficiency of the whole system.

A fan coil system is basically a small scale CAV system, which is commonly used in office buildings. The air handling equipment in such a system is a fan coil unit, which comprises basically a fan and a chilled water coil housed within a casing. It is an 'air-water' system whereas CAV and VAV systems are 'all-air' systems. In this system, it requires chilled water pipes to be extended into the occupied spaces, and a separate ductwork for distribution of fresh air supply to individual spaces. The indoor air temperature is usually controlled in a range by ON/OFF control.

In conventional air-conditioning systems, indoor temperature is the main control objective and is actively controlled, while the indoor humidity control is usually ignored.

There are some problems in these systems that more or less impact the indoor environment and energy performance.

2.1.2 Problems of Conventional Air-conditioning Systems

In practical applications, conventional air-conditioning schemes are facing a series of challenges. Four main problems of them are analyzed as follows. (1) In CAV and VAV systems, when one air handling unit serves a multi-zone space, an identical fresh air fraction is inevitably employed for different zones with different occupancy densities. Consequently, over ventilation which causes energy waste, or inadequate ventilation which causes poor indoor air quality may occur (Xu and Wang 2007). It is almost impossible to verify that the ASHRAE ventilation standard 62.1-2007 has been met with an all-air system (ASHRAE 2007). (2) In conditioned space, the optimum indoor relative humidity is from 40% to 60% RH, and 50% RH is ideal for building occupants to avoid the hazards of fungi, bacteria, viruses, and respiratory difficulties (Kittler 1996). However, in comfort air-conditioning systems, indoor relative humidity tends to rise under part load conditions. This problem is serious in hot and humid regions, like south China, especially for CAV and FCU systems. (3) In all-air air-conditioning systems, recirculation air is used, which may cause bacterium and virus transmission among multiple zones in conditioned space (Zhang and Niu 2003). In this situation, occupants are at high risks of infection when diseases breakout, such as SARS (Severe Acute Respiratory Syndrome) and bird flu. In the view of environmental safety, air-conditioning systems should reduce the possibility of internal air circulation between different zones. (4) Wet surface of cooling coil is inevitable in supply air cooling and dehumidification process in conventional air-conditioning systems, which is beneficial

for the generation and growth of microbial and mould. It is harmful for the indoor air quality, hence health and productivity of occupants in space.

2.2 Dedicated Outdoor Air-chilled Ceiling Systems

As presented in the previous chapter, energy savings and indoor environment are two significant concerns in HVAC systems. In order to improve system energy performance and solve the above-mentioned problems, research on new air-conditioning systems and technologies is very active in recent years. A novel air conditioning system which integrates a dedicated outdoor air system (DOAS) with parallel sensible load treatment equipments, such as chilled ceiling panels, thermal storage units and dry fan-coil units, has been attracting a lot of interests (Niu 1995, Mumma 2002). The DOAS and the parallel unit in a DOAS-integrated system are two independent subsystems. The DOAS takes charge of the total latent load and a part of sensible load of space, while the parallel terminal bears the remainder sensible load. Therefore, the DOAS-integrated air-conditioning scheme can decouple the treatment of sensible load and latent load and realizes independent indoor temperature control and humid control. In DOAS-integrated systems, the amount of fresh air distributed to each zone is independent and solely determined by the occupant number in that zone; therefore it can verify the ventilation air distribution required by ASHRAE ventilation standard 62.1-2007. The outdoor air ventilation in this system hence is more effective than that in a traditional VAV system. In addition, because the outdoor air does not mix with re-circulated air in DOAS, the possibility of disease transmission among different zones can be reduced significantly.

2.2.1 Dedicated Outdoor Air System

Dedicated outdoor air system is an 100-percent outdoor-air system, which conditions the outdoor ventilation air separately from the return air from the conditioned space. It is responsible for the moisture load treatment and a part of sensible load of the air conditioned space, as well as for meeting the ventilation requirement of occupants in the space. Figure 2.1 shows a typical dedicated outdoor air system (Mumma 2001a).

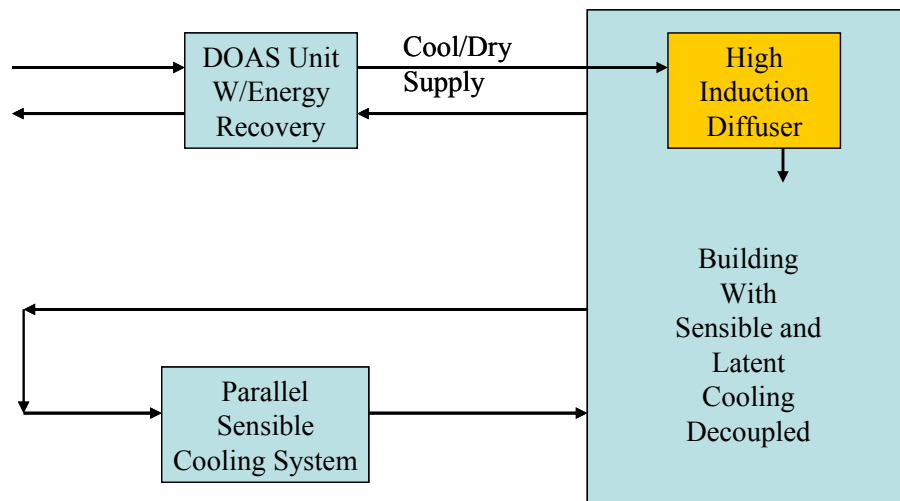


Figure 2.1 Schematic of a dedicated outdoor air system (Mumma 2001a)

It is common practice in commercial building air conditioning to combine ventilation air with return air from the building, condition (cool or heat) this air as needed, and distribute the conditioned air to the interior space, with or without zoned temperature control. The dedicated outdoor air system conditions the outdoor ventilation air separately from the return air from the conditioned space. This approach to handling ventilation air has received considerable attention in past several years. The impetus for this attention has been the growing realization of the penalties and difficulties involved in meeting ASHRAE Standard 62 (*Ventilation for Acceptable Indoor Air Quality*)

requirements throughout the conditioned space of a commercial building, with effective humidity control, particularly in the energy efficient approaches such as VAV systems. The difficulty of achieving good ventilation performance with a VAV system was illustrated in several references (Kettler 1998, Shelquist and Amborn 2001, Xu and Wang 2007).

Handling the treatment and distribution of ventilation air and of return air from the occupied space with separate, parallel systems offers a number of potential advantages over conventional VAV systems that help to overcome the problems discussed above. Many of these advantages directly result in significant energy savings.

Firstly, the ventilation air system can be sized and operated to provide the ventilation air flow rate required by code to provide acceptable indoor air quality and provide this flow rate regardless of the interior temperature, without any need to oversize the ventilation rate. Moreover, a DOAS allows easy verification that the system supplied the minimum outdoor air quantities to different portions of a building.

Secondly, the predominant humidity load in most commercial building in most climate area is the humidity brought in with the ventilation air. Consequently, the entire humidity load for the building can be handled efficiently by separately conditioning the air so that excess ambient humidity is removed. Moreover, energy recovery heat exchanger between the make-up air and exhaust air is readily implemented in this system.

Thirdly, when the ventilation air is separately conditioned, with the entire building humidity load handled in the process, the indoor air conditioning system (parallel

sensible cooling system) can be operated to maintain temperature control. Because this is intended for sensible cooling only, the cooling can be operated at a higher than normal temperature preventing moisture condensation and increasing the COP of the compressor. In addition, some energy-efficient, sensible only cooling approaches, such as radiant ceiling cooling can be employed.

2.2.2 Chilled Ceiling System

DOAS supplies the outdoor ventilation air required by ASHRAE Standard 62.1 to the individual occupied spaces, generally cooled and dehumidified to provide a portion of the terminal space sensible cooling and the entire space latent cooling requirements. Consequently, terminal equipment is required to accommodate the sensible cooling loads not met by the DOAS. Many optional terminal equipments can be selected. Those choices include: dry fan coil units, heat pumps, multi-split units, constant or variable volume all-air systems, active or passive chilled beams, chilled ceiling panels, etc.

The chilled ceiling panels are the most well-known and the best parallel system choice for use with the DOAS. Chilled ceiling system incorporates pipes in the ceilings of the buildings through which cold water flows. The pipes lie close to the ceiling surfaces or in panels and cool the room via natural convection and radiative heat transfer, as shown in Figure 2.2. It can improve indoor thermal comfort, because cooling is provided directly and more evenly to the occupants without causing drafts in the radiant systems.

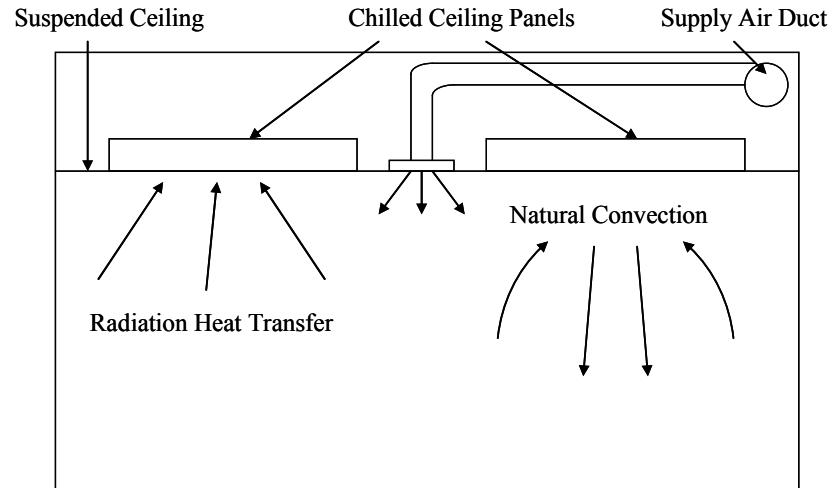


Figure 2.2 Principles of radiant ceiling panel cooling

However, applications of chilled ceiling to hot and humid regions are much more challenging because of condensation risks, initial cost and cooling capacity (Mumma 2002), which limits the popularity of chilled ceilings. Several studies on radiant ceiling systems for cooling have been conducted about cooling capacity and condensation control in US, China, Japan and some European countries (Imanari 1999, Niu 2002, Hao 2007, Conroy 2001, Jeong 2003). It is concluded that combining chilled ceiling systems with dedicated outdoor air systems is an effective way to overcome the problems. In addition, to ensure indoor air quality and removal of the moisture load in the room, radiant cooling panels do need to be used in conjunction with a dehumidification and ventilation system.

For initial cost, in the new construction, the installed costs of chilled ceiling systems plus an appropriately sized DOAS system with enthalpy recovery are similar to conventional VAV system. A number of sources, indicated below have made similar statements about comparative costs. Mumma (2001b) posited that a cooling panel

system, when used in combination with a dedicated outdoor air system outfitted with sensible and enthalpy transfer devices, cost less to construct than a VAV system. Similarly, Springer (2001) stated that costs were competitive with VAV system, due in large part to lower ventilation costs. One case study by Energy Design Resources (2001) showed a 40-55% reduction in space requirements for mechanical equipment and ductwork due to less ducting. In new construction, this can be translated in lower construction costs and more rentable floor space. A Dedanco system only cost 2% more than a VAV system, with large decreases in costs of ducts and fan equipment (Dedanco, 2001).

In addition, when combining with a dedicated outdoor air subsystem, the chilled ceiling system is energy efficient compared with conventional air conditioning systems. Like the first-cost analysis, the operating cost data favours the DOAS-CC system, which consumes 15%-20% less than that of a conventional VAV system (Roth et al. 2002, Mumma 2001b). One of the basic energy savings mechanisms is the ability to operate with higher chilled water temperature, allowing the evaporation temperature of chillers to be correspondingly higher, and thus reducing the chillers energy consumption. The chilled water temperature required in this system can be 6-10°C higher than that in the conventional systems. Other than higher chilled water temperature, the system can save energy due to reduced air flow. When implemented with dedicated outdoor air system, the chilled ceiling system can save energy by reducing total ventilation air flow and by handling sensible cooling loads more efficiently. This leads to a reduced power for ventilation (only 25% to 30% of the air flow rate required for peak cooling loads in an all-air system).

Dedicated outdoor air-chilled ceiling system, as an alternative air conditioning manner, has been widely investigated and successfully utilized in Europe (Wilkins 1992, Diaz 2011), America (Stetiu 1999, Conroy 2001), Asian countries (Imanari 1999, Matsuki 1999, Zhang and Niu 2003) and other place (Chowdhury 2008) in the last decade. There are increased interests in this system in recent years, since it can achieve independent control of indoor air temperature and humidity, provide more effective ventilation, prevent virus and bacteria transmission among different zones, etc. Compared with conventional air-conditioning schemes, the DOAS-CC system can improve indoor thermal comfort and indoor air quality, as well as consume less energy, especially when adopting some energy-saving technologies, such as total energy recovery (Zhang 2002, 2006) and liquid desiccant dehumidification (Liu 2006, Xiong 2010).

2.2.3 Total Heat Recovery

In air-conditioning field, about 20-40% of the overall energy consumption of air conditioning system is consumed in fresh air handling process. The ratio can be even higher in hot and humid regions where latent load from fresh air is as heavy as 50% of the cooling load (Zhang and Xiao 2008). Therefore, decreasing the energy consumption during the fresh air handling process is essentially important to improve system energy efficiency.

For the DOAS, which is a 100-percent outdoor-air system, energy recovery is required in most cases according to ANSI/ASHRAE/IESNA Standard 90.1-2007, and the energy-recovery system should be with at least 50-percent recovery effectiveness

(ASHRAE 2007b). Heat recovery ventilators (HRVs) are frequently used to save cooling/heating loads of buildings by retrieving part of the thermal energy included in the exhaust air (Zhong 2009, Lazzarin 1998). Cooling systems can be downsized when energy recovery is used, because energy recovery systems reduce peak cooling requirements. There are several types of HRVs commonly used, including a parallel plate type, a rotary type, a run-around type, and a heat pipe type (ASHRAE 2008). The plate heat exchanger, run-around coil and heat pipe heat exchanger have some advantages, such as robust construction, no moving parts and little or no possibility of cross contamination of airstreams. But they are sensible heat recovery only except when condensation occurs on exchanger surfaces in warmer air stream.

Energy wheels, or rotary heat exchangers, consists of a matrix in the shape of a wheel located inside both of the adjacent fresh air and exhaust air ducts of the building air conditioning or ventilation system, transfer sensible or latent energy (or both) between the exhaust air and the incoming outside air. A total energy wheel can have a sensible and latent effectiveness as high as 75%, which results in a total effectiveness of 75%. However, large spaces are required for installation and cross contamination cannot be avoided in the rotary heat exchanger. In addition, energy wheels have moving parts and pressure drops in the air streams are higher. Figure 2.3 shows a schematic of an energy wheel.

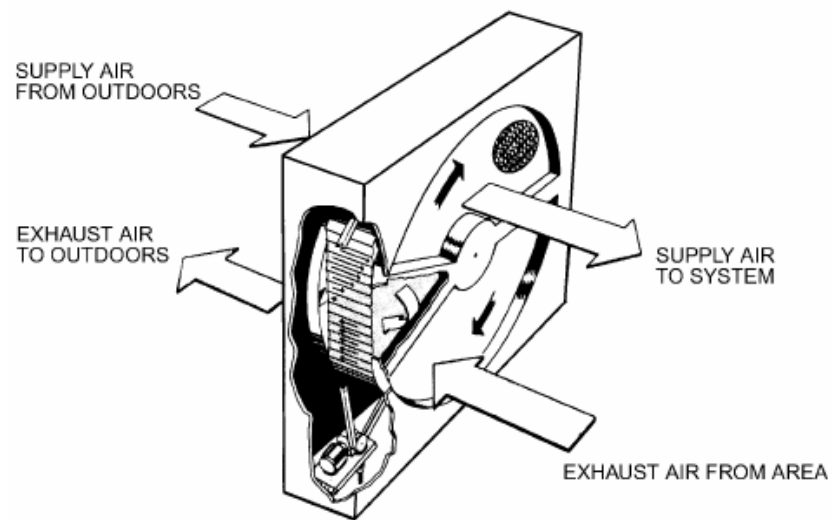


Figure 2.3 Schematic of an energy wheel (ASHRAE System and Equipment Handbook 2008)

Membrane-based total heat exchanger is a new kind of enthalpy exchanger. Figure 2.4 shows the schematic of cross-flow and counter-flow membrane-based HRVs. In the exchanger, some new materials with vapour-permeable capabilities are used as the plates. Therefore, both the sensible heat and the latent heat (moisture) can be exchanged between two air flows. The membrane based HRV has some merits, such as higher heat and moisture recovery effectiveness, no mechanical components, no cross contamination, and lower pressure drops, etc. (Zhang et al. 2000, Zhang and Niu 2001).

Air to air energy recovery heat exchangers can significantly reduce the energy needed to treat ventilation air. Many studies have been conducted in recent years on theoretical and experimental analysis of energy recovery, and results revealed that total heat recovery could save 29-42% of primary energy depending on the system involved (Zhang 2008, Abe 2006, Zhang 2006).

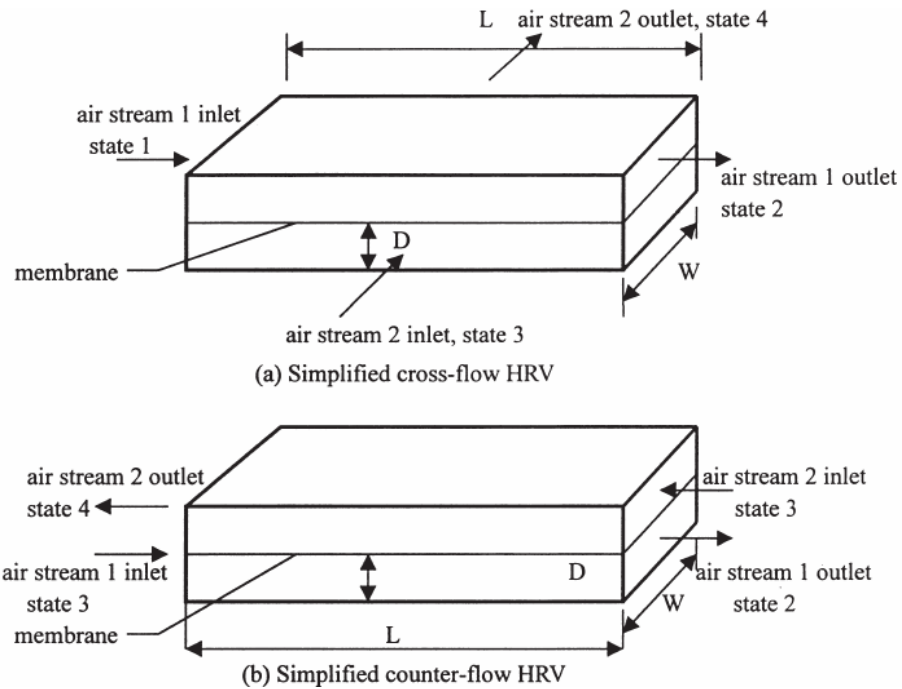


Figure 2.4 Schematic of cross-flow and counter-flow membrane HRVs (Zhang et al. 2000)

2.2.4 Liquid Desiccant Dehumidification

As presented above, the dehumidification and cooling process of supply air in air-conditioning systems is energy-intensive, especially in hot and humid regions. Different dehumidification methods can be employed, including mechanical dehumidification and desiccant dehumidification (or chemical dehumidification) methods. In the conventional mechanical dehumidification and cooling process, in order to remove the moisture from supply air, the process air should be cooled below its dew-point temperature, and reheating is sometimes needed to ensure comfortable supply air temperature. The overcooling and reheating process is energy-intensive, which leads to low evaporating temperature, a poor COP value for the chiller and higher energy consumption of the system. When the sensible heat ratio (SHR) of the conditioned space

is low, the sum of these two components increases dramatically (Daou 2006). In addition, the condensed water provides a breeding ground for duct bacteria, which impacts the indoor air quality. Furthermore, the refrigerants used in the air conditioning technology are more or less CFCs (Chloro-fluoron-carbon) based ones, that many countries are taking steps to phase out or are considering doing so. Therefore, the new-fangled energy-saving as well as environmental-friendly dehumidification technologies are needed.

Desiccant dehumidification technology has been proposed as an alternative to conventional mechanical cooling in the air-conditioning field owing to its merits in handling latent heat. A desiccant dehumidification system can avoid the energy penalty caused by the overcooling and reheating process and the bacteria generation caused by condensed water. It can also significantly reduce the electricity peak load caused by air-conditioning systems, especially in hot and humid regions. Desiccant systems are thus more energy efficient, healthy and environmentally friendly than conventional vapour compression air-conditioning systems (Dai 2001, Liu 2004, Kinsara 1996).

Desiccants may be either solid or liquid. Solid desiccants widely used in air-conditioning systems include silica gel and molecular sieves, while liquid desiccants include lithium chloride (LiCl), lithium bromide, calcium chloride (CaCl₂), and triethylene glycol. Liquid desiccants have a number of advantages over solid desiccants, including a lower pressure drop in air-flow across the desiccant material, energy storage capacity, and the capability to remove pollutants. Moreover, a liquid desiccant system can be driven by low-grade heat sources such as solar energy or waste heat (Factor 1980).

Figure 2.5 presents a basic configuration of a liquid desiccant dehumidification system. The liquid desiccant air conditioner removes moisture and latent load (and, possibly, sensible heat) from process air via a liquid desiccant material, such as lithium chloride. It consists of two primary units, an absorber (or dehumidifier) where concentrated liquid desiccant solution absorbs moisture from the process air, and a regenerator where the moisture taken on by the liquid desiccant in the absorber is removed from the liquid desiccant, thus regenerating the liquid desiccant to the higher concentration.

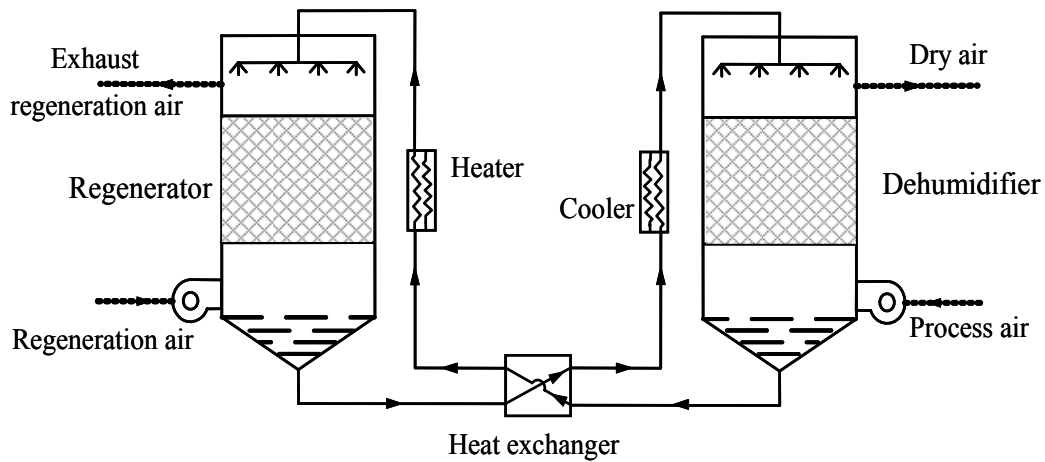


Figure 2.5 Basic configuration of a liquid desiccant dehumidification system

Recent years have witnessed rapid advances in the research and development of liquid desiccant system, with a number of fundamental studies on the dehumidification and regeneration processes carried out. Chen et al. (2006), Babakhani and Soleymani (2009), and Gandhidasan (2004), for example, presented simplified analytical solutions for the heat and mass transfer processes that occur in counter-flow packed-type liquid desiccant equipment. Yin et al. (2008) and Liu et al. (2009) investigated the performance of internally cooled/heated dehumidifiers and regenerators in liquid desiccant systems.

They concluded that these dehumidifiers and regenerators exhibited better mass transfer performance than adiabatic units. Fumo and Goswami (2002) conducted theoretical and experimental analysis of the mass and heat transfer in air-liquid desiccant packed towers with a counter-flow configuration. They employed a finite difference model to predict the dehumidification and regeneration processes, finding that desiccant concentration, desiccant temperature, the air flow rate and the air inlet humidity ratio have the greatest impact on the dehumidifier's performance, whereas desiccant temperature, desiccant concentration and the air flow rate have the greatest impact on that of the regenerator. They also noted that the dehumidification or regeneration process was virtually unaffected by the air temperature or the desiccant solution flow rate. Research on the cross-flow configuration of liquid desiccant dehumidification systems has also been reported (Liu 2007, Dai 2004).

Numerous investigations of the performance analysis of liquid desiccant air-conditioning systems have also been carried out in recent years. For instance, a study in the US showed that, in compare with a conventional primary air handling unit, the liquid desiccant air conditioning system can offer 20-25% energy saving for outdoor preconditioning process (Roth 2002). Dai et al. (2001) compared the performance of a hybrid liquid desiccant cooling system with that of a vapor compression air-conditioning system. Their results showed that the cooling production and coefficient of performance (COP) of the hybrid system were significantly better. Kinsara et al. (1996, 1997) carried out parametric studies on the effects of different key variables, such as the ambient temperature, the inlet temperature of the liquid desiccant, and the effectiveness of the heat exchanger, on the COP of a hybrid air-conditioning system with calcium chloride

(CaCl₂) employed as the desiccant. Tu et al. (2009) proposed a novel energy-efficient air-conditioning system utilizing a lithium chloride solution as the desiccant, and then employed simulation tests to analyze the effects of certain key variables on the system's performance. Xiong et al. (2010) reported a novel two-stage liquid desiccant dehumidification system utilizing a CaCl₂ solution. They demonstrated that the thermal coefficient performance of the proposed system could be increased from 0.24 to 0.73 under given conditions.

In sum, significant research efforts have been devoted to the heat and mass transfer and system performance analysis of liquid desiccant systems in recent years. However, the control issues surrounding such systems have received little attention. Reliable control is a prerequisite for the normal and continuous operation of a liquid desiccant system. Moreover, reliable control is beneficial in terms of energy savings and improving the quality of the built environment, an issue that has been intensively studied and comprehensively applied in conventional air-conditioning systems. Therefore, control strategies for the liquid desiccant system are desirable to develop.

2.3 Control and Optimization of HVAC Systems

2.3.1 Control and Optimization of Conventional HVAC Systems

The fundamental objective of any form of building HVAC system control is to provide a comfortable, efficient, and productive environment. Control functions (or control strategies) of HVAC system play a substantial role in creating these qualities in a

building environment. The effectiveness of various control functions significantly impacts the degree to which this overall objective is achieved.

Control functions of building air-conditioning systems can be generally divided into two categories, i.e., local control functions and optimal (or supervisory) control functions.

Local control functions mainly focus on local processes control or local loops control. The local control is the low level control, which is designed to ensure the robust operation and keep track of the set-point considering the dynamic characteristics of the local process environment. The typical local control method used in the HVAC field is PID (Proportional Integral Derivative) control, which is used in over 80 percent of closed control loops in building air-conditioning applications. ON/OFF control, step control and modulating control are also effective control actuation schemes of the local process control loops in HVAC practice (Wang 2010).

Optimal control is the high level control, which is based on a broader perspective—the performance of the total HVAC system. Optimal control highlights the importance of the overall system performance involving energy or cost efficiency, indoor environment quality, etc. It aims at seeking the minimum energy input or operating cost to provide the satisfied indoor comfort and healthy environment, taking into account the ever-changing indoor and outdoor conditions as well as the characteristics of HVAC systems. Therefore, optimal control is to optimize the operation of HVAC system using a systematic approach by considering the system level characteristics and interactions among the overall system.

A foundation of an optimal control problem is to predict the response of a system studied. Different optimal control methods can be applied to evaluate the responses of the system to the changes of control variables. An overall classification of main optimal control methods used in HVAC systems is illustrated in Figure 2.6 (Wang 2010). They can be classified into four categories, including model-based optimal control method, model-free optimal control method, hybrid optimal control method, and performance map-based optimal control method. The control methods using physical models, grey-box models and black-box models can be classified into the category of model-based methods while the methods using expert systems and pure learning approaches can be grouped into the model-free category. Model-based optimal control method is the most commonly adopted in the HVAC field.

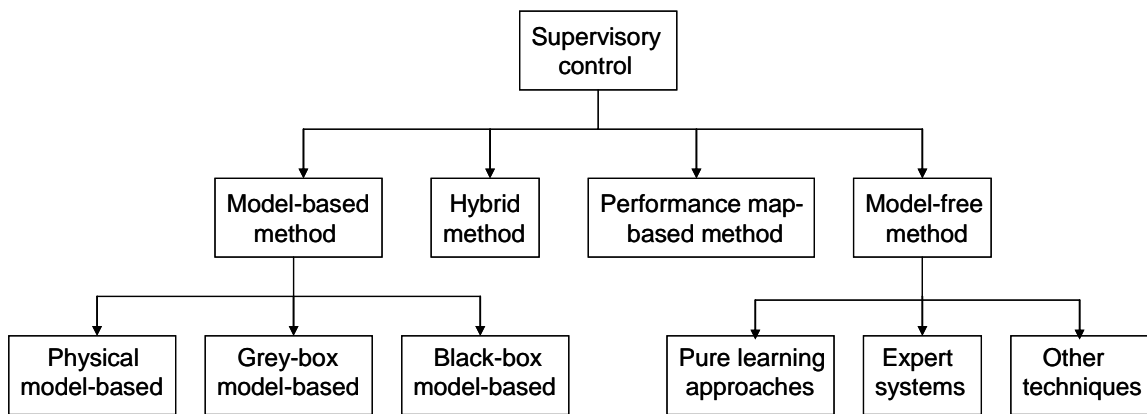


Figure 2.6 Classification of optimal control methods in HVAC systems (Wang 2010)

In model-based optimal control, the main function of the models is to predict the system energy and environment performance as well as the system response to the changes of control settings. All the models are related to power consumption and/or operating cost directly.

Identifying the model parameters is another key issue of system optimal control. The use of online identification techniques allows the models used to be reasonably simple. Online measurements collected from Building Automation Systems (BASs) are used to tune the model parameters to make them represent the actual system. Different parameters estimation approaches, including the least squares estimated algorithm, the recursive least square (RLS) algorithm, the time-varying parameters estimated algorithm, exponential forgetting RLS estimated algorithm, etc., can be applied to identify the model parameters under various conditions (Sun 2010a).

Another equally important issue of optimal control scheme is to find the solution to an optimal problem with optimization techniques. In general, the optimization techniques developed in the optimal control field could be summarized into two categories: linear optimization techniques and nonlinear optimization techniques. The linear optimization technique is a simple and straightforward technique since there is always a unique optimum in a linear optimization problem. The linear optimization technique includes direct method, recursive method, iterative method, etc. Compared to the linear optimization technique, the nonlinear optimization technique is complex and sophisticated since many local optimums exist in a nonlinear optimization problem. It is also difficult to find the global optimum.

In HVAC field, the primary role of optimization techniques is to seek the energy-efficient control settings (i.e. operation mode and set-points) to minimize the system energy inputs and/or operating cost while still maintaining satisfactory controlled variables. Searching for the optimal values of the set points in HVAC systems is usually a nonlinear optimization process. A number of studies have been carried out on the

development and application of various nonlinear optimization techniques in HVAC systems, such as the direct search method (Nelles 2001) , conjugate gradient method (Nizet et al. 1984), sequential quadratic programming (Sun et al. 2005, Chang 2004, Bassily et al. 2005), branch and bound (B&B) method (Nelles 2001), genetic algorithm (Wang et al. 2000, Chang 2005, Xu et al. 2007b), and evolutionary programming (Beyer 2001).

Among all of these techniques, genetic algorithm (GA) is attracting growing attention of building professionals and has been widely used in academic research for global optimizations. The genetic algorithm is a better optimization method especially when an optimal problem is not perfectly smooth and unimodal, or is not well understood, or the fitness function is noisy. The genetic algorithm can quickly find a sufficiently good solution and can be applied when a task does not require an absolute optimum. It therefore well fits the characteristics of an on-line optimization problem since it requests to find a near optimal solution quickly and the fitness function might be noisy because it is based on the on-line signals of sensors which are prone to errors. GA is thought to perform robustly in the presence of small amounts of noises since it works by accumulating fitness statistics over many generations.

Control functions are indispensable for modern air-conditioning systems. Great efforts towards the development and application of various control strategies for HVAC systems have been made.

Ardehali and Smith (1997) evaluated the performances of various operational strategies, such as night purge (NP), fan optimum start and stop (OSS), condenser water

reset (CWR), and chilled water reset (CHWR), applied to older- and newer-type commercial office buildings utilizing HVAC systems. The results showed that, in general, NP was not an effective strategy in buildings with low thermal mass storage, OSS reduced fan energy, and CWR and CHWR could be effective for chillers with multi-stage unloading characteristics. The most energy-efficient operational strategies were the combination of OSS, CWR, and CHWR for the older-type building, and OSS for the newer-type building.

Mathews et al. (2001) investigated the effect of some retrofit techniques on the comfort enhancement and energy saving potential of HVAC systems. These techniques included air-bypass control on cooling coils, reset and setback control, improved HVAC system start-stop times and economizing on outside air intake. Through the integrated simulation of a building, improved HVAC system start-stop times together with air-bypass, reset and setback control was found to be the most lucrative. Predicted annual energy savings were 66%.

Wang and Xu (2002, 2004) introduced an energy-efficient outdoor ventilation control strategy for VAV systems, which combining demand-controlled ventilation and economizer control can achieve adequate and even better indoor air quality with less energy consumption in buildings. A robust control strategy, using ‘freezing’, gain scheduling, I-term reset and feedback transition control for different transition processes, was developed addressing the instability problems faced during the transition processes between different control modes when combined DCV control with economizer control in applications. It can reduce the possibility of alternation and oscillation in the transient region and significantly increase the control stability. The optimization strategy

combining DCV and economizer can achieve significant energy saving as much as 41.7% compared with that of fixed minimum fresh air control and improve IAQ under in-situ measurements.

Chow (2002, 2004), Chang (2005), Ma (2011) etc. studied the system-based optimization approaches for chiller plant implementations. For instance, Chow et al. (2002) introduced a new concept of integrating neural network and genetic algorithm in the optimal control of absorption chiller system. The chilled and cooling water mass flow, the chilled water supply temperature, and the cooling water return temperature were optimized in the system. It was concluded that more energy saving could be achieved when more control variables were brought in the optimal control strategy.

Chapter 41 of the 2007 ASHRAE Handbook-HVAC Applications (ASHRAE 2007) provided a critical overview of supervisory and optimal control strategies and optimization for HVAC systems. The chapter consists of three major sections. The first section defines the systems and control variables considered. The background on the effects and opportunities associated with adjusting control variables is also presented. The second section presents a number of strategies, including the cooling tower fan control, chilled water reset with fixed and variable speed pumps, sequence and loading of multiple chillers, strategies for boilers, strategies for air-handling units, strategies for building zone temperature set points, cooling thermal storage control, etc, that can be utilized in practice for optimal control of HVAC systems. The third section presents basic methods for optimization of systems both with and without significant thermal energy storage.

Xu et al. (2009) presented an optimal ventilation control strategy for a multi-zone VAV air-conditioning system. The temperature set point of the critical zone was optimized to reduce the required fresh air fraction, hence to reduce the total fresh air flow rate and the system energy consumption. The results illustrated that the optimal strategy could achieve about 4% of energy saving and maintained acceptable thermal comfort and indoor air quality.

Ning and Zaheeruddin (2010) proposed a neural network based optimal supervisory operation strategy to find the optimal set points for chilled water supply temperature, discharge air temperature and VAV system fan static pressure in a VAV system such that the indoor environment was maintained with the least chiller and fan energy consumption. In the study, the optimal control strategy was developed based on dynamic system model. A multi-layer feed forward neural network was constructed and trained in unsupervised mode to minimize the cost function. Simulation results showed that compared to the conventional night reset operation scheme, the optimal scheme saved around 10% energy under full load condition and 19% energy under partial load conditions.

The results obtained from above mentioned studies demonstrated that system performance can be improved when optimization methods or optimal control are implemented in the air-conditioning systems, since the setpoints of control variables are optimized and reset during operation to follow dynamic operating conditions. Meanwhile, model-based optimization method is effective.

2.3.2 Control and Optimization of DOAS-CC Systems

Robust control is prerequisite for reliable operation of air conditioning systems besides proper design and maintenance. It also has significant impacts on energy use as well as occupants' comfort, healthy and productivity. During the last decade, a number of research has been carried out on the control issues of the DOAS-CC systems or similar systems.

Zhang and Niu (2003b) proposed a novel air conditioning system which combining a pre-cooling desiccant cooling cycle with chilled ceiling panels. In the study, the system latent load was treated by a rotary desiccant wheel and indoor air temperature was controlled by the chilled ceiling panels. The simulation results indicated that the system had good performance. It could save up to 40% of primary energy consumption in comparison with a conventional constant volume system.

Mumma and his collaborators have paid considerable efforts to develop control strategies for dedicated outdoor air-chilled ceiling. Mumma and Jeong (2005a, 2005b) investigated the basic control methods for a single-zone DOAS-CC system. In the research, dual wheels (i.e. enthalpy wheel and sensible wheel) and a cooling coil in the DOAS subsystem were adopted for indoor air humidity control, while the supply water flow rate of chilled ceiling was regulated for indoor air temperature control. These single-zone control logics can also be extended to include large multi-zone buildings.

Lim et al. (2006) presented two control methods for indoor temperature control and condensation control in a single room served by a floor radiant cooling system, i.e. modulation of the supply water temperature and of the supply water flow rate in the

radiant cooling panels respectively. Simulation and experimental results showed that the supply water temperature control was better than the water flow control with respect to the indoor air temperature fluctuation and condensation prevention. But for multi-zone applications, the variable supply water temperature control is difficult to realize in the system. Some additional small water pumps are needed for supply water temperature regulation.

Liu et al. (2006) studied the annual performance of an independent temperature and humidity control HVAC system. Capozzoli et al. (2006) presented two hybrid air conditioning systems with chemical dehumidification, i.e. solid desiccant dehumidification and liquid desiccant dehumidification, for supply air humidity control in supermarket applications. In the proposed systems, liquid desiccant dehumidification system was employed for independent control of the supply air humidity.

Mossolly et al. (2008) developed optimized operation strategies for a combined chilled ceiling displacement ventilation (DV) system in Beirut climate. In the work, three control strategies based on control of single parameter (chilled ceiling temperature) or simultaneous control of multiple parameters (DV system flow rate and temperature or all the DV and CC systems parameters) were optimized using a multi-objective genetic algorithm for minimal energy consumption during operation of the system. Simulation results showed that the optimized control strategy that involved varying all system design variables had been shown to consume the lowest energy when compared with optimized strategies when one or two variables are optimized during operation. Savings of up to 15% were realized with the optimal strategy as compared to the base strategy when only the chilled ceiling temperature was varied.

Labs21 (2009) introduced several key strategies to ensure effective design, construction and operation of chilled beams in laboratories. For the supply air dehumidification control, different methods, including traditional cooling and reheating dehumidification, run-around coil dehumidification, face-and-bypass dehumidification, etc., were proposed. In addition, in order to prevent condensation on the chilled beam, moisture sensors were placed on the chilled water supply lines, and if moisture was detected, the water valve was closed.

Most of previous studies on control of DOAS-CC systems or similar air conditioning systems focused on local control, i.e. how to effectively maintain a variable at its setpoint; but rarely concerned about the selection of setpoints to achieve optimal performance of the entire system. This may be attributed to the limited understanding of characteristics of the entire system even though individual components in such a system is well understood. Projects adopting DOAS-CC systems integrated with liquid desiccant dehumidification increase rapidly in recent years. It is the critical time to study optimal control of such systems during their operations.

Considering that there are relatively few and inadequate studies related to optimal control of the DOAS-CC system and reliable models, either complicated numerical models or simplified models, of the major components including chilled ceiling (Diaz 2010), liquid desiccant dehumidifier and regenerator (Yin 2007, Gandhidasan 2004, 2005) as well as the membrane-based total heat exchanger (Zhang 2006) are available at present, this study therefore aims at developing a model-based optimal control strategy for the integrated DOAS-CC system to optimize the overall system energy performance

and indoor environment. The performance of this strategy is tested and evaluated in a simulated multi-zone space under various operating conditions.

2.4 Summary

The DOAS-CC system is a promising air-conditioning system which can overcome the problems encountered by conventional HVAC systems. Some new energy savings technologies that can improve the energy performance of the integrated system are reviewed in this chapter, such as the total energy recovery and liquid desiccant dehumidification. At the same time, the roles and effects of control and optimization on the performance of HVAC systems, and the current research on DOAS-CC system, including local control and optimization of the whole DOAS-CC system, are presented as well. All these research outcomes will provide a significant theoretical basis and guidance for my PhD study to develop control and optimization strategies for the proposed DOAS-CC integrated system.

CHAPTER 3 BUILDING SYSTEM AND SIMULATION PLATFORM

This chapter mainly presents the proposed dedicated outdoor air-chilled ceiling system and mathematical models for the main components in the system. Validation of major models by experimental data is also presented. Section 3.1 describes the investigated building and air-conditioning system. Section 3.2 presents the mathematical models of major components and the validation results. The performance tests of the integrated system are shown in Section 3.3.

3.1 Building and System Descriptions

The prototype of the investigated building is a commercial building located in South China. The usable floor area is about 302 m². It is divided into five zones. Four of them, i.e. Zone 1-3 and Zone 5, are perimeter zones and Zone 4 is an interior zone, as shown in Figure 3.1. The function and area of each zone are shown in Table 3.1.

Thickness of the external wall of the building is 163 mm and the heat transmission coefficient U-value for the opaque part of the façade is 1.506 W/ (m².K). Insulating glazing windows having a U-value of 2.83 W/ (m².K) is used. Blinds are installed for shading. The floor to ceiling height of the conditioned space is 2.7 m and the area ratio of window to wall is 40% for external walls. In the open space, about 70% of the ceiling

is covered by chilled ceiling panels. The design occupant numbers of the five zones are 5, 2, 1, 13, and 56 persons, respectively.

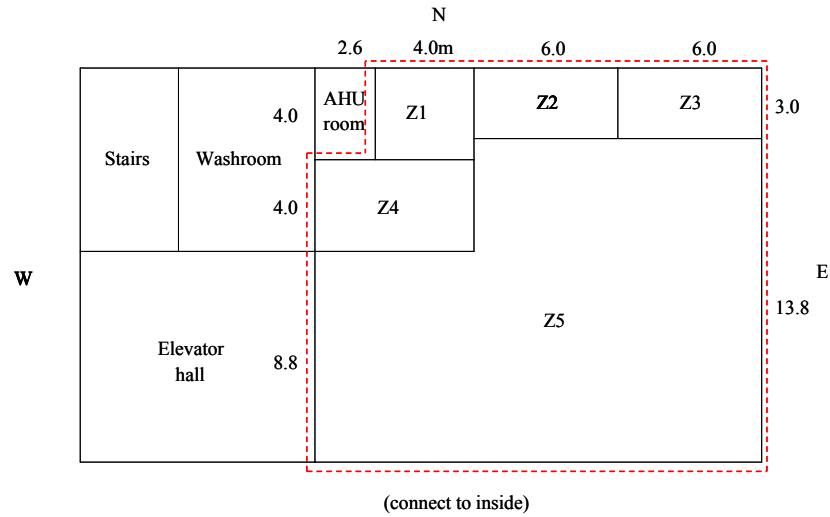


Figure 3.1 Layout of half a typical floor

Table 3.1 Basic data of the multi-zone space

	Zone1	Zone2	Zone3	Zone4	Zone5
Function	Meeting room	Manager room 1	Manager room 2	Conference room	Office room
Area (m ²)	16	18	18	26.4	224

Figure 3.2 shows the schematic of the proposed DOAS-CC system and its control system. In the integrated system as illustrated in Figure 3.2(a), the DOAS subsystem is responsible for satisfying ventilation demand and removing the moisture load of the conditioned space. The fresh air flow rate from the DOAS can be either fixed or determined by demand controlled ventilation strategy. A membrane-based total heat exchanger is employed to recover the energy of exhaust air and improve the system energy efficiency. A liquid dehumidifier is used to dehumidify the humid outdoor air to

the supply air humidity ratio set-point ($\omega_{sup,sp}$), which can be constant or variable that is determined by optimization strategy. The dry cooling coil after the dehumidifier is used to cool down the supply air to a comfort level, i.e. 19°C. The supply fan and the exhaust fan run at variable speeds. The supply fan is modulated to maintain the supply air static pressure, and the exhaust fan is controlled to maintain a difference between the supply and exhaust air flow rates. The chilled ceiling subsystem is responsible for removing the remainder sensible load of each zone, and independently controlling the indoor air temperature.

The detailed structure of the liquid desiccant cooling module is shown in Figure 3.2(b). Lithium chloride (LiCl) solution is used as the liquid desiccant in the dehumidification system. The supply air humidity ratio of the DOAS system is controlled by regulating the strong solution inlet temperature into the liquid dehumidifier, which is achieved by adjusting the cooled water flow rate entering the cooler. The supply air temperature is maintained by modulating the supply cooled water flow rate into the dry cooling coil. In the solution regeneration process, the outlet solution concentration from the regenerator is controlled by regulating the inlet solution temperature into the regenerator, which is realized by adjusting the hot water flow rate entering the heater.

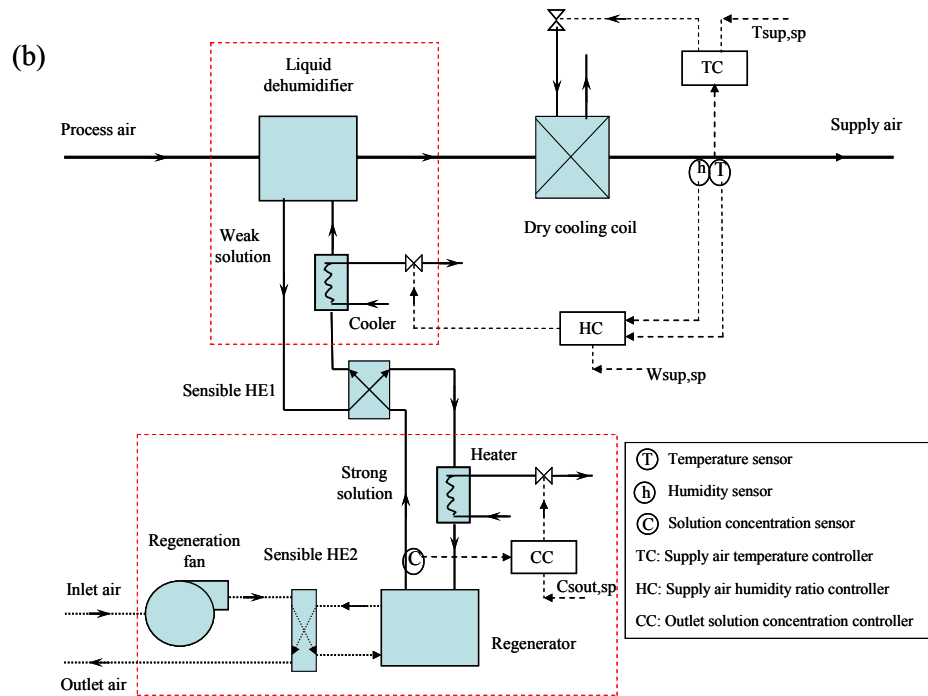
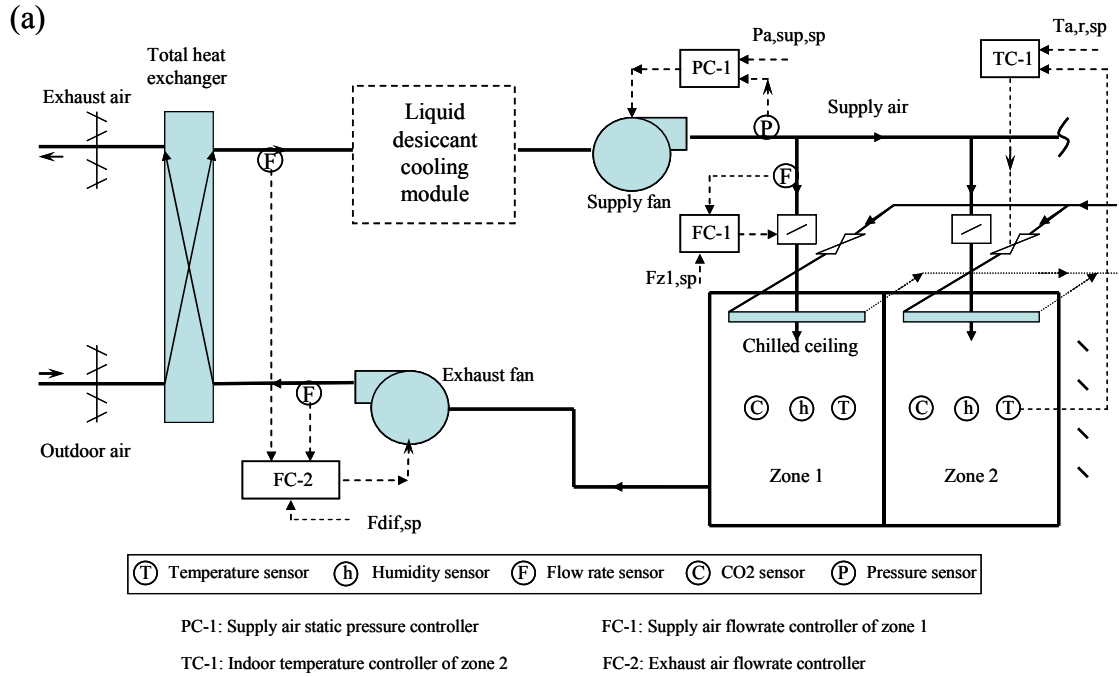


Figure 3.2 Schematic of the DOAS-CC system and its control system: (a) the whole DOAS-CC system; (b) liquid desiccant cooling module

3.2 Development of the System Simulation Platform

In this section, mathematic models of major components in the dedicated outdoor air-chilled ceiling system are developed and validated by experimental data.

3.2.1 Introduction of the Simulation Platform

TRNSYS, a transient systems simulation program with a modular structure, is used as the platform for the simulation tests of the proposed dedicated outdoor air-chilled ceiling integrated system in this thesis. TRNSYS recognizes a system description language in which the user specifies the components that constitute the system and the manner in which they are connected. The TRNSYS library includes many of the components commonly found in thermal and electrical energy systems, as well as components routines to handles inputs of weather data or other time-dependent forcing functions and outputs of simulation results. The modular nature of TRNSYS gives the program tremendous flexibility, and facilitates the addition to the program of mathematical models not included in the standard TRNSYS library. TRNSYS is well suited to detailed analyses of any system whose behavior is dependent on the passage of time (Klein et al. 2006).

Compared with other simulation programs, i.e. DOE-2, EnergyPlus, etc., TRNSYS focuses on transient simulation of associated thermal system rather than the whole building. Therefore, TRNSYS is more suitable for dynamic performance study (including control issue) for building air-conditioning systems.

To analyze the performance of the proposed system under different outdoor and indoor conditions, the models of major components of the integrated system are needed. These models are built according to TRNSYS' requirements to predict the system energy performance, environment quality as well as the system response to the changes of control settings. The major component models used to construct this system simulation platform are summarized in the following briefly.

3.2.2 Mathematic Models of Major Components

Models of major components in the DOAS-CC system, such as multi-zone building, membrane-based total heat exchanger, liquid dehumidifier, desiccant solution regenerator, cooling coil, etc., are introduced as follows.

3.2.2.1 Multi-zone building model

A multi-zone building model, Type 56 in TRNSYS 16, is used to simulate the dynamic balance of energy and moisture of the conditioned space. It is suitable for testing the control, energy and environmental performances of on-line local and supervisory control strategies.

The building model in Type 56 is a non-geometrical balance model with one air node per zone, representing the thermal capacity of the zone air volume and capacities which are closely connected with the air node (furniture, for example). Thus the node capacity is a separate input in addition to the zone volume.

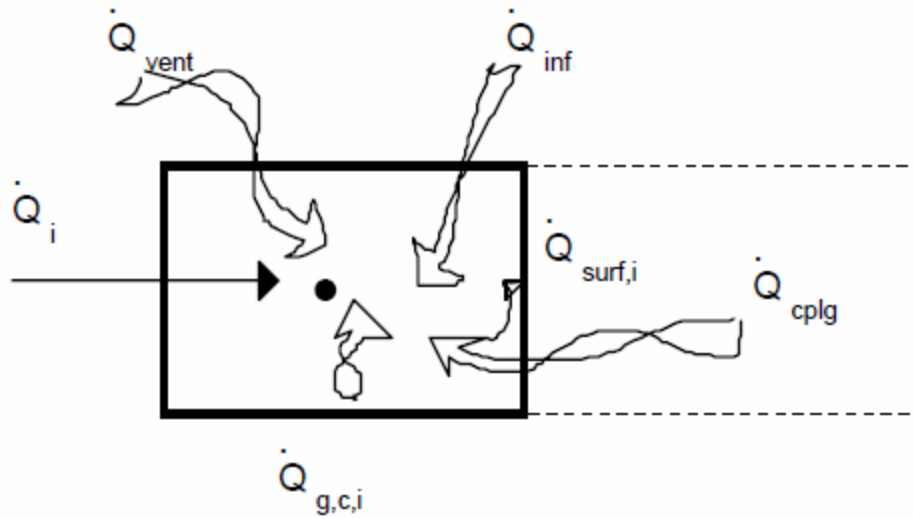


Figure 3.3 Heat balance on the zone air node (Klein et al. 2006)

The heat balance of one zone is shown in Figure 3.3. It can be expressed by Equation (3.1).

$$C_i \frac{dT_i}{dt} = Q_i \quad (3.1)$$

where C_i is the thermal capacitance of zone i , Q_i is the net heat gain.

$$Q_i = Q_{surf,i} + Q_{inf,i} + Q_{vent,i} + Q_{g,c,i} + Q_{cplg,i} \quad (3.2)$$

where $Q_{surf,i}$ is the surface gains (gain from external walls, external windows, etc.), $Q_{inf,i}$ is the infiltration gains (air flow from outside only), $Q_{vent,i}$ is the ventilation gains (air flow from a user-defined source, like an HVAC system), $Q_{g,c,i}$ is the internal convective gains (by people, equipment, illumination, radiators, etc.), $Q_{cplg,i}$ is the gains due to air flow from adjacent zone or boundary condition. More detailed information about these terms can refer to menu of TRNSYS 16 (Klein et al. 2006).

A moisture balance for zone i can be expressed by

$$M_{eff,i} \frac{dw_i}{dt} = m_{inf,i} (w_a - w_i) + \sum_k^{n,vent} m_{v,k,i} (w_{v,k,i} - w_i) + W_{g,i} + \sum_{surfaces} m_{cp1g,s} (w_j - w_i) \quad (3.3)$$

where $M_{eff,i}$ is the effective moisture capacitance of the zone, w_i is the humidity ratio of the zone, w_a is the ambient humidity ratio, $w_{v,k,i}$ is the humidity ratio of the ventilation air from ventilation type k , $W_{g,i}$ is the internal moisture gains, w_j is the humidity ratio of an adjacent zone j .

In the multi-zone building model (Type 56), pollutant concentration balance, such as CO₂ concentration, is not considered. In order to evaluate the indoor air quality represented by indoor CO₂ concentration, a building CO₂ model is developed additionally. It can be expressed by Equation (3.4).

$$V_i \frac{dC_i}{dt} = v_{inf,i} (C_a - C_i) + \sum_k^{n,vent} v_{v,k,i} (C_{v,k,i} - C_i) + CS_{g,i} + \sum_{surfaces} v_{cp1g,s} (C_j - C_i) \quad (3.4)$$

where V_i is the total air volume of the zone, C_i is the CO₂ concentration of the zone, C_a is the ambient CO₂ concentration, $C_{v,k,i}$ is the CO₂ concentration of the ventilation air from ventilation type k , $CS_{g,i}$ is the internal CO₂ generation rates, C_j is the CO₂ concentration of an adjacent zone j .

3.2.2.2 Membrane-based total heat exchanger

Both a finite difference model and an effectiveness-number transfer unit (ϵ -NTU) model can be adopted to simulate membrane-based total heat exchangers. The former is

detailed and quite accurate, but is time-consuming, whereas the latter is simple and fast with acceptable accuracy (Liang 2010).

In this study, the ε - NTU model is adopted to model the membrane-based total heat exchanger. A parallel-plate structure is applied in the membrane exchanger, as fins have little use in enhancing the heat and mass transfer of the membrane (Zhang 2008), as shown in Figure 3.4.

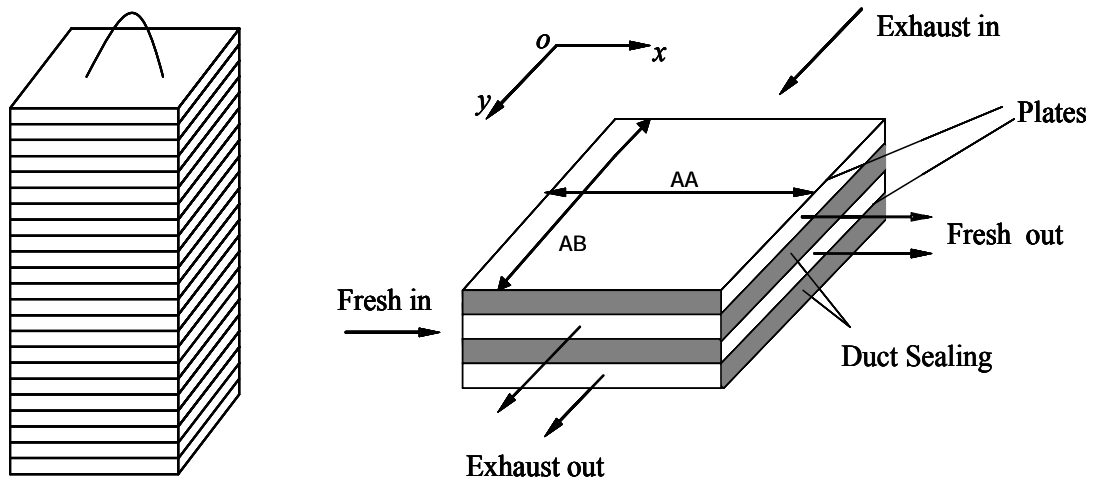


Figure 3.4 Schematic of a membrane-based parallel-plates enthalpy exchanger

For the membrane-based enthalpy exchanger, the sensible effectiveness and latent effectiveness are defined as

$$\varepsilon_S = \frac{T_{f,in} - T_{f,out}}{T_{f,in} - T_{ex,in}} \quad (3.5)$$

$$\varepsilon_L = \frac{W_{f,in} - W_{f,out}}{W_{f,in} - W_{ex,in}} \quad (3.6)$$

For sensible effectiveness

$$\varepsilon_s = 1 - \exp\left[\frac{\exp(-NTU_s^{0.78}) - 1}{NTU_s^{-0.22}}\right] \quad (3.7)$$

where NTU_s is an overall number of transfer units for sensible effectiveness. For the total heat exchanger that has equal area on both sides, NTU_s is calculated by:

$$NTU_s = \frac{UA}{(m_a c_{pa})_{\min}} \quad (3.8)$$

The correlation for latent effectiveness can be written as

$$\varepsilon_L = 1 - \exp\left[\frac{\exp(-NTU_L^{0.78}) - 1}{NTU_L^{-0.22}}\right] \quad (3.9)$$

$$NTU_L = \beta \cdot NTU_s \quad (3.10)$$

where NTU_L is an overall number of transfer units for latent effectiveness, and β is the ratio of latent to sensible total transfer units, assuming equal specific heat for two air streams, which is related to material properties (Liang 2010, Zhang 2005).

3.2.2.3 Dehumidifier and regenerator

In the proposed liquid desiccant air-conditioning system, the implemented dehumidifier and regenerator have counter-flow configurations. The mathematical model can be constructed based on the control volume

$$m_a dh_a = m_s dh_s \quad (3.11)$$

$$dm_s = m_a dw_a \quad (3.12)$$

$$\frac{dh_a}{dy} = \frac{NTU}{L} [Le \cdot (h_a - h_e) + (1 - Le) \cdot \lambda \cdot (w_a - w_e)] \quad (3.13)$$

$$\frac{dw_a}{dy} = \frac{NTU}{L} (w_a - w_e) \quad (3.14)$$

The Lewis number and NTU are defined as follows.

$$Le = \frac{F_H}{F_M \cdot c_{pa}} \quad (3.15)$$

$$NTU = \frac{F_M \cdot vAL}{m_a} \quad (3.16)$$

An integrated analytical solution to adiabatic heat and mass transfer in packed-type liquid desiccant equipment is adopted to model the dehumidifier and regenerator. Readers are referred to (Chen 2006) for a more detailed description.

3.2.2.4 Cooling/heating coil

A first-order differential equation is used to represent the dynamics of a cooling/heating coil with a lumped thermal mass, as shown in Equation (3.17) (Wang 1999). A dynamic equation based on energy balance ensures that the energy is conserved.

$$C_c \frac{dT_c}{d\tau} = \frac{T_{a,in} - T_c}{R_1} - \frac{T_c - T_{w,in}}{R_2} \quad (3.17)$$

where T_c is the mean temperature of the coil, $T_{a,in}$ and $T_{w,in}$ are the inlet air and water temperatures, C_c is the overall thermal capacity of the coil, and R_1 and R_2 are the overall heat transfer resistances at the air and water sides, respectively.

3.2.2.5 Chilled ceiling model

The specific TRNSYS module developed for radiant ceiling is used in this study. Figure 3.5 shows the schematic of a chilled ceiling panel (Klein et al. 2006). It considers it as an ‘active layer’ added to the wall, floor or ceiling definition.

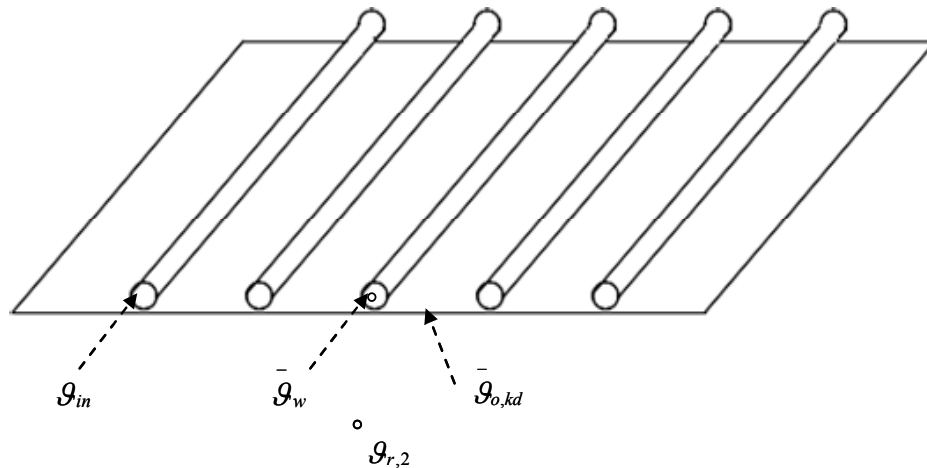


Figure 3.5 Schematic of chilled ceiling panel (Klein et al. 2006)

TRNSYS chilled ceiling panels model is based on the German norm DIN 4715-1; therefore some additional parameters to define the performance in this type of test conditions are required. These parameters as specific norm power, specific norm mass flow rate, norm area and norm number of loops can be obtained from the producer of chilled ceiling panels. Besides the test results, the heat transfer coefficient U_{wrx} is needed. It can be calculated internally from the specific norm power using the following approximation for common used chilled ceiling panels.

$$U_{wrx} = 0.6 \exp\left(\frac{0.0469 P_{sp_norm}}{3.6}\right) 3.6 \quad (3.18)$$

where P_{sp_norm} is the specific norm power after DIN 4715-1.

Also the temperature difference dT_{surf_norm} between mean fluid temperature $\bar{\theta}_w$ and mean surface temperature $\bar{\theta}_k$ if know for test conditions can be used to calculate the heat transfer coefficient U_{wrx} with the following equation:

$$U_{wrx} = \frac{P_{sp_norm}}{dT_{surf_norm}} \quad (3.19)$$

3.2.2.6 Power models

The electric power consumed by the chiller is calculated as

$$E_{ch} = \frac{Q_{ch}}{COP_{ch}} \quad (3.20)$$

where Q_{ch} is the cooling energy consumed by the integrated system, and COP_{ch} is the chiller's coefficient of performance.

Fan power is calculated by

$$E_{fan} = \frac{V \cdot \Delta p}{3600 \eta_{fan}} \quad (3.21)$$

where V is the volumetric flow rate of the fan, Δp is the total pressure rise of the pump, and η_{fan} is fan efficiency. In this study, the pressure rises of the supply fan, return fan,

and regeneration air fan are assumed to be fixed in the operation period. They are 1000Pa, 400Pa, and 300Pa, respectively. The efficiency of the fans is 0.6.

The other components in the simulator, such as the controllers, the sensible heat exchangers, etc. are obtained from the TRNSYS model base. The sensible effectiveness of the heat exchangers is 0.8.

3.2.3 Validations of the Component Models

3.2.3.1 Validation of membrane-based total heat exchanger model

To study the heat and mass transfer performance of the membrane-based total heat exchanger, an experimental rig is set up in the Key Laboratory of Enhanced Heat Transfer and Energy Conservation of Education Ministry, South China University of Technology, as shown in Figure 3.6. Two parallel air ducts with a 200mm×200mm cross-section are assembled. Each duct is comprised of a variable speed blower, a wind tunnel, a set of nozzles, wind straighteners, electric heating coils, steam humidification tubes, temperature and humidity sensors. The heating power and the steam generation currents can be adjusted according to the set points of temperature and humidity. The whole test rig is built in a constant temperature and constant humidity room, so the inlet temperature and humidity can be controlled and maintained very well even under very hot and humid ambient weather conditions. A 10 mm thick plastic foam insulation layer is pasted on the outer surfaces of the ducts to prevent heat dissipation from the system to the surroundings.

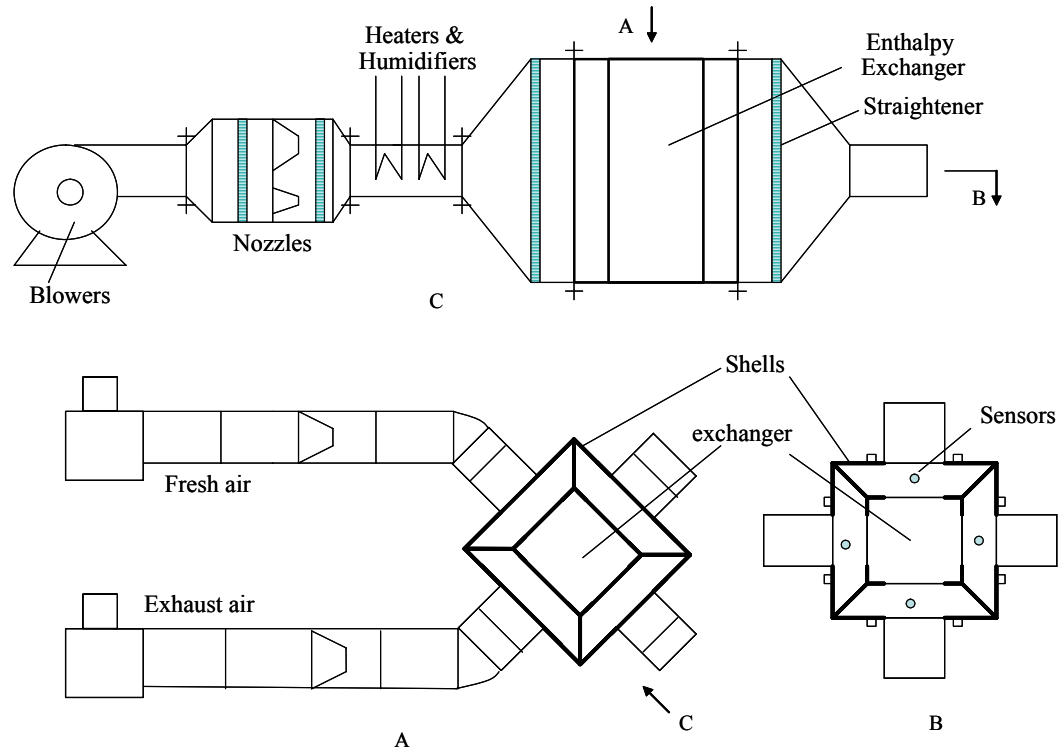


Figure 3.6 Experimental rig of the membrane-based enthalpy exchanger

The structural parameters and nominal operating condition of the exchanger is listed in Table 3.2. During the experiment, equal air flow rates are kept for the two ducts. Though the design air flow rates are $150\text{m}^3/\text{h}$ in the test, they can be adjusted by variable speed blowers to have different air velocities. Temperature, humidity, and volumetric flow rates are monitored at the inlet and outlet of the exchanger. Volumetric air flow rates are varied from 100 to $200\text{m}^3/\text{h}$, corresponding to frontal air velocities from 0.37 to 0.74m/s which are typical for enthalpy exchangers.

Table 3.2 Structural parameters and nominal operating condition of the exchanger

Item	Symbol (unit)	Value
Number of channels for each flow	n	115
Channel length	x_F, y_F (mm)	185
Channel height	a (mm)	2.0
Vapor diffusivity in air	D_a (m ² /s)	2.85×10^{-5}
Heat conductivity of air	λ_a (W m ⁻¹ K ⁻¹)	0.0263
Inlet fresh air temperature	T_{fin} (°C)	35
Inlet exhaust air temperature	T_{ein} (°C)	27
Inlet fresh air humidity	RH _{fin} (%)	59
Inlet exhaust air humidity	RH _{ein} (%)	54

The experimental data, including inlet and outlet states of fresh air and exhaust air from the test rig is shown in Table 3.3. According to the experimental results, it can be found that the sensible effectiveness and latent effectiveness of the enthalpy exchanger decrease as the increase of air flow rate. These steady-state measurements are used to validate the mathematical model.

Table 3.3 Experimental results of the total heat exchanger

Flow rate (m ³ /h)	Fresh air				Exhaust air				Effectiveness	
	T_{in}	RH _{in}	T_{out}	RH _{out}	T_{in}	RH _{in}	T_{out}	RH _{out}	E_S	E_L
100	35	0.69	28.5	0.601	26.9	0.511	33.8	0.635	0.827	0.742
125	35.1	0.665	28.7	0.629	27	0.527	33.7	0.618	0.809	0.701
150	34.9	0.66	28.7	0.645	27	0.552	33.5	0.61	0.796	0.675
175	34.9	0.69	28.8	0.645	26.9	0.551	33	0.638	0.763	0.672
200	34.9	0.656	28.8	0.651	26.9	0.658	32.6	0.635	0.738	0.665

The comparisons of experimental data and the simulation results are shown in Figure 3.7 for the sensible effectiveness and latent effectiveness validations. Comparing the experimental data and the simulation results, it can be found that the maximum error of effectiveness is less than 6%. The results illustrate that the simplified physical model is feasible to calculate the effectiveness of the membrane-based total heat exchanger.

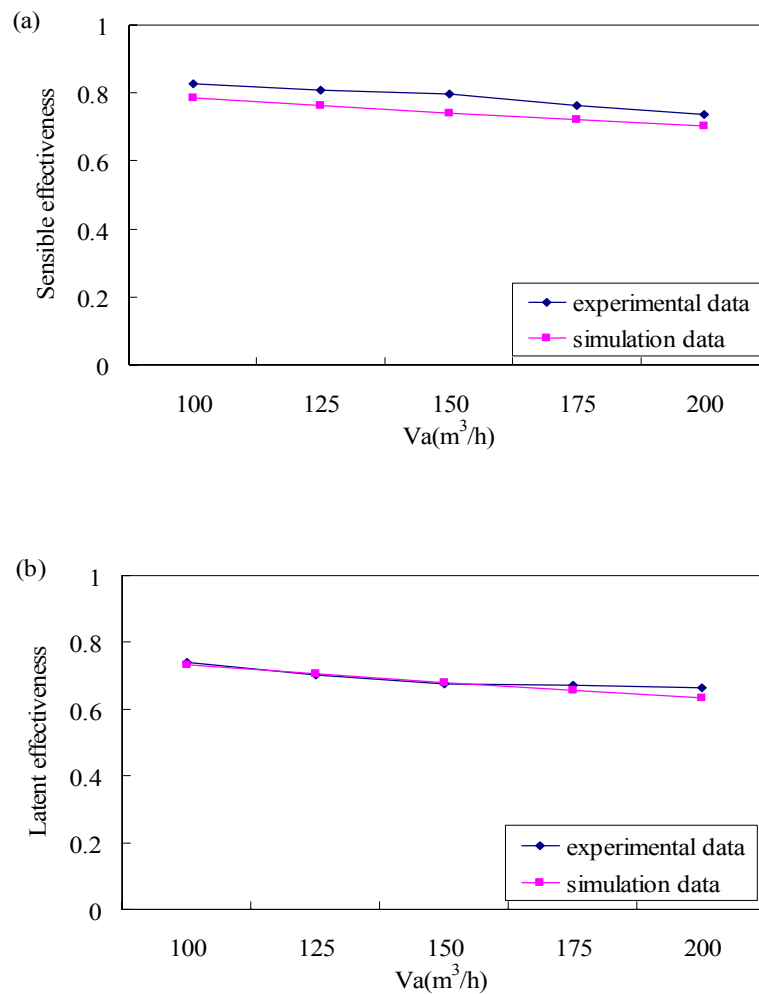


Figure 3.7 Comparison of experimental and simulation results: (a) sensible effectiveness; (b) latent effectiveness

3.2.3.2 Validation of dehumidifier and regenerator models

To validate the dehumidifier and regenerator models, comparisons are made between the analytical solutions of the models used in this study and the experimental data available from the literature (Fumo and Goswami 2002). Reliable sets of experimental data using LiCl as the liquid desiccant were reported by Fumo and Goswami (2002). In their experiments, the diameter of the packed bed was 24 cm, the height of the tower was 60 cm, and polypropylene Rauschert Hiflow rings with a specific surface area of $210\text{m}^2/\text{m}^3$ were selected as the packing material. The comparison results are given in Table 3.4 and Table 3.5. The analytical solutions are also compared with the results obtained by Gandhidasan (2004) in Table 3.4. In the present study, the Lewis number is assumed to be unity and the mass transfer coefficient F_M is $0.013\text{kg}/\text{m}^2\text{s}$ in the air dehumidification process; the Lewis number is assumed to be 0.95 and the mass transfer coefficient F_M is $0.02\text{kg}/\text{m}^2\text{s}$ in the solution regeneration process. According to the results presented in Tables 3.4 and 3.5, there is very good agreement between the experimental data and the analytical solutions of the process air outlet state and desiccant outlet state obtained in this study. In all cases, the maximum difference is less than 8% for the air dehumidification process and less than 7% for the desiccant regeneration process.

Table 3.4 Comparison of experimental data (Fumo and Goswami 2002) with analytical solutions for the dehumidification process

	$T_{a,out}$ (°C)	$W_{a,out}$ (kg/kg)	$T_{s,out}$ (°C)	$C_{s,out}$ (%)
<i>Case 1: $m_a=1.180$ kg/m²s, $T_{a,in}=30.1$ °C, $W_{a,in}=0.0181$ kg/kg, $m_s=6.227$ kg/m²s, $T_{s,in}=30.3$ °C, $C_{s,in}=34.7\%$</i>				
Experimental results	32.20	0.0108	32.60	34.60
Present study	31.07	0.0106	31.32	34.66
Percentage difference	-3.51	-1.85	-3.93	0.17
Gandhidasan (2004)			31.35	34.65
Percentage difference			-3.83	0.14
<i>Case 2: $m_a=1.513$ kg/m²s, $T_{a,in}=30.2$ °C, $W_{a,in}=0.0181$ kg/kg, $m_s=6.113$ kg/m²s, $T_{s,in}=30.0$ °C, $C_{s,in}=34.3\%$</i>				
Experimental results	32.20	0.0108	32.70	34.10
Present study	31.14	0.0116	31.18	34.26
Percentage difference	-3.29	7.41	-4.65	0.47
Gandhidasan (2004)			31.38	34.24
Percentage difference			-4.04	0.41
<i>Case 3: $m_a=1.189$ kg/m²s, $T_{a,in}=35.5$ °C, $W_{a,in}=0.0188$ kg/kg, $m_s=6.290$ kg/m²s, $T_{s,in}=30.3$ °C, $C_{s,in}=34.5\%$</i>				
Experimental results	32.80	0.0112	32.60	33.70
Present study	32.45	0.0109	31.58	34.46
Percentage difference	-1.07	-2.68	-3.13	2.26
Gandhidasan (2004)			31.73	34.45
Percentage difference			-2.67	2.20
<i>Case 4: $m_a=1.214$ kg/m²s, $T_{a,in}=30.3$ °C, $W_{a,in}=0.0142$ kg/kg, $m_s=6.273$ kg/m²s, $T_{s,in}=30.1$ °C, $C_{s,in}=33.9\%$</i>				
Experimental results	31.10	0.0103	31.50	33.80
Present study	30.77	0.0100	30.72	33.88
Percentage difference	-1.06	-2.91	-2.48	0.24
Gandhidasan (2004)			30.70	33.88
Percentage difference			-2.54	0.24
<i>Case 5: $m_a=1.190$ kg/m²s, $T_{a,in}=30.1$ °C, $W_{a,in}=0.0180$ kg/kg, $m_s=5.019$ kg/m²s, $T_{s,in}=30.2$ °C, $C_{s,in}=34.4\%$</i>				
Experimental results	32.20	0.0113	32.70	34.20
Present study	31.06	0.0108	31.44	34.35
Percentage difference	-3.54	-4.42	-3.85	0.44
Gandhidasan (2004)			31.39	34.35
Percentage difference			-4.01	0.44
<i>Case 6: $m_a=1.198$ kg/m²s, $T_{a,in}=29.9$ °C, $W_{a,in}=0.0177$ kg/kg, $m_s=6.269$ kg/m²s, $T_{s,in}=25.0$ °C, $C_{s,in}=34.7\%$</i>				
Experimental results	28.20	0.0088	28.40	34.50
Present study	27.04	0.0088	26.42	34.65
Percentage difference	-4.11	0	-6.97	0.43
Gandhidasan (2004)			26.62	34.64
Percentage difference			-6.27	0.40

<i>Case 7: $m_a=1.182 \text{ kg/m}^2\text{s}$, $T_{a,in}=29.9^\circ\text{C}$, $W_{a,in}=0.0179 \text{ kg/kg}$, $m_s=6.164 \text{ kg/m}^2\text{s}$, $T_{s,in}=30.1^\circ\text{C}$, $C_{s,in}=33.1\%$</i>				
Experimental results	32.40	0.0114	32.20	33.00
Present study	30.84	0.0113	31.02	33.07
Percentage difference	-4.81	-0.88	-3.66	0.21
Gandhidasan (2004)			31.00	33.06
Percentage difference			-3.73	0.18

Table 3.5 Comparison of experimental data (Fumo and Goswami 2002) with analytical solutions for the regeneration process

	$T_{a,out} (^\circ\text{C})$	$W_{a,out} (\text{kg/kg})$	$T_{s,out} (^\circ\text{C})$	$C_{s,out} (\%)$
<i>Case 1: $m_a=1.098 \text{ kg/m}^2\text{s}$, $T_{a,in}=30.1^\circ\text{C}$, $W_{a,in}=0.0180 \text{ kg/kg}$, $m_s=6.206 \text{ kg/m}^2\text{s}$, $T_{s,in}=65.1^\circ\text{C}$, $C_{s,in}=34.1\%$</i>				
Experimental results	59.30	0.0532	57.80	34.80
Present study	58.67	0.0533	60.13	34.27
Percentage difference	-1.06	0.19	4.03	-1.52
<i>Case 2: $m_a=1.438 \text{ kg/m}^2\text{s}$, $T_{a,in}=29.8^\circ\text{C}$, $W_{a,in}=0.0177 \text{ kg/kg}$, $m_s=6.479 \text{ kg/m}^2\text{s}$, $T_{s,in}=65.1^\circ\text{C}$, $C_{s,in}=34.5\%$</i>				
Experimental results	57.50	0.0488	56.60	35.20
Present study	56.44	0.0479	59.66	34.68
Percentage difference	-1.84	-1.84	5.41	-1.48
<i>Case 3: $m_a=1.097 \text{ kg/m}^2\text{s}$, $T_{a,in}=35.1^\circ\text{C}$, $W_{a,in}=0.0180 \text{ kg/kg}$, $m_s=6.349 \text{ kg/m}^2\text{s}$, $T_{s,in}=65.1^\circ\text{C}$, $C_{s,in}=33.4\%$</i>				
Experimental results	58.50	0.0551	57.40	34.10
Present study	59.28	0.0563	60.22	33.57
Percentage difference	1.33	2.18	4.91	-1.55
<i>Case 4: $m_a=1.132 \text{ kg/m}^2\text{s}$, $T_{a,in}=30.2^\circ\text{C}$, $W_{a,in}=0.0143 \text{ kg/kg}$, $m_s=6.370 \text{ kg/m}^2\text{s}$, $T_{s,in}=65.2^\circ\text{C}$, $C_{s,in}=34.0\%$</i>				
Experimental results	57.60	0.0513	57.20	34.70
Present study	58.34	0.0530	59.82	34.19
Percentage difference	1.28	3.31	4.58	-1.47
<i>Case 5: $m_a=1.101 \text{ kg/m}^2\text{s}$, $T_{a,in}=29.9^\circ\text{C}$, $W_{a,in}=0.0180 \text{ kg/kg}$, $m_s=7.541 \text{ kg/m}^2\text{s}$, $T_{s,in}=65.2^\circ\text{C}$, $C_{s,in}=34.3\%$</i>				
Experimental results	59.00	0.0556	57.90	34.90
Present study	58.84	0.0535	61.07	34.44
Percentage difference	-0.27	-3.78	5.47	-1.32
<i>Case 6: $m_a=1.111 \text{ kg/m}^2\text{s}$, $T_{a,in}=30.0^\circ\text{C}$, $W_{a,in}=0.0187 \text{ kg/kg}$, $m_s=6.245 \text{ kg/m}^2\text{s}$, $T_{s,in}=60.3^\circ\text{C}$, $C_{s,in}=34.4\%$</i>				
Experimental results	55.80	0.0447	54.20	34.80
Present study	54.67	0.0416	56.79	34.51
Percentage difference	-2.03	-6.94	4.78	-0.83
<i>Case 7: $m_a=1.099 \text{ kg/m}^2\text{s}$, $T_{a,in}=29.7^\circ\text{C}$, $W_{a,in}=0.0177 \text{ kg/kg}$, $m_s=6.400 \text{ kg/m}^2\text{s}$, $T_{s,in}=64.8^\circ\text{C}$, $C_{s,in}=32.8\%$</i>				
Experimental results	57.60	0.0542	56.80	33.40
Present study	58.29	0.0573	59.52	32.98
Percentage difference	1.20	5.72	4.79	-1.26

3.3 Tests of the System Simulation Platform

According to the above developed or selected component models, a simulator of the whole dedicated outdoor air-chilled ceiling system is built on the platform of TRNSYS. In this section, the responses of basic control loops, such as supply air humidity control and supply air temperature control loops, etc., and indoor air state responses are tested to evaluate the simulation platform performance of the dedicated outdoor air-chilled ceiling system. In addition, the effect of membrane-based total heat exchanger on the system energy performance is also tested.

The performance of the DOAS-CC system is tested in a summer day. The weather data of the tested day is shown in Figure 3.8. The operation period of air-conditioning system is from 9:00 to 18:00. The expected indoor air conditions in the office are 25°C of dry bulb temperature and no more than 60% of relative humidity (RH). Constant ventilation flow rate is used for occupant ventilation in this test case. The fresh air requirement is computed according to the number of design occupants, i.e. 10 l/s per person for the office rooms and the meeting room. The actual occupancy profiles of each zone and the total occupancy profile are presented in Figure 3.9. The CO₂, moisture and sensible heat generation rates per person are assumed to be 5×10^{-6} m³/s, 2.2×10^{-5} kg/s and 65 W, respectively. Internal loads are taken as 10 W/m² for lighting and 20 W/m² for equipments. In addition, a moisture disturbance of 1.02 kg/hr is introduced into Zone 5 from 9:00 to 18:00 in the test day.

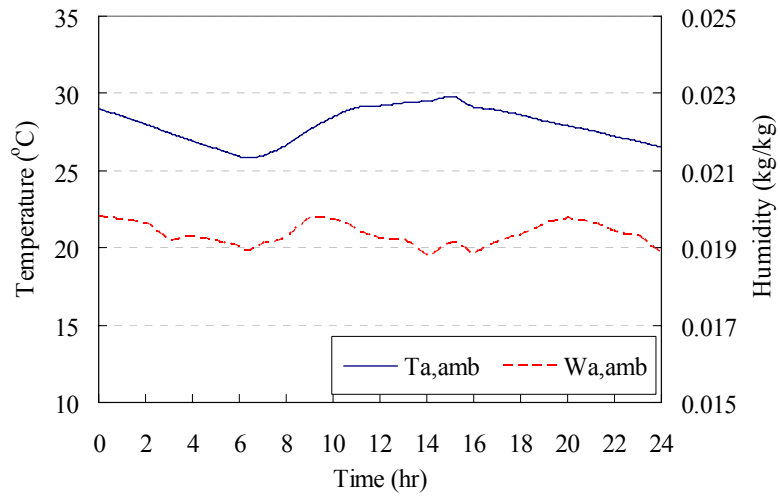


Figure 3.8 Outdoor air temperature and humidity on the summer test day

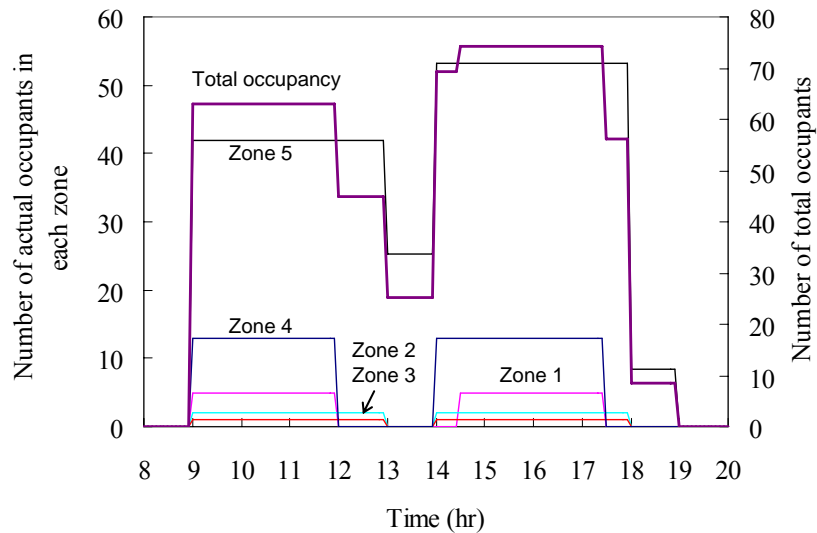


Figure 3.9 Occupancy profiles of individual zones and the total occupancy profile

3.3.1 System Responses Tests

In the dedicated outdoor air subsystem, a liquid dehumidifier is implemented to dehumidify air and control the supply air humidity. The inlet temperature of strong

solution into dehumidifier is regulated to achieve the supply air humidity set point, i.e. 9.3g/kg in the study. The supply air humidity response in the DOAS system is shown in Figure 3.10. It can be found that the liquid dehumidifier is feasible to control supply air humidity, since the actual outlet humidity is almost the same as the set point. In addition, the strong solution inlet temperature entering the dehumidifier is also shown in the figure. It changes between 28°C and 29°C. It can be seen that the solution inlet temperature is lower in the morning period, since the latent load treated by the dehumidifier is higher in morning, which is caused by higher outdoor air humidity ratio in the morning period, as shown in Figure 3.8.

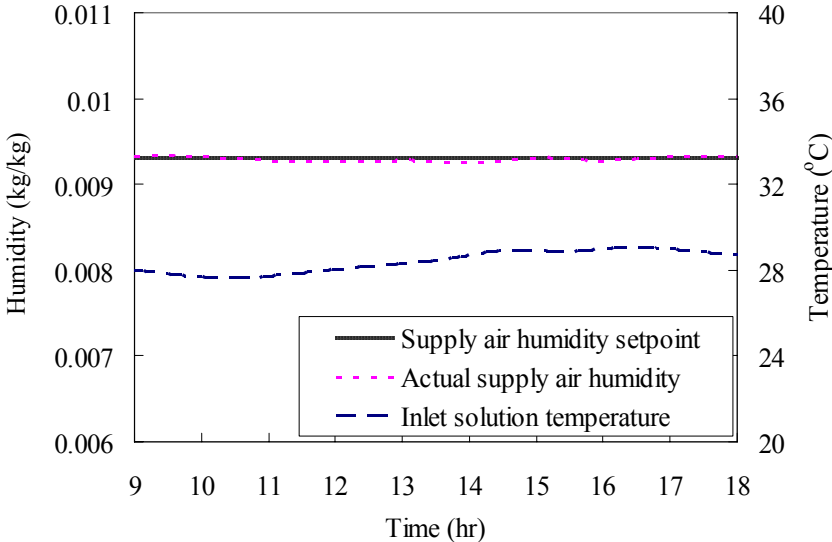


Figure 3.10 Supply air humidity responses

A dry cooling coil is employed to cool down the supply air after the liquid dehumidifier. The supply water flow rate is modulated to control the outlet air temperature to the set point, i.e. 19°C. The supply air temperature response is shown in Figure 3.11. The actual supply air temperature well approaches the set point. The supply

water flow rate is also shown in the figure, which changes slightly and almost is 1.1 kg/s.

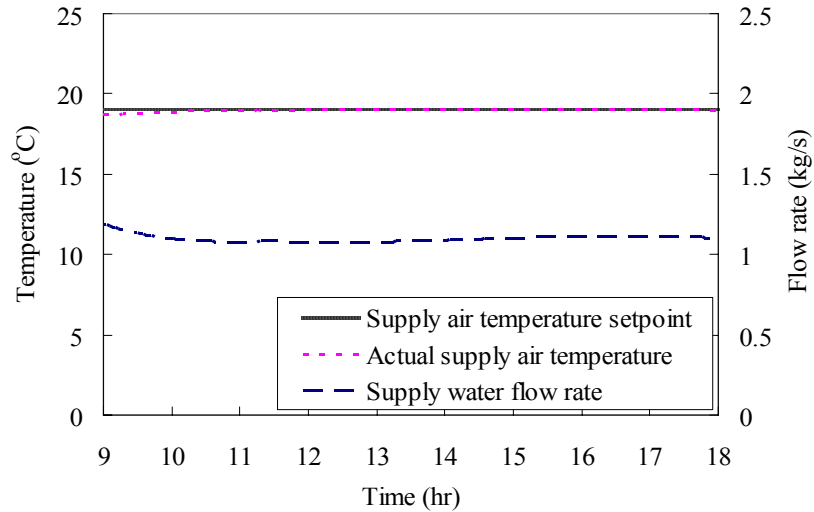


Figure 3.11 Supply air temperature responses

When the DOAS-CC system operates in the working period, the indoor air temperature and indoor RH responses of Zone 5 are shown in Figure 3.12. The data is shown for zone 5 since it has the highest load variation and would be representative of the thermal response of the system. It can be found that the indoor air is well controlled to the set point, i.e. 25°C, except for some fluctuations in the morning and noon periods. There are larger load changes and disturbances in the periods. The indoor air relative humidity changes between 50% and 60%. Since the ventilation flow rate is constant in this test, the relative humidity is lower in the morning and noon periods, which is caused by the lower occupant number in the periods, as shown in Figure 3.9. The indoor air CO₂ concentration is shown in Figure 3.13. The maximum indoor air CO₂ concentration is about 800ppm. The CO₂ concentration is lower in the morning and noon periods, since constant ventilation flow rate is supplied.

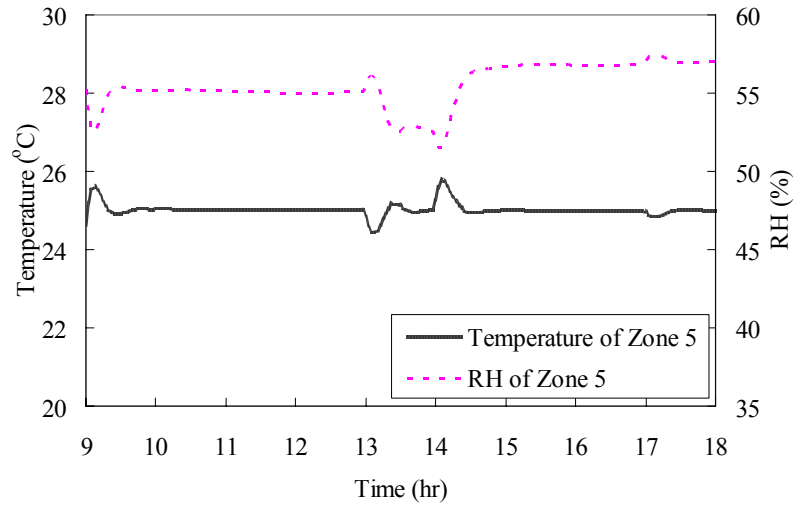


Figure 3.12 Indoor air temperature and humidity responses

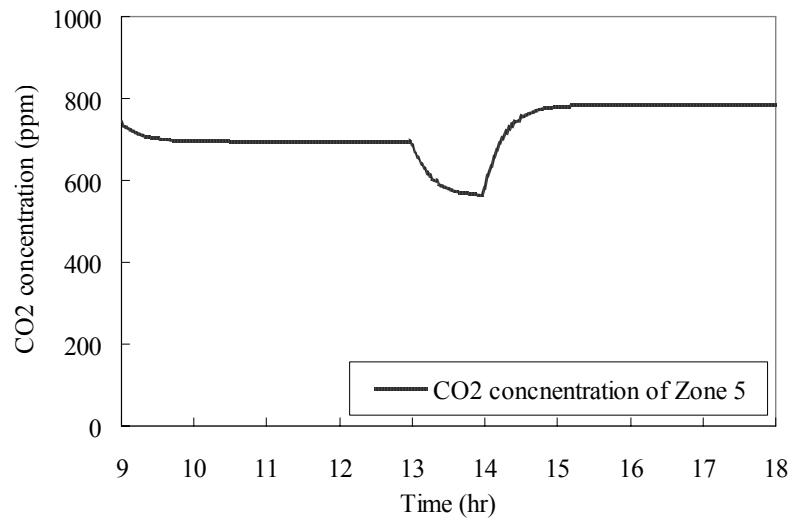


Figure 3.13 Indoor CO₂ concentration response

In addition, in the operation of the DOAS-CC system, the responses of chilled ceiling are shown in Figure 3.14. The supply water flow rate changes from 0 to 0.4 kg/s. In the noon period, the supply water flow rate is comparatively lower, since the sensible cooling load is lower in this period. The outlet water temperature is also presented in this

figure, which changes from 21°C to 24°C. It can be found that the temperature rising in the noon period is higher than that in morning and afternoon periods.

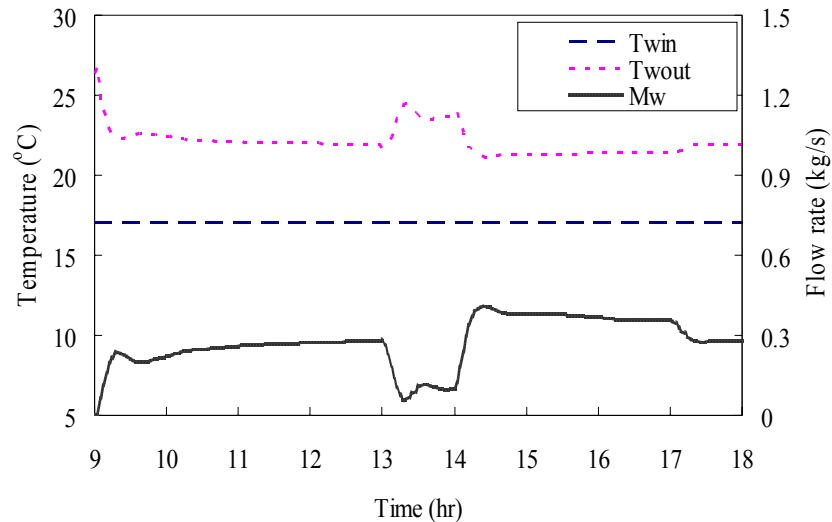


Figure 3.14 Chilled ceiling responses

3.3.2. Effect of Total Heat Exchanger on System Energy Performance

In this section, a case study is conducted to investigate the effect of the membrane-based total heat exchanger on the energy performance of the proposed dedicate outdoor air-chilled ceiling system. In the simulation tests, the whole system performance is evaluated at two kinds of conditions, with membrane-based energy recovery (*With membrane-ER*) and without membrane-based energy recovery (*Without membrane-ER*), in the whole August.

Table 3.6 presents the energy consumption of the DOAS-CC integrated system under these two conditions. Simulation results indicate that the effect of the membrane-based total heat recovery on the performance of DOAS-CC system is

prominent, which can save about 27.1% of cooling consumption for supply air dehumidification and cooling, and about 21.7% of heating requirement for desiccant solution regeneration. Consequently, it can totally reduce about 23.2% of energy consumption of the integrated system. Apart from significant energy saving in the system, the inlet air state, i.e. temperature and humidity, entering the liquid dehumidifier is more stable when the total heat recovery is applied in the system, even though the ambient air state has large variations. In this situation, the control of air dehumidification is more robust and the control system is more stable.

Table 3.6 Breakdown of primary energy consumption of the integrated system

Items	Without membrane-ER	With membrane-ER
Heater	56418.98	44193.35
Total heating(MJ)	56418.98	44193.35
<i>Saving (%)</i>	--	21.67%
Cooler	44709.84	26266.11
Dry coil	11603.86	11036.57
Chilled ceiling	14797.89	14527.06
Total cooling(MJ)	71111.59	51829.75
<i>Saving (%)</i>	--	27.11%
Supply fan	4864.80	4864.80
Return fan	1945.92	1945.92
Regeneration fan	1339.20	1339.20
Total fan energy (MJ)	8149.92	8149.92
<i>Saving (%)</i>	--	0%
Overall energy(MJ)	135680.49	104173.02
<i>Saving (%)</i>	--	23.22%

3.4 Summary

In this chapter, the investigated building and the dedicated outdoor air-chilled ceiling system adopting membrane-based total heat recovery and liquid desiccant dehumidification technologies are introduced firstly. Then the mathematic models of major components in the DOAS-CC system are set up and they are validated by experimental data from site measurements or literature of other researchers. The validation results show that these mathematic models are applicable to study the performance of the components. For the membrane-based enthalpy exchanger, the sensible effectiveness and latent effectiveness decrease as the increase of air flow rate. Lastly, a simulator of the whole DOAS-CC system is built on the platform of TRNSYS. The responses of major local control loops in the integrated system are tested. The test results show that the developed simulator is reliable to study the performance of the integrated system. In addition, the effect of membrane-based total heat exchanger on the energy performance of the whole DOAS-CC system is investigated, which can save about 23.2% of total energy consumption of the integrated system in the whole August.

CHAPTER 4 CONTROL OF THE LIQUID DESICCANT SYSTEM

This chapter mainly presents the developed control strategies for the liquid desiccant system and the characteristics of the system under various operation conditions. Section 4.1 develops control methods for the supply air dehumidification and cooling process in the dehumidifier side and methods for the liquid desiccant regeneration in the regenerator side. The control feasibilities of different control methods are also evaluated. Section 4.2 presents the control performance of the liquid desiccant system under various operation conditions. Section 4.3 presents a case study about outdoor air ventilation strategy of the liquid desiccant based air-conditioning system.

4.1 Control Strategies of the Liquid Desiccant System

To realize normal and continuous operation and to follow the changing cooling, dehumidification, and ventilation loads, the liquid desiccant cooling system requires reliable control. The supply air humidity and temperature directly influence the thermal comfort in the air-conditioned space. The strong solution concentration determines the dehumidification capability and energy consumption in the solution regeneration process. The supply air temperature can be controlled by regulating the water valve of the dry cooling coil. Different methods are available for controlling the supply air humidity and the strong solution concentration, and they are presented in this section.

A schematic of the proposed liquid desiccant air-conditioning system is presented in Figure 4.1. It is a dedicated outdoor air system, and the supply air is 100% fresh air. The system can be adopted alone or integrated with such terminal sensible cooling equipment as chilled ceiling and dry fan-coil units to provide independent temperature, humidity, and ventilation control for air-conditioned spaces. The proposed system contains three loops: the process air loop, the liquid desiccant solution loop, and the regeneration air loop.

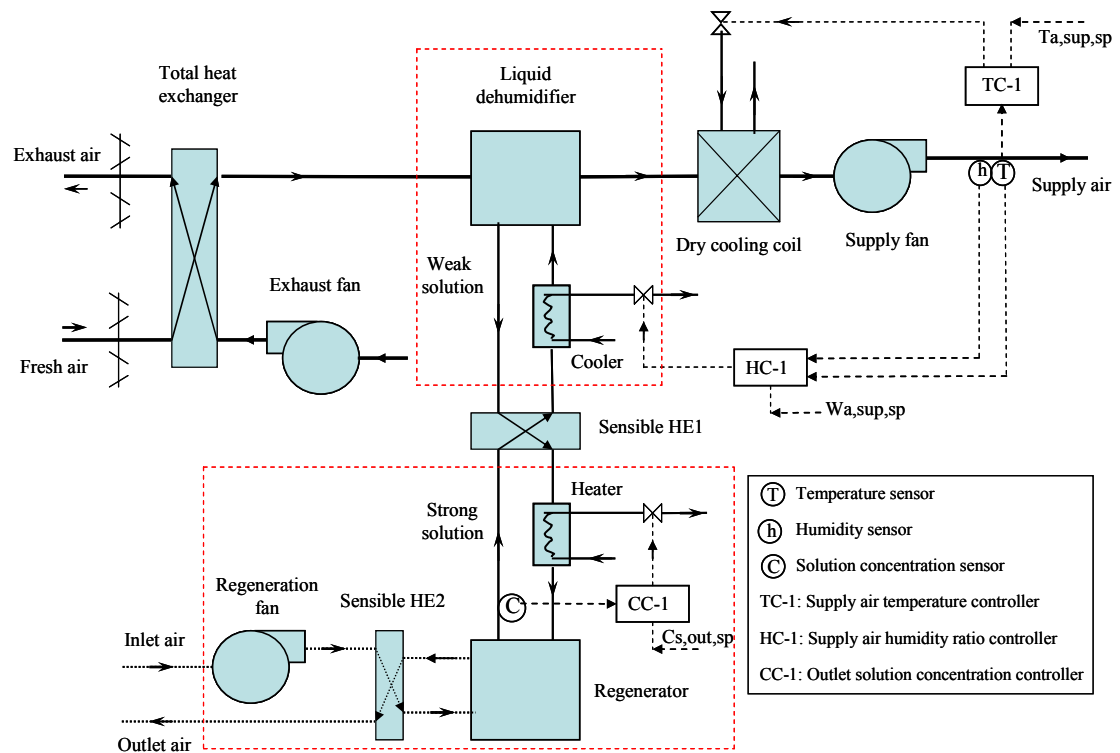


Figure 4.1 Schematic of the proposed liquid desiccant-based dedicated outdoor air system

The process air loop comprises a membrane-based total heat exchanger, a liquid desiccant solution loop, and a dry cooling coil. Fresh air flows through the total heat exchanger, where it exchanges heat and moisture with the exhaust air from the conditioned space.

The air leaving the heat exchanger is dehumidified by the liquid dehumidifier, and then sensibly cooled down to a pre-set state by the dry cooling coil. Exhaust air from the conditioned space passes through the total heat exchanger and is exhausted to the outside. In this study, a membrane-based total heat exchanger was selected to recover the heat and moisture from the exhaust air.

The solution loop is composed of a water cooler, a dehumidifier, a solution-to-solution heat exchanger (*Sensible HE1*), a hot water heater, and a regenerator. The desiccant is a lithium chloride solution. The re-concentrated solution is pre-cooled by the heat exchanger and then cooled by the water cooler before being sprayed onto the packing of the dehumidifier. The diluted solution leaving the dehumidifier is pre-heated by the sensible heat exchanger, further heated by the water heater, and then finally re-concentrated in the regenerator. Although low-grade heat resources, such as waste heat and solar energy, are preferred for solution regeneration, they are not always readily and stably available. Therefore, diluted solution heating was performed by the hot water heater in this study.

The regeneration air loop consists of an air-to-air sensible heat exchanger (*Sensible HE2*) and a regenerator. The inlet air (ambient air) in the solution regeneration process is first pre-heated by the heat exchanger, and then fed into the regenerator to absorb the moisture in the weak solution. The temperature of the air leaving the regenerator is higher than that of the inlet air. Hence, the outlet air is used to pre-heat the inlet air in the heat exchanger sensibly before it is extracted to the outside.

4.1.1 Control Methods of Air Dehumidification Process

Two control methods are proposed for supply air humidity control in the supply air treatment process. *Method (a): Variable strong solution inlet temperature.* The proposed system's supply air humidity ratio is controlled by regulating the strong solution inlet temperature in the liquid dehumidifier. It is realized by adjusting the cooled water flow rate entering the cooler, as shown in Figure 4.1. *Method (b): Variable strong solution flow rate.* The supply air humidity ratio is controlled by regulating the strong solution flow rate in the dehumidifier. The supply air temperature increases in the dehumidification process, and it is maintained at its set-point ($T_{a,sp}$) by modulating the supply water flow rate into the dry cooling coil.

4.1.2 Control Methods of Solution Regeneration Process

Two control methods are also proposed for controlling the outlet solution concentration in the solution regeneration process. *Method (c): Variable diluted solution inlet temperature.* The outlet solution concentration from the regenerator is controlled by regulating the diluted solution inlet temperature, which is realized by adjusting the hot water flow rate entering the heater, as shown in Figure 4.1. *Method (d): Variable regeneration air flow rate.* The outlet solution concentration is controlled by modulating the regeneration air flow rate entering the regenerator, while the diluted solution inlet temperature in the regenerator is kept constant.

4.1.3 Effectiveness of Control Methods

The design parameters of the liquid desiccant system are listed in Table 4.1. In the proposed system, the design supply air humidity ratio ($w_{a,sup}$) is 6.0g/kg.da and the supply air temperature is 19°C. In this section, the effectiveness of the control methods in controlling the supply air humidity and the strong solution concentration after regeneration is analyzed.

Table 4.1 System design parameters

Items	Value
Ambient air temperature ($T_{a,amb}$)	31°C
Ambient air humidity ($w_{a,amb}$)	21.6g/kg
Volume flux of supply air in dehumidifier ($V_{a,sup}$)	0.8m ³ /s
Volume flux of solution in packed beds (V_s)	0.9 l/s
Volume flux of regeneration air ($V_{a,rgn}$)	1.6 m ³ /s
Outlet solution concentration from regenerator ($C_{s,out}$)	35%
Solution inlet temperature into dehumidifier ($T_{s,deh}$)	20.9°C
Solution inlet temperature into regenerator ($T_{s,rgn}$)	56.1°C
Supply air humidity ($w_{a,sup}$)	6.0g/kg

4.1.3.1 Control methods for air dehumidification process

The control performance of the proposed system with two different control methods applied is shown in Figure 4.2. As shown in Figure 4.2(a), the water condensation rate ($\Delta w_{a,sup}$) from the supply air decreases significantly with an increase in the strong solution inlet temperature ($T_{s,deh}$). The dehumidification capacity of the dehumidifier varies from 9.3g/kg.da to 4.1g/kg.da when the inlet temperature of the strong solution rises from 21°C to 35°C. Correspondingly, the supply air humidity ratio ($w_{a,sup}$) changes from 6.0g/kg.da to 11.2g/kg.da. The solution concentration variation ($\Delta C_{s,deh}$) varies

from 0.228% to 0.100% in the air dehumidification process, which is proportional to the water condensation rate from the supply air. The supply air humidity is sensitive to variation of the inlet solution temperature, and the supply air humidity ratio can be easily controlled by regulating the inlet solution temperature in the dehumidifier when the supply air latent load is altered. Hence, the variable strong solution inlet temperature method is effective in controlling the supply air humidity.

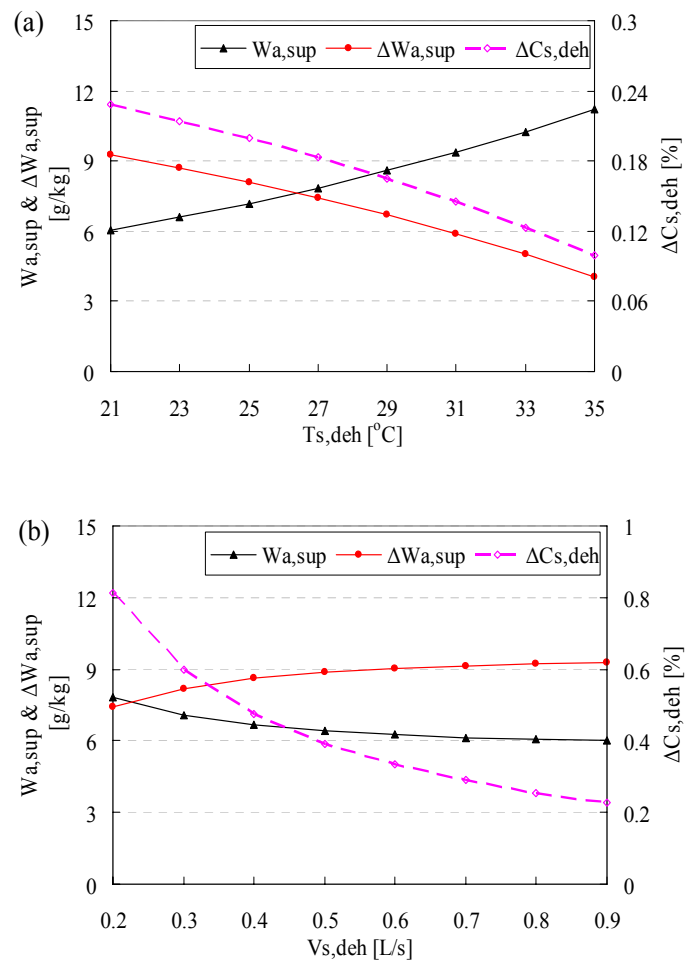


Figure 4.2 Control performance in the air dehumidification process: (a) variable strong solution inlet temperature method; (b) variable strong solution flow rate method

The control performance of the air dehumidification process is shown in Figure 4.2(b), when the variable strong solution flow rate method is implemented. The water condensation rate ($\Delta w_{a,sup}$) from the supply air varies from 7.4g/kg.da to 9.3g/kg.da when the strong solution flow rate changes from 0.2l/s to 0.9l/s. The dehumidification capacity of the dehumidifier is slightly increased with an increase of the strong solution flow rate ($V_{s,deh}$). Correspondingly, the supply air humidity ratio ($w_{a,sup}$) changes from 7.8g/kg.da to 6.0g/kg.da. The supply air humidity exhibits a small variation with a significant change in the desiccant solution flow rate. In addition, the inlet and outlet solution concentration difference of dehumidifier ($\Delta C_{s,deh}$) varies from 0.812% to 0.229% with an increase of the strong solution flow rate. This method is not beneficial in maintaining sufficient soaking of the absorber and enough partial pressure difference on the interface in the dehumidifier in part load conditions, since less desiccant solution is used. Hence, the variable strong solution flow rate method is not recommended for controlling the supply air humidity.

4.1.3.2 Control methods for solution regeneration process

Figure 4.3 shows the control performance in the solution regeneration process when different control methods are adopted. In this process, the dehumidification side is assumed to work on the design condition. As shown in Figure 4.3(a), the variation in the desiccant solution concentration before and after the regenerator (ΔC_s) decreases with a decrease in the inlet temperature of the diluted solution entering the regenerator ($T_{s,rgn}$). The vapor pressure of the desiccant solution is highly dependent on the temperature. The higher the temperature, the higher the vapor pressure and, consequently, the greater the

potential for water evaporation from the desiccant solution. The variation in the solution concentration decreases from 0.235% to 0.106% when the inlet temperature of the diluted solution decreases from 58°C to 40°C. Moreover, the variation range of the solution concentration in the solution regeneration process is comparable to that in the dehumidification process, as shown in Figure 4.2(a). Thus, the variable diluted solution inlet temperature method is effective in controlling the solution outlet concentration in the regeneration process.

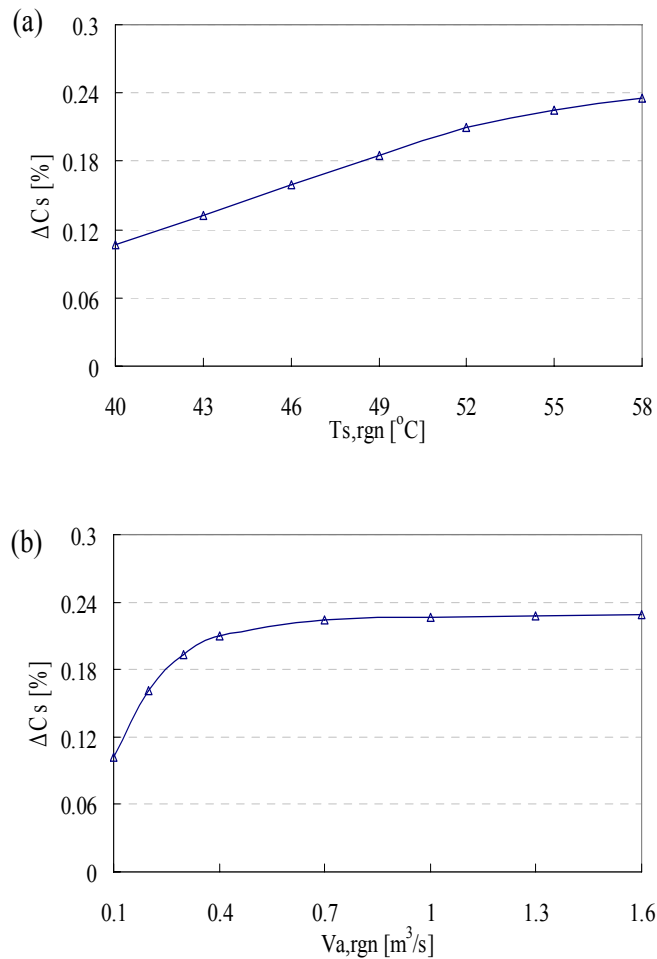


Figure 4.3 Control performance in the solution regeneration process: (a) variable diluted solution inlet temperature method; (b) variable regeneration air flow rate method

Figure 4.3(b) shows the control performance in the solution regeneration process when the variable regeneration air flow rate method is used. As illustrated in this figure, the variation in the desiccant solution concentration before and after the regenerator reduces with a decrease in the flow rate of the regeneration air entering the regenerator ($V_{a,rgn}$). The variation in the solution concentration decreases from 0.229% to 0.102% when the regeneration air flow rate changes from $1.6\text{m}^3/\text{s}$ to $0.1\text{m}^3/\text{s}$. The variation range of the solution concentration in the solution regeneration process is comparable to that in the dehumidification process, as shown in Figure 4.2(a). Thus, the variable regeneration air flow rate method is effective in controlling the strong solution concentration. However, it should be pointed out that the solution concentration variation ratio (slope) is larger in the lower regeneration air flow rate range, i.e., $0.1\sim 0.7\text{m}^3/\text{s}$, whereas the solution concentration variation remains almost fixed in the higher range, i.e., above $0.7\text{m}^3/\text{s}$.

According to the foregoing effectiveness analysis, the two following control strategies are suitable for the proposed system. *Control strategy 1*: the strong solution inlet temperature is regulated to control the supply air humidity, and the diluted solution inlet temperature is modulated to control the solution concentration after regeneration. *Control strategy 2*: the strong solution inlet temperature is regulated to control the supply air humidity, and the regeneration air flow rate is modulated to control the solution concentration after regeneration.

4.2 Control Performance of the Liquid Desiccant System

This section discusses the influences of system parameters such as the desiccant solution concentration, solution flow rate, regeneration air flow rate, supply air flow rate, ambient air temperature, and humidity. The steady-state control performance of the proposed system under different conditions is analyzed with the two control strategies implemented. Only one parameter is changed in each test, with the other parameters kept fixed.

The performance of the proposed system can be evaluated with two performance indexes, i.e., the electric coefficient of performance (ECOP) and the coefficient of performance for the whole system (COP). They are calculated by Equations (4.1) and (4.2), respectively (Dai 2001).

$$ECOP = \frac{Q_C}{E} \quad (4.1)$$

$$COP = \frac{Q_C}{Q_T + E/0.3} \quad (4.2)$$

where Q_C is the cooling production of the system and Q_T is its thermal energy consumption, that is, the heat input required to re-concentrate the diluted liquid desiccant. E is the total electric power consumption of the fans and the chilling system for the chilled water supply to the cooler and cooling coil. The overall performance coefficient of the chilling system is assumed to be 3.5 as a constant when calculating the

electricity use (Capozzoli 2006). In addition, the equivalent coefficient of electric power and thermal energy in Hong Kong is taken as 0.3.

Figure 4.4~4.6 illustrate the effects of the strong solution concentration, solution flow rate, and ambient air temperature on the system's ECOP and COP, respectively. It can be seen that the ECOP and COP values of the liquid desiccant system are almost the same in both control strategies. The main reason for the similarity is that the latent heat load of the supply air undergoes no change when the system parameters change and the current latent load of this air equals the design latent load.

As shown in Figure 4.4, the COP decreases slightly with an increase in the strong solution concentration, primarily because the regeneration heat required is slightly higher at a higher solution concentration. The impact of solution concentration on system performance is negligible in the tested range. However, it should be noted that it is difficult to measure the solution concentration continuously and accurately in practical applications. Hence, it is acceptable to allow a proper range for the outlet solution concentration variation in the regeneration process.

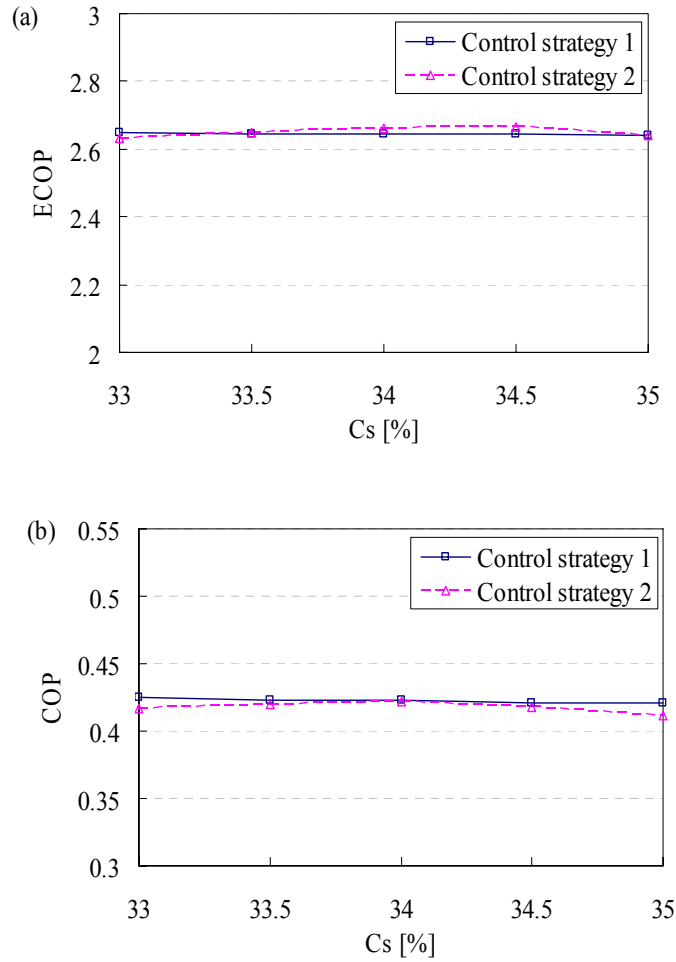


Figure 4.4 Effect of strong solution concentration on ECOP and COP

Figure 4.5 shows the effect of the solution flow rate on system performance. The system's ECOP and COP decrease markedly as the desiccant solution flow rate increases. The explanation for this decrease is that greater desiccant solution flux provides little benefit to the dehumidification capacity of the system, although the regeneration heat consumption demanded by the heater and the cooling requirement of the cooler increase greatly with an increase in the solution flow rate. Hence, in practice, the desiccant solution flow rate for dehumidification applications is expected to be as low as possible, and a certain minimum flow rate must be ensured for normal operation.

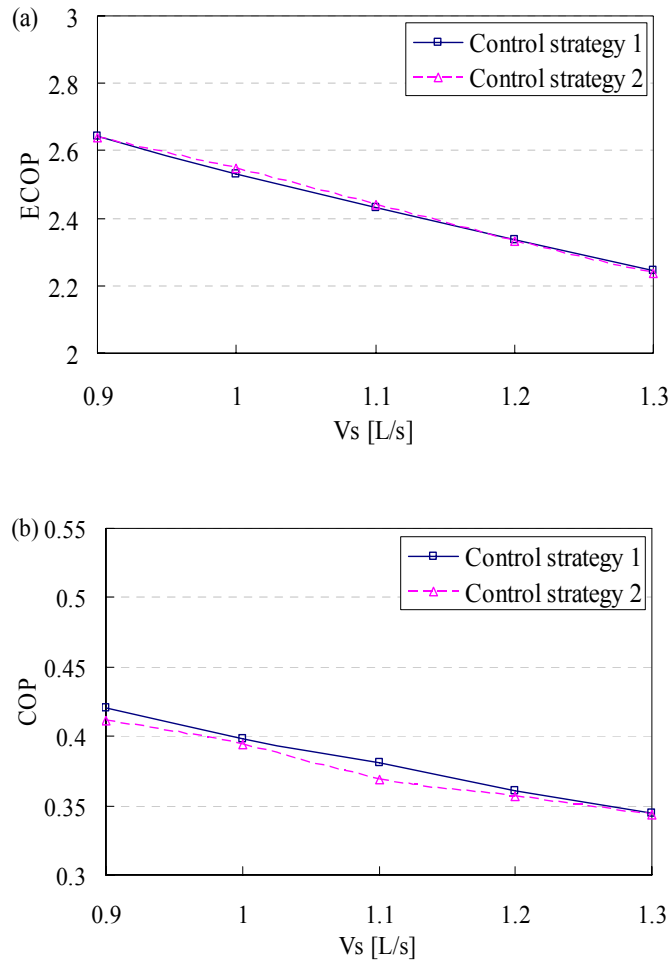


Figure 4.5 Effect of solution flow rate on ECOP and COP

In practical applications, the ambient air state changes with time. Figure 4.6 illustrates the effect of the ambient air temperature on system performance. It can be seen that the system's ECOP and COP increase with a rise in the ambient air temperature. This is because the cooling production of the proposed system increases significantly with an increase in the ambient air temperature, whereas the increase in total energy consumption in the dehumidification and regeneration processes is less. It can thus be concluded that the proposed system is more suitable for hot climates.

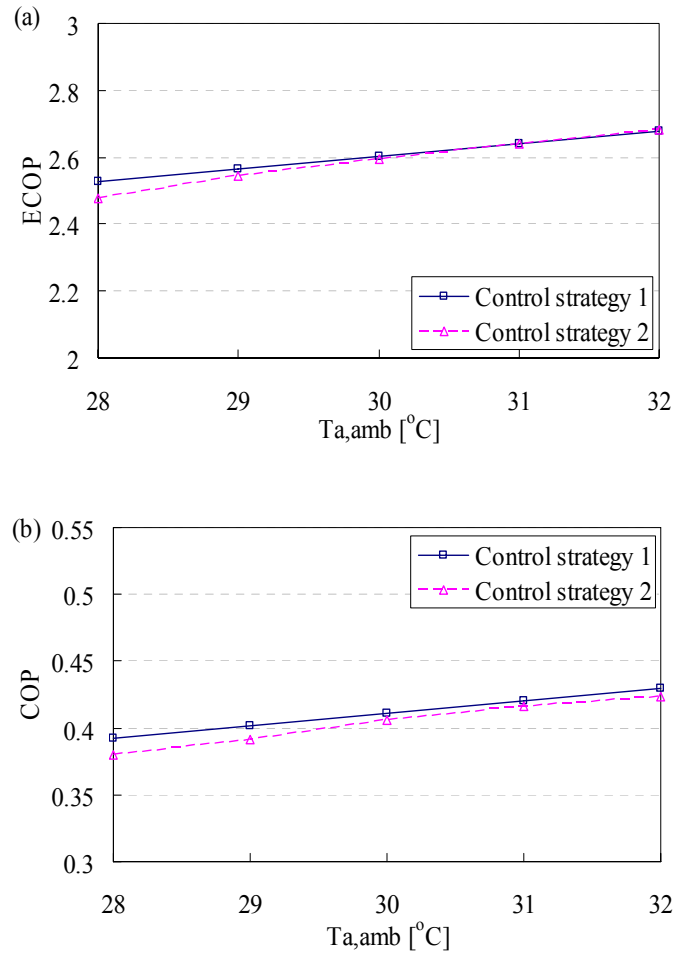


Figure 4.6 Effect of ambient air temperature on ECOP and COP

Figures 4.7~4.9 illustrate the effects of ambient air humidity, supply air flow rate, and supply air humidity on system performance, respectively. As shown in Figure 4.7, the system's ECOP and COP decrease as the outdoor air humidity ratio decreases, which indicates that the proposed system is more suitable for humid regions.

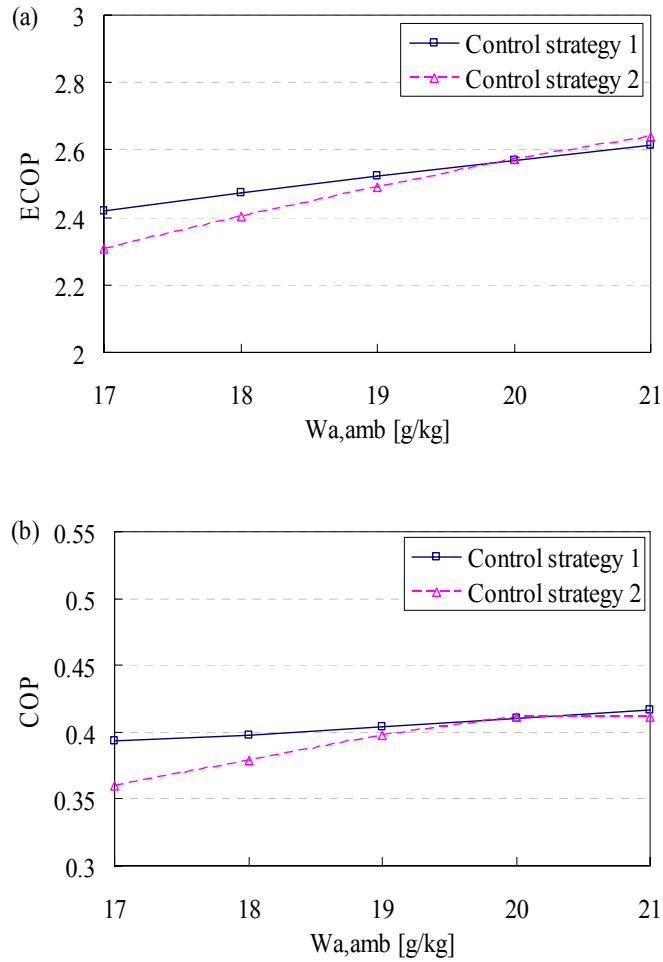


Figure 4.7 Effect of ambient air humidity ratio on ECOP and COP

Figure 4.8 illustrates the supply air flow rate's effect on system performance. With a decrease in this rate, the system's ECOP and COP both decrease dramatically. The explanation is that the cooling production reduces rapidly and the total energy consumption of the system reduces slowly when the supply air flux decreases. Hence, the proposed liquid desiccant system is appropriate for high supply air flow rate cases.

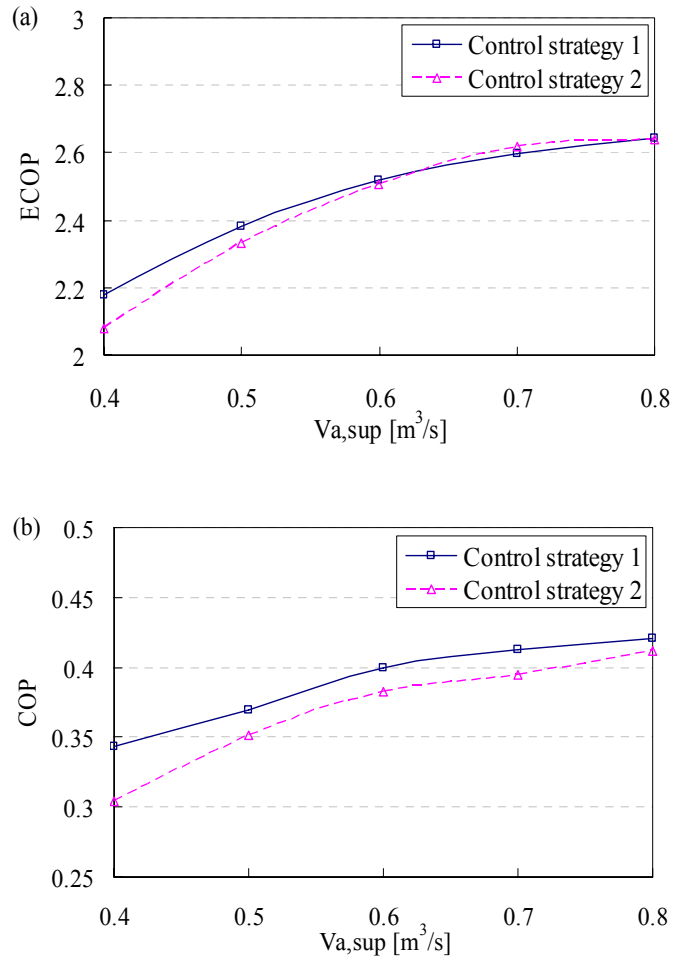


Figure 4.8 Effect of supply air flow rate on ECOP and COP

Figure 4.9 shows the effects of different supply air humidity ratios on system performance. It can be seen that the system's ECOP and COP rise as the supply air humidity increases. The reason for this ascent is that the cooling production of the proposed system decreases slightly with an increase in the supply air humidity ratio, and there is a significant reduction in total energy consumption in the dehumidification and regeneration processes.

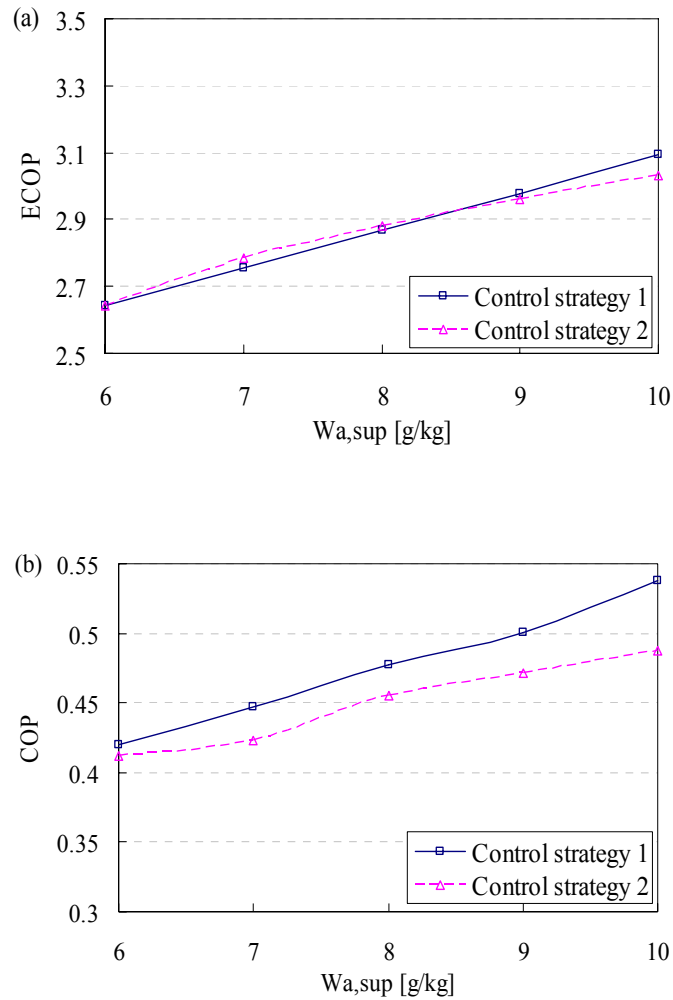


Figure 4.9 Effect of supply air humidity ratio on ECOP and COP

As shown in Figures 4.7~4.9, the system's ECOP and COP are a little higher when control strategy 1 is adopted instead of control strategy 2. One reason for the higher values is that in part load conditions, in which the actual supply air latent load is lower than the design latent load, the regeneration air flow rate in control strategy 2 is lower than that in control strategy 1, i.e., $1.6\text{m}^3/\text{s}$. The effect of the regeneration air flow rate on the system's performance is shown in Figure 4.10. As this rate decreases, the system's COP reduces accordingly. Another reason is that in part load conditions, the diluted solution inlet temperature in the regenerator in control strategy 1 is lower than

the fixed diluted solution inlet temperature in control strategy 2, i.e., 56.1°C. The effect of the regeneration solution inlet temperature on system performance is shown in Figure 4.11. As this temperature decreases, the system's COP increases slightly.

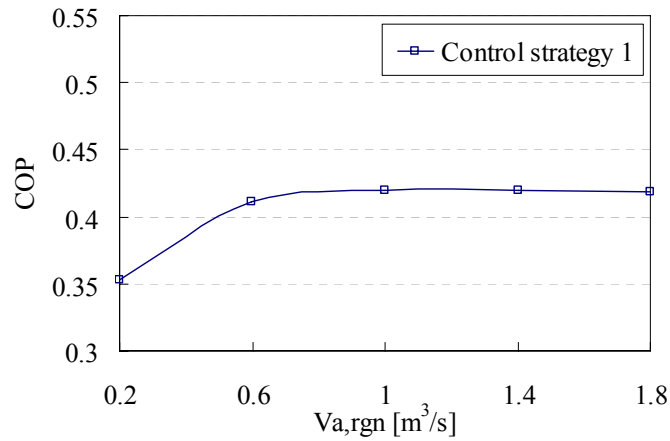


Figure 4.10 Effect of regeneration air volume on COP

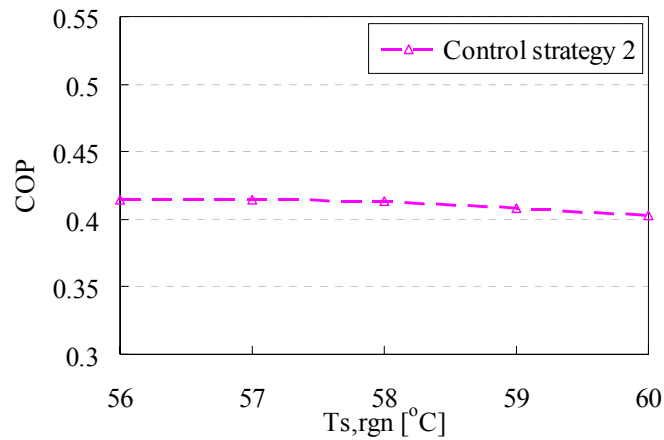


Figure 4.11 Effect of regeneration solution inlet temperature on COP

A simulation exercise is conducted to test the energy performance of the proposed liquid desiccant system on a summer day using the two control strategies. The outdoor air dry bulb temperature and humidity on the test day is shown in Figure 3.8. The

operation period of the proposed system is from 9:00 to 18:00. The supply air humidity ratio is controlled at 7.1g/kg.da, and the supply air temperature is 19°C in the operation period.

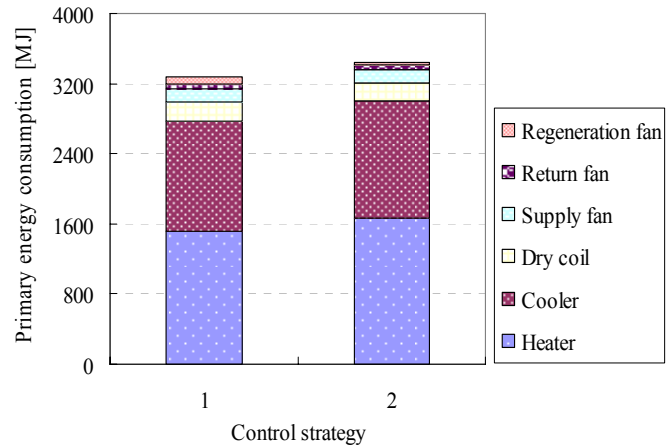


Figure 4.12 Energy consumption of the proposed system using different control strategies

Figure 4.12 presents a comparison of the proposed system's energy consumption when the two control strategies are employed on the summer day. It can be seen that control strategy 2 consumes about 3.3% more energy than control strategy 1. In addition, this figure also illustrates the dominance of the energy consumption of the air dehumidification and solution regeneration processes, which account for about 85% of the total such consumption. When control strategy 1 is applied in the liquid desiccant system, 47.1% of the total energy is consumed by the heater in the diluted solution re-concentration process, and 37.9% is consumed by the cooler in cooling the strong desiccant solution in the dehumidifier. In addition, the dry cooling coil accounts for about 6.3% of the total energy consumption in cooling down the supply air after dehumidification. It is very interesting to find that the performance of the proposed

liquid desiccant system can be enhanced with the adoption of energy conservation technologies. When evaporation cooling techniques are utilized to provide the necessary cooling water for the cooler and the cooling coil, and free solar energy or waste heat is available for desiccant solution regeneration, the energy efficiency of this system can be dramatically improved.

4.3 Outdoor Air Ventilation Strategy in Liquid Desiccant Based Air-Conditioning Systems

Outdoor air ventilation flow rate is a crucial variable for air-conditioning systems, which significantly influence indoor air quality and energy consumption of air-conditioning systems. In conventional air-conditioning systems, minimum outdoor air flow rate is usually provided and supplied into the conditioned space in order to save energy and ensure acceptable indoor air quality, according to the ventilation code (ASHRAE Standard 62.1). The liquid desiccant dehumidification is an effective alternative way to remove the latent load of air, and it can reduce the energy consumption of system. Considering the energy savings potential and its characteristics of liquid desiccant dehumidification, more outdoor air flow rate can be taken in the liquid desiccant based air-conditioning systems to improve the indoor air quality and maintain lower energy consumption.

In this section, a liquid desiccant based air-conditioning system, as shown in Figure 3.2(b), operating under typical climate conditions in Hong Kong is studied. Outdoor air is mixed with return air before processed. The performance of the system under different

fresh air ratios is simulated. The energy saving potential compared with a typical conventional air-conditioning system with primary return air is evaluated.

The air handling processes of the liquid desiccant based air-conditioning system and the conventional system are shown on a psychrometric chart in Figure 4.13. Points O, R, C and S are the state points of outdoor air, return air, mixed air and supply air, respectively.

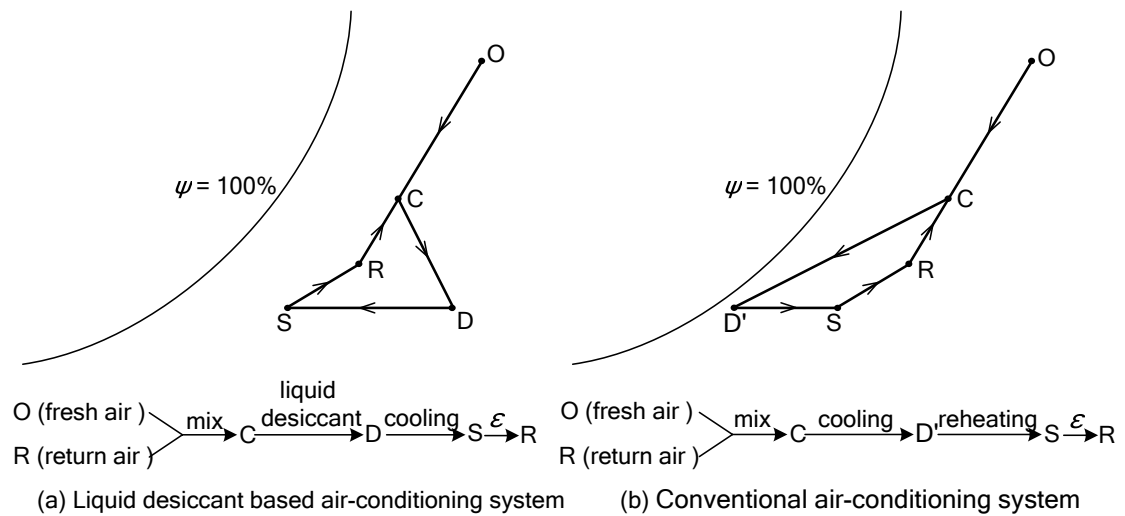


Figure 4.13 Air handling processes of the two systems

Figure 4.13(a) shows the air handling process of the liquid desiccant based air-conditioning system. The outdoor air (O) is mixed with part of the return air (R). The moisture in the mixed air (C) is removed by the desiccant solution in the dehumidifier so that the humidity ratio of the air after dehumidification is identical to that of the supply air. Then, the dry air after dehumidification (D) is cooled to the supply air state (S). Here, the coolant is only responsible for sensible load removal and its temperature is thus higher than the air dew point temperature. Finally, the dry and cool air is delivered into the indoor space.

Figure 4.13(b) shows the common air-handling process of a conventional air-conditioning system with primary return air. Firstly, the mixed fresh and return air is cooled to the apparatus dew point (D'). As the cooling process must remove the latent and sensible loads simultaneously, the cooling temperature should be lower than that of the air dew point. Then, in consideration of occupant comfort, the air is reheated to the supply state (S) and delivered to the indoor space.

4.3.1 Test Condition

A case study is conducted to compare the performance and power consumption of the liquid desiccant based system and a conventional system with primary return air in an educational building in Hong Kong. The comparisons are made under different fresh air ratios (R_f), increasing from 20% to 100% gradually at intervals of 10% in simulation tests. The outdoor weather conditions with the highest humidity in a typical meteorological year are adopted for the simulation study. The dry bulb temperature (T_O) is 29.6°C, the relative humidity (RH_O) is 94.9%, and the corresponding humidity ratio (ω_O) is 25.45g/kg. The indoor air design conditions are as follows. The dry bulb temperature (T_R) is 23°C and the relative humidity (RH_R) is 55%. The set point of the supply air temperature (T_S) is 18 °C. The area of the simulated indoor air-conditioning space in the educational building is 100m², and the occupant density is assumed to be 1 person/m². According to the empirical data of load estimation in Hong Kong, the heat excess of the indoor space is assumed to be 20kW. The supply air mass flow rate is 1.98kg/s.

In the liquid desiccant system, variable strong solution flow rate method is used to control the supply air humidity, and variable regeneration air flow rate method is used to control the outlet concentration of regeneration solution. The strong solution entering the dehumidifier has a temperature of 28°C and a mass concentration of 36%. The temperature of the diluted solution at the inlet of the regenerator is set as 60°C, and the mass concentration at the inlet of the regenerator is determined by the outlet states of the dehumidifier. The concentrated solution is cooled by cooling water from the cooling tower before entering the dehumidifier. The cooling energy consumption for solution cooling is hence ignored in the study.

4.3.2 Results Analysis

In simulation tests, the outdoor fresh air (O), the return air (R) and the supply air (S) in both systems, as well as the state of apparatus dew point (D') in the conventional system, are fixed under different fresh air ratios. The values of the aforementioned state points are listed in Table 4.2.

Table 4.2 States of several points of the air handling process

Point	Description	Dry bulb temperature $T(^{\circ}\text{C})$	Relative humidity $RH(\%)$	Humidity ratio $\omega(\text{g/kg})$	Specific enthalpy $h(\text{kJ/kg})$
O	fresh air	29.60	94.90	25.15	94.02
R	return air	23.00	55.00	9.64	47.64
S	supply air	18.00	59.80	7.67	37.54
D'	apparatus dew point	10.87	95.00	7.67	30.30

The states of the mixed air (C) are firstly determined, as listed in Table 4.3. As the states of the air to be handled are different, the corresponding latent loads and sensible loads in air handling process are also various. Figure 4.14 indicates that, both the sensible load and the latent load increase with the increase of the fresh air ratio. However, the trends of the increments of both loads are not the same. The increment of the latent load is much sharper than that of the sensible load. The latent load accounts for 67.3% of the total load when the fresh air ratio is 20%, but when that ratio is 100%, the latent load only accounts for 79.5% of the total load. In the liquid desiccant based system, the latent load is removed by the desiccant solution rather than by compression refrigeration cooling.

Table 4.3 States of the mixed air with different fresh air ratios

Point	Fresh air ratio $R_f(\%)$	Dry bulb temperature $T(^{\circ}\text{C})$	Relative humidity $RH(\%)$	Humidity ratio $\omega(\text{g/kg})$	Specific enthalpy $h(\text{kJ/kg})$
C	20	24.32	66.85	12.74	56.90
	30	24.98	71.91	14.29	61.52
	40	25.64	76.46	15.85	66.16
	50	26.30	80.53	17.40	70.79
	60	26.96	84.16	18.95	75.43
	70	27.62	87.38	20.50	80.07
	80	28.28	90.23	22.05	84.72
	90	28.94	92.72	23.60	89.36
	100	29.60	94.90	25.15	94.02

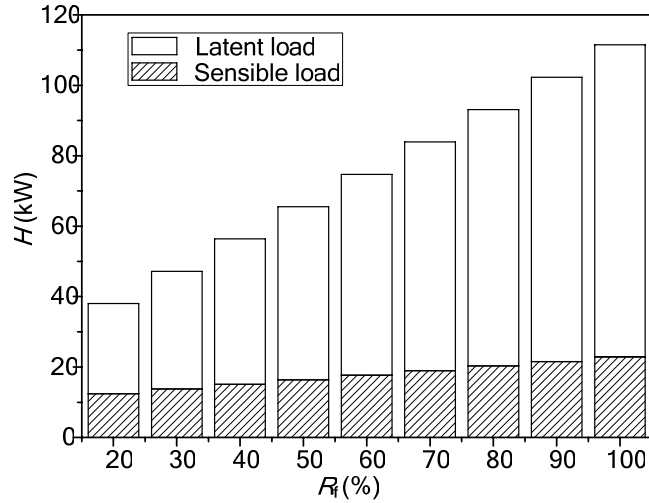


Figure 4.14 Latent load and sensible load distribution under different fresh air ratios

When the fresh air ratio increases, more desiccant solution is needed in the dehumidification process to maintain the outlet humidity ratio of the air. As shown in Figure 4.15, there are sharp increases in the desiccant solution mass flow rate when the fresh air ratio increases. In addition, the larger the fresh air ratio is, the greater is the increment in the solution flow rate. When total fresh air ($R_f=100\%$) is used in the system, the solution mass flow rate rises to 8 times that of the system adopting a fresh air ratio of 20%, which indicates that a greater amount of heat energy should be input into the solution for its regeneration.

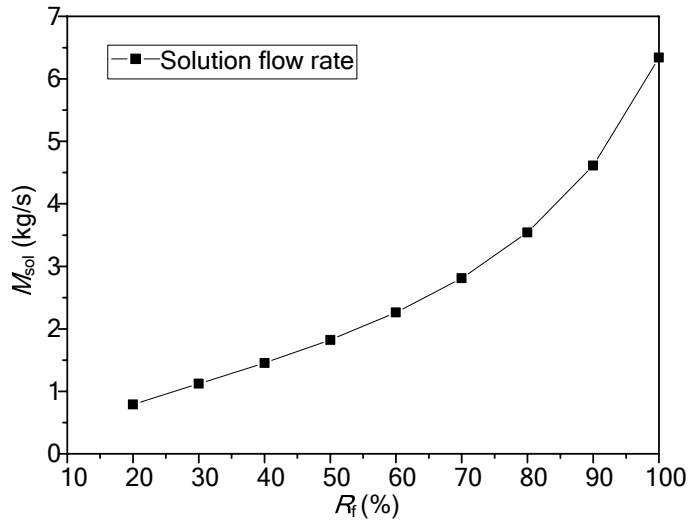


Figure 4.15 Desiccant solution mass flow rate under different fresh ratios

Figure 4.16 shows that, the heating requirement for the regeneration of the diluted solution increases considerably with the increase of fresh air, which accounts for a great percentage of the total energy consumption of the system. The heat energy consumed when R_f is 100% is 5 times that of the system with a fresh air ratio of 20%.

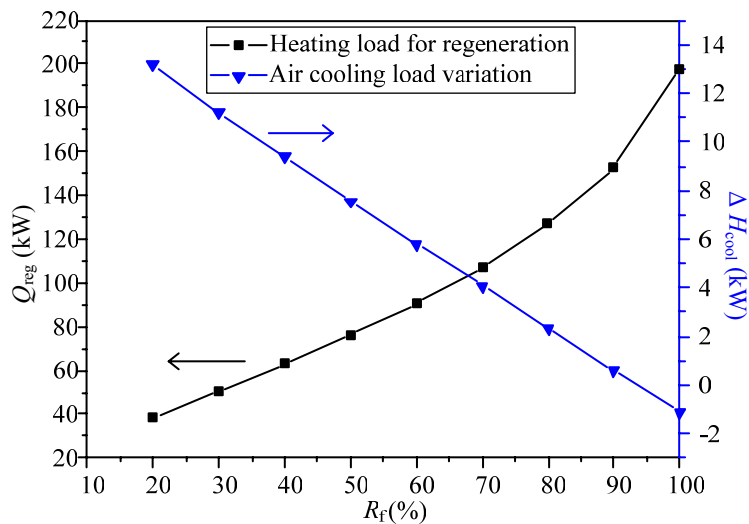


Figure 4.16 Heating load for solution regeneration and air cooling load variations under different fresh air ratios

The states of the mixed air after dehumidification by the desiccant solution (point D) under various fresh air ratios are listed in Table 4.4. The temperatures and specific enthalpies of the mixed air after moisture removal vary slightly with the increase in the fresh air ratio. Consequently, the difference in the amount of energy consumed in cooling the dry air to the supply air state is small under all fresh ratios. However, comparing the temperatures in Table 4.4 with the states of the mixed air (point C), the temperature differences before and after dehumidification are very different under the different fresh air ratios. The mixed air with an R_f of 20% has the largest temperature rise after dehumidification, and the value of the temperature rise drops with the increase in the fresh air ratio. The temperature of the air with an R_f of 100% even decreased after the desiccant solution removed the latent load.

Table 4.4 States of the air after dehumidification by liquid desiccant

Point	Fresh air ratio R_f (%)	Dry bulb temperature $T(^{\circ}\text{C})$	Relative humidity $RH(\%)$	Humidity ratio $\omega(\text{g/kg})$	Specific enthalpy $h(\text{kJ/kg})$
D	20	30.93	27.60	7.67	49.76
	30	30.60	28.11	7.67	49.43
	40	30.34	28.54	7.67	49.17
	50	30.09	28.94	7.67	48.92
	60	29.87	29.31	7.67	48.70
	70	29.66	29.67	7.67	48.49
	80	29.45	30.03	7.67	48.28
	90	29.25	30.39	7.67	48.08
	100	29.04	30.74	7.67	47.87

The abovementioned temperature variations in the dehumidification process result in the variations of the air cooling load, which is also shown in Figure 4.16. The positive value in the figure represents the increase in the air cooling load, and the negative value

represents the decrease in the air cooling load. The largest increase in the air cooling load appears at the fresh air ratio of 20%, and the load increment drops gradually when the fresh air ratio increases. Finally, the air cooling load variation turns negative: that is, it decreases when the fresh air ratio is 100%. This is caused by the following factors. Firstly, the temperatures of all of the mixed air point except for the points with the fresh air ratio of 100% before dehumidification are lower than the temperature of the desiccant solution, which causes the heat to transfer from the solution to the air handled. With the increase in the fresh air ratio, the temperature difference between air and solution gradually becomes smaller and smaller, and the temperature of the air with the fresh air ratio of 100% is even higher than that of the solution. Thus, the air can be cooled by solution. Secondly, as heat is released in the dehumidification process, the temperature of the air and the solution increase in this process. However, the flow rate of the desiccant solution also increases with the increase in the fresh air ratio, which reduces the temperature rise in the air. Both factors cause the variation in the air cooling load shown in Figure 4.16, which also indicates that the desiccant solution with lower temperature is beneficial to the sensible load reduction and corresponding energy consumption in load removal.

Figure 4.17 shows the variations of the COP of the liquid desiccant based air-conditioning system under different fresh air ratios. The trend of variation can be divided into three sections. In the first section, as the fresh air ratio increases from 20% to 40%, the COP grows slightly from 0.94 to 0.97, which means that the increase in the heating load of solution regeneration is lower than that of the air enthalpy difference between the mixed-air state and the supply-air state. In the second section, as the fresh

air ratio increases from 40% to 60%, the COP drops gradually from 0.97 to 0.93. In the third section, the COP decreases rapidly from 0.93 to 0.72 when the fresh air ratio increases from 60% to 100%, which indicates that the increase in the energy consumed in solution regeneration becomes much more prominent.

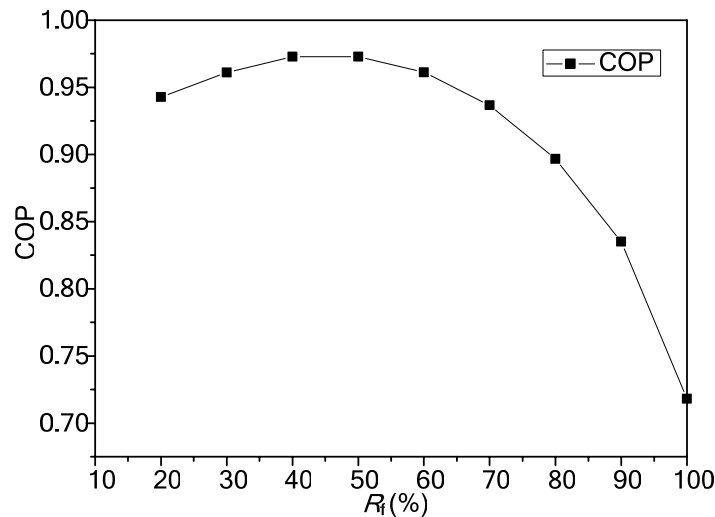


Figure 4.17 COP of the liquid desiccant based system under different fresh air ratios

The performance of the liquid desiccant based system studied in this section is a little different from that presented in the previous sections. Since the total heat recovery is not applied in this study and the control strategies adopted are different. The system configuration and control strategies affect the characteristics of air-conditioning systems.

Figure 4.18 shows the comparison of the total power consumption between the liquid desiccant-based air-conditioning system and the conventional air-conditioning system with primary return air. Firstly, it can be seen that the power consumption in the both systems increases with the increase in the fresh air ratio. However, the increase in the liquid desiccant based system is sharper than that of the conventional system because more power is needed to provide heating driving regeneration, as mentioned previously.

For the conventional system, when the fresh air ratio increases, both the temperature and humidity of the mixed air increases, and consequently more power is needed in the air cooling and moisture removal. Secondly, the figure shows clearly that power can be saved if liquid desiccant is applied in air handling process. The maximum power saving ratio is up to 58.9% when the fresh air ratio is 20%. The power saving ratio drops with the increase in fresh air volume, which is mainly attributable to the increase in power consumption of solution regeneration. The power saving ratio reaches a minimum of 4.6% when the fresh air ratio is 100%. The heat resource used in this study is provided by a vapor compression heat pump. If the solution could be heated by a low grade heat resource not driven by electricity, such as solar energy, industrial waste heat, etc., then the power would be consumed only by the air cooling and the transportation of solution and cooling water. The total power saving then would be much more considerable.

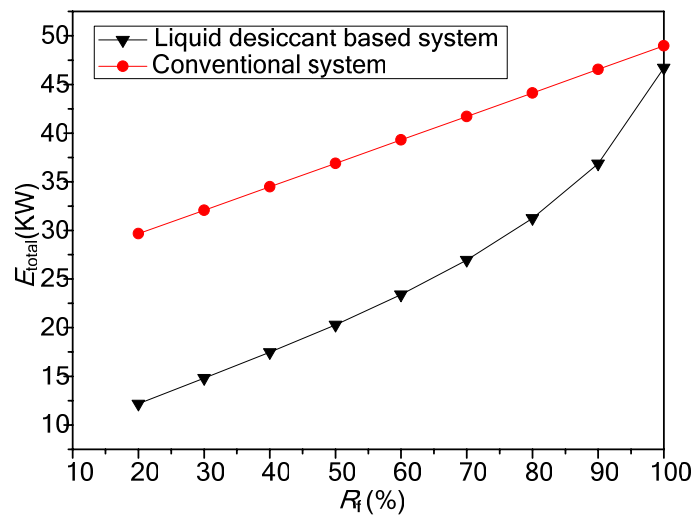


Figure 4.18 Total power consumption of the two systems compared

According to ASHARE standards 62.1-2007, the typical recommended fresh air volume of the educational building in this study is 4.0L/s per person; the corresponding

fresh air ratio is about 23%. Based on the power consumption comparison shown in Figure 4.18, even when fresh air accounts for nearly 75% of the air in the liquid desiccant based air-conditioning system, the power consumption is still lower than that of the conventional system adopting the typical recommended fresh air ratio of 23%. When the fresh air ratio increases from 23% to 50%, the power consumed in the liquid desiccant based system only increases by 7.1kW. In addition, as shown in Figure 4.17, the highest COP of the liquid desiccant based system appears when the fresh air ratio is in the range of 40% to 50%. This range is recommended in practice because, on one hand, the IAQ is expected to improve greatly as the fresh air volume is increased, and on the other hand, the power consumption does not increased very much.

4.4 Summary

This chapter proposes a hybrid liquid desiccant air-conditioning system and develops control methods for the supply air dehumidification and desiccant solution regeneration processes. The effectiveness of these control methods is analyzed, and the control performance of the proposed system is investigated under different operation conditions.

In the air dehumidification process, the variable strong solution inlet temperature control method is found to be effective. The dehumidification capacity of the liquid desiccant system is more sensitive to variation in the solution inlet temperature. In the desiccant solution regeneration process, the performance of the variable diluted solution inlet temperature method is found to be better than that of the variable regeneration air flow rate method under part latent load conditions. Simulation tests demonstrate that it

consumes about 3.3% less energy on a summer day. The simulation results also show that the proposed liquid desiccant system is more suitable for hot and humid climates, a higher supply air flow rate, and higher supply air humidity ratio conditions. In addition, a lower solution flow rate and a higher regeneration air flow rate are preferable in this hybrid system for improving its energy performance.

Liquid desiccant dehumidification is an energy efficient method to remove the latent load of process air compared with conventional cooling dehumidification manner. When the liquid desiccant dehumidification is used in practical applications, more outdoor air flow rate can be considered in the liquid desiccant based air-conditioning systems to improve the indoor air quality and maintain lower energy consumption. The optimal outdoor air ventilation flow rate can be determined by the practical air-conditioning system characteristics (which may be affected by the system configuration and control strategies) and operation conditions.

CHAPTER 5 INDEPENDENT TEMPERATURE AND HUMIDITY CONTROL IN MULTI-ZONE DEDICATED OUTDOOR AIR SYSTEMS

This chapter mainly presents the control and optimization strategies for independent temperature and humidity control in the multi-zone dedicated outdoor air systems. The performance of these strategies is also investigated. Section 5.1 briefly reviews the independent temperature and humidity control system. Section 5.2 presents various control methods, including supply air humidity reset and demand controlled ventilation strategy, for the system studied. Section 5.3 presents the control performance of these control strategies and their energy performance.

5.1 Brief of Independent Temperature and Humidity Control System

Many commercial buildings, such as offices, schools, restaurants, theaters, etc., suffer from humidity-related problems that cannot be resolved with conventional air conditioning systems because they are not effective at controlling humidity. The temperature and humidity independent control system is a kind of new air-conditioning system, which controls the temperature and humidity independently with different equipments, while the conventional air-conditioning system disposes the latent load and sensible load together only using conventional mechanical cooling manner. Compared to conventional air-conditioning systems, the independent temperature and humidity

control system can not only reduce risks or liabilities such as mold, bacteria, and material damage but also can create a more comfortable, odor-free environment while saving energy associated with ventilation and overcooling. The investigation and application of independent temperature and humidity control air-conditioning system have been extended rapidly, contribution to high attention on the energy saving.

Spears and Judge (1997) conducted a two months test of energy consumption of an independent temperature and humidity control system with desiccant system and a conventional air-conditioning system in two supermarkets where the independent temperature and humidity control system saved 13% energy consumption. Niu et al. (2002) proposed a 100% outdoor air displacement ventilation system consisting of a desiccant cooling system combined with a chilled ceiling. The results showed that the proposed integrated system could save up to 44% of primary energy consumption in comparison with a conventional constant air volume system. Jeong et al. (2003) reported a DOAS-radiant panel cooling system for a studio in a university. They indicated that the annual energy consumption of the novel system was 42% less than that of a conventional variable air volume system with air-side economizer. Sekhar (2004) introduced a single-coil twin-fan air conditioning system which involved the independent control of temperature and humidity and had a potential to save energy up to 12%. Liu (2008) adopted the empirical average COP to analysis the energy performance difference between independent control and conventional air conditioning systems, and pointed out that the independent control system can save 20%~30% compared to the conventional system.

In previous studies, separate controls of indoor temperature and humidity as well as performance analysis of air-conditioning systems were investigated with the focus on single-zone applications, while less attention had been paid to applications in multi-zone spaces. In addition, open literature rarely considered the optimization control of the independent temperature and humidity control system.

5.2 Control Strategies of the Dedicated Outdoor Air System

The dedicated outdoor air system is a typical independent temperature and humidity control system. In the DOAS-integrated system, indoor air temperature is controlled by a parallel system, such as the chilled ceiling subsystem, while the DOAS is responsible for the indoor air humidity control and provides required outdoor air flow rate to meet the ventilation requirement. In previous research, constant ventilation flow rate (Niu et al. 2002) and constant supply air humidity, i.e. 7.15g/(kg dry air) (Mumma and Jeong 2005) were usually adopted in DOAS. Actually, the ventilation flow rate and the supply air humidity ratio of DOAS are two crucial variables for DOAS-integrated systems, which significantly influence indoor thermal comfort, indoor air quality and energy consumption of the integrated system and can be optimized. In the present study, a liquid desiccant based dedicated outdoor air-chilled ceiling system is proposed for serving a multi-zone space. Two optimization control strategies are proposed to optimize the aforementioned two variables and improve the system performance. To evaluate the performances of these two strategies, a basic control method, i.e. the method adopting constant ventilation flow rate and constant supply air humidity ratio, is selected as the benchmark. A description of these strategies is given in this section.

5.2.1 Basic Strategy

The basic strategy maintains the temperature in each conditioned zone at its set point by regulating the chilled water flow rate through chilled ceiling, while allows indoor RH freely float, which is similar to controls in conventional air conditioning systems. In the basic method, the ventilation flow rate of each zone and the supply air humidity ratio in the DOAS subsystem are constant. The ventilation rate of each zone is determined by the designed occupants' number. According to the ASHRAE Standard 62.1-2007, the ventilation rate of fresh air for occupied space shall be determined as follows:

$$DVR = R_p P + R_B A \quad (5.1)$$

where R_p and R_B are the outdoor air requirements per person and per unit area, respectively. A is the occupied area and P is the number of occupants.

In simulation tests, it is found that the CO_2 concentration in the office room is much higher than the prescribed level (i.e. about 700ppm above the fresh air CO_2 concentration) when the latest standard (ASHRAE 2007) is used. Therefore, in this study, the following rule is used to calculate the fresh air requirement of each zone. The fresh air requirement is computed according to the number of occupants, i.e. 10 l/s per person for the office rooms and the meeting room (ASHRAE 2001) while the minimum fresh air requirement is taken according to the air-conditioning area, i.e. 0.3 l/s per square meter for these rooms (ASHRAE 2007). This rule considers the minimum fresh air rate for occupant-generated pollutants and the minimum fresh air rate for diluting

non-occupant-generated pollutants simultaneously. The supply air humidity ratio of the DOAS is fixed and equals to the design value, i.e. 9.3g/(kg dry air) in this study. This strategy is used as a reference in the comparison with the strategies reported as follows.

5.2.2 Supply Air Humidity Ratio Set-point Reset

In this control strategy, the ventilation flow rate is fixed and identical to the flow rate in basic control strategy, but the supply air humidity ratio set-point in the DOAS is varying with the instant latent load of conditioned zones.

An online supply air humidity ratio set point reset strategy is developed and the control logic is shown in Figure 5.1. Different from the temperature control, which aims at maintaining the indoor temperature at a fixed set point, i.e. 25°C in this study, the indoor air relative humidity of each zone is expected to be controlled in the range of 30% to 60%RH (Kittler 1996), and the maximum RH of all zones is expected to be always close but not exceeding 60%RH to save energy consumed by air dehumidification. The set point of the humidity ratio is determined according to the relative humidity measurements of all zones. The maximum and minimum values of relative humidity in all zones are monitored. When the maximum RH of the five zones (RH_{max}) is larger than 58%, the supply air humidity ratio set point (ω_{sp}) will be decreased, while the minimum RH (RH_{min}) is less than 32%, the humidity set point will be increased. If the relative humidity of all zones is well controlled in the range of 30%-60%, the set point will not be changed.

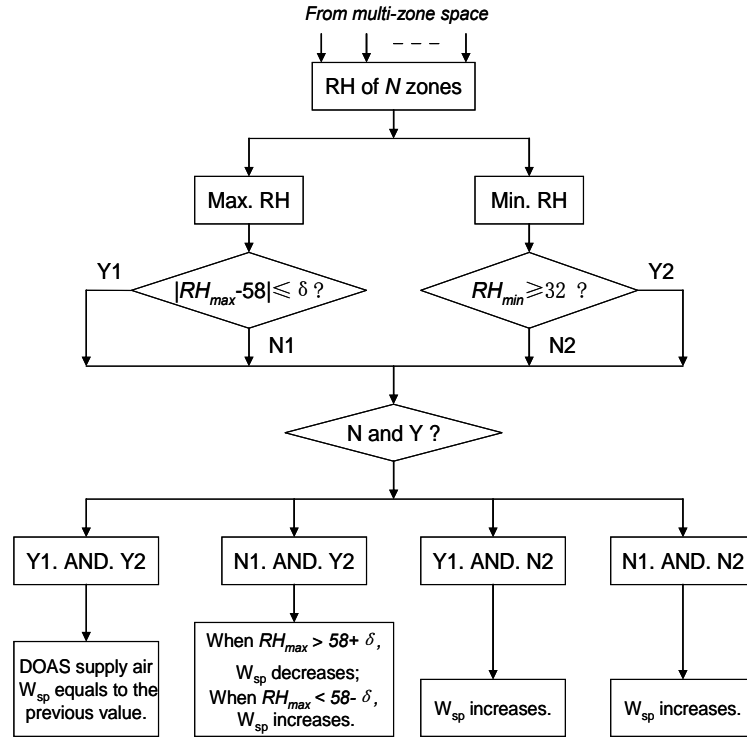


Figure 5.1 Flowchart of supply air humidity ratio set point reset strategy

5.2.3 Demand-controlled Ventilation Based Supply Air Humidity Reset

In this combined control strategy, the ventilation flow rate is variable, which is determined by detected actual occupant number based on demand-controlled ventilation strategy (Xu 2009, Wang 1998). An online dynamic strategy, as presented by Equation (5.2), is adopted to detect the actual number of occupants in this study and the ventilation rate of each zone is computed by detected real-time occupants' number in the space as shown in Equation (5.1).

$$P_{zone,i}^k = \frac{E_{ac}(V_{s,zone,i}^k + V_{s,zone,i}^{k-1})(C_{zone,i}^k - C_s^k)}{2S} + V_{zone,i} \frac{C_{zone,i}^k - C_{zone,i}^{k-1}}{\Delta t} \quad (5.2)$$

where C_s is the CO₂ concentration of the supply air, V is the air volume in the conditioned space/zone, P is the number of occupants, and S is the average CO₂ generation rate of an occupant, $zone,i$ indicates the i -th zone. E_{ac} is the air change effectiveness.

The supply air humidity ratio set-point in the DOAS in this strategy is variable and determined by the strategy as illustrated in Figure 5.1.

5.3 Performance of Various Control Strategies

In this section, performance of the DOAS-CC system in a summer day is investigated. The outdoor air dry bulb temperature and the humidity profiles on the testing day have been shown in Figure 3.8.

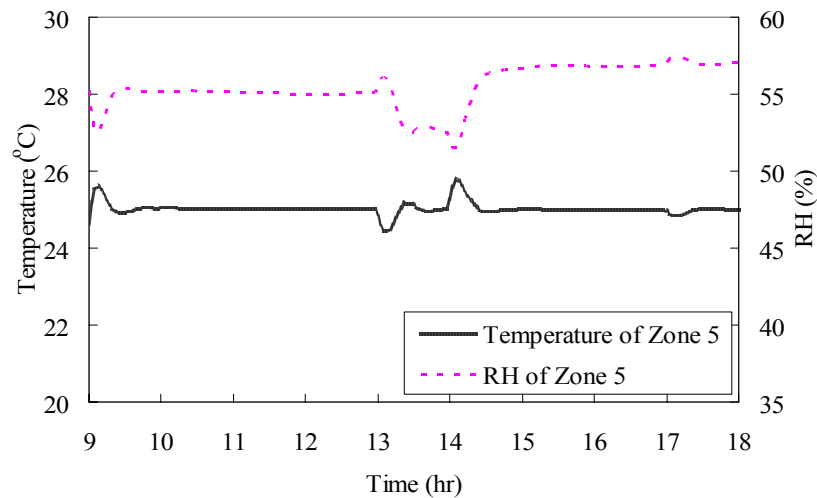


Figure 5.2 Indoor air temperature and humidity responses when adopting basic control strategy

In the DOAS-CC system, the indoor air temperature is controlled by regulating the supply water flow rate in the chilled ceiling subsystem, which is comparatively easy to

achieve the set point. Figure 5.2 shows the indoor air temperature and relative humidity responses in zone 5 when the basic control strategy is used in the integrated system. The data is shown for zone 5 since it has the highest load variation and would be representative of the thermal response of the system. It can be found that indoor air temperature is well controlled in the design value, i.e. 25°C, in the stable operating period. As depicted in the figure, the indoor air relative humidity is about 55%RH in the stable operation period. The indoor air relative humidity is lower from 13:00 to 14:00, since the actual occupant number in zone 5 is lower in the lunch time period.

As far as the IAQ is concerned, the basic control strategy proved to be sufficient for the occupants' ventilation in the conditioned zones. The variation of the CO₂ concentration in zone 5 is plotted in Figure 5.3. The CO₂ concentration varies according to the actual occupant number in the space, and the maximum value is about 800ppm in the operation period.

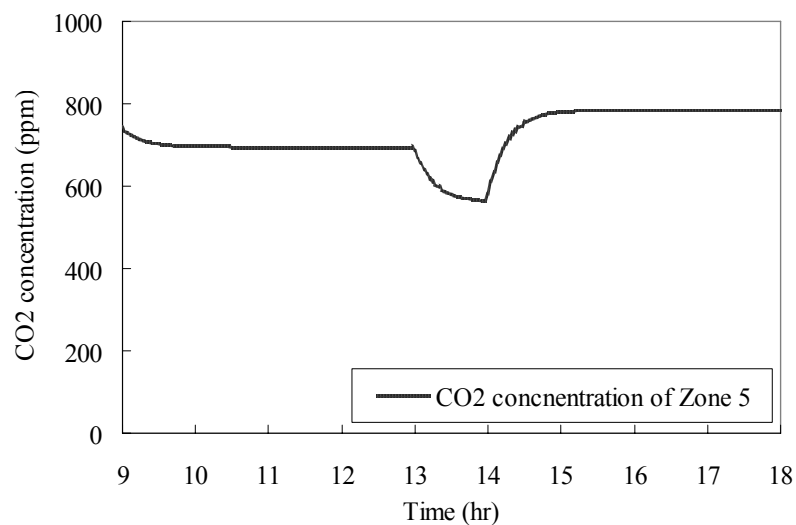


Figure 5.3 CO₂ concentration response when adopting basic control strategy

As the supply air humidity ratio set point reset strategy is employed, the supply air humidity ratio set point in DOAS is determined by the maximum and minimum indoor air relative humidity values in five zones. In this study, the supply air humidity ratio is mainly affected by the maximum RH, since the tested day is a typical summer day. Figure 5.4 shows the supply air humidity ratio set-point ($\omega_{sup,sp}$) and the maximum RH value in five zones (RH_{max}). It can be found that the maximum relative humidity keeps about 60%, except for the beginning operating hours. The supply air humidity ratio set point varies in the range from 0.006 to 0.012kg/(kg dry air). The actual supply air humidity of the DOAS subsystem (ω_{sup}) is also depicted in the figure, which well follows the variation of supply air humidity set point. It is demonstrated that the adopted liquid desiccant dehumidification method is reliable to control the supply air humidity in the DOAS. In this case, the indoor air temperature is well controlled and its response is similar to that when adopting basic control strategy, since indoor air temperature is also independently regulated by chilled ceiling subsystem.

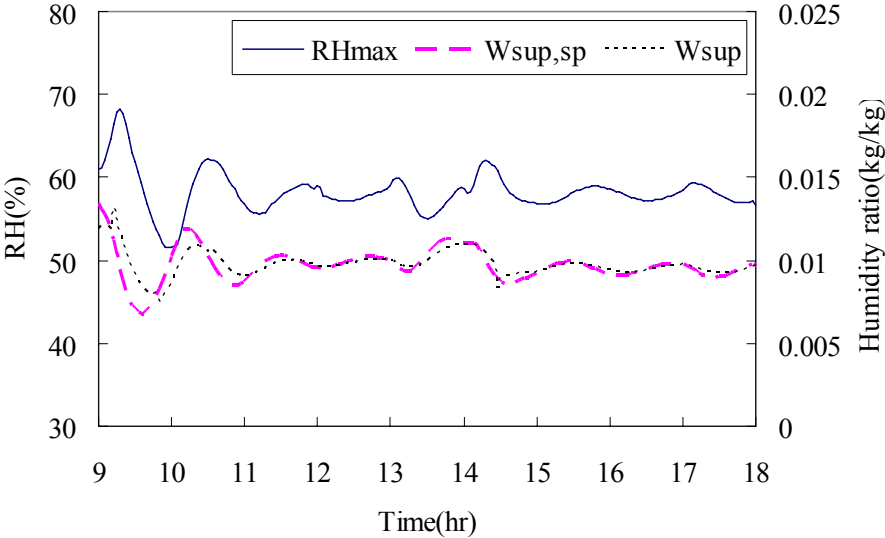


Figure 5.4 Supply air humidity ratio and maximum RH when adopting the supply air humidity ratio set point reset

Figure 5.5 presents the detected occupancy of zone 5 by the occupancy detector as shown in Equation (5.2) when the occupancy-based DCV strategy is used in the air-conditioning system. The difference between the detected occupancy and the actual occupancy can be observed and is small in the operation period, which will not affect the DCV to set the outdoor air flow rate set-point.

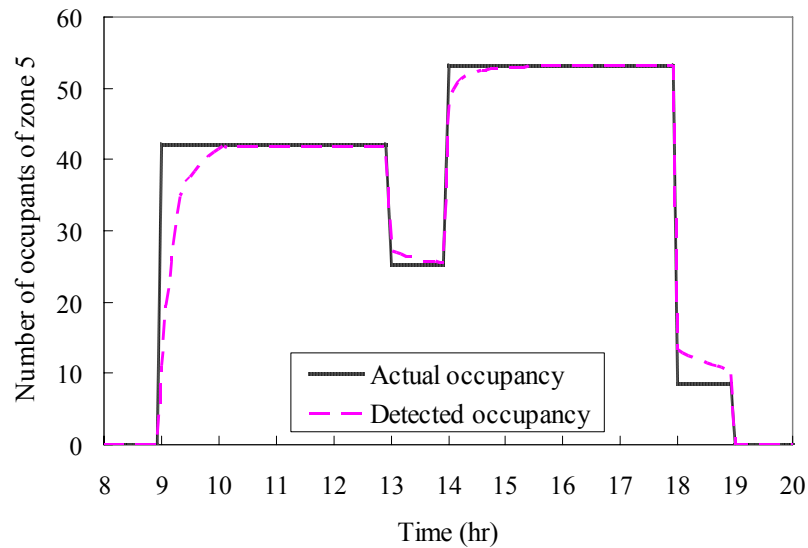


Figure 5.5 Comparison between actual occupancy and detected occupancy

The DCV strategy determines the required fresh air flow rate in each zone according to the detected occupant number in that zone, consequently reduces the energy consumption for air dehumidification and air distribution by fans. Figure 5.6 shows the variation of the CO₂ concentration in zone 5 when DCV-based supply air humidity reset strategy is applied. The CO₂ concentration slightly varies and is almost close to the maximum value, i.e. 800ppm, in the operating period. The supply air humidity ratio of the DOAS subsystem, the indoor air relative humidity and temperature variations are similar to those of the supply air humidity ratio set point reset strategy.

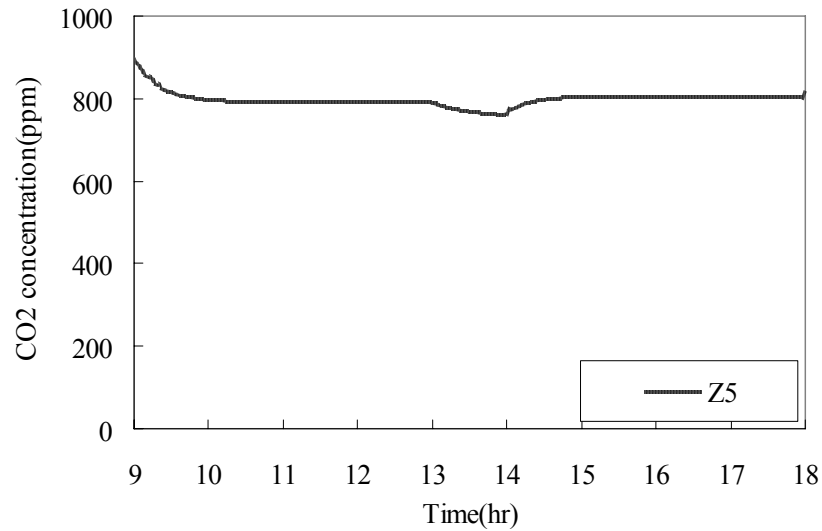


Figure 5.6 Indoor air CO₂ concentration response when adopting DCV strategy

In order to evaluate the energy performance of the supply air humidity ratio set point reset strategy and the DCV strategy, the DOAS-CC system is simulated to operate for a long period, i.e. the whole August in Hong Kong. Table 5.1 presents the primary energy consumption of the main components of the integrated system in this period when various control strategies are used. When adopting the supply air humidity ratio set point reset strategy (i.e. proposed strategy 1 in Table 5.1), the supply air humidity ratio of the DOAS subsystem is higher than the fixed supply air humidity, which reduces about 18.3% of heating consumption for the liquid desiccant regeneration and about 2.2% of cooling requirement for the supply air dehumidification and cooling. Consequently, the supply air humidity ratio set point reset strategy can save about 8.8% of overall energy consumption during the test period. When the DCV-based supply air humidity reset strategy (i.e. proposed strategy 2 in Table 5.1) is adopted in the system, the demanded fresh air flow rate varies with the estimated occupant numbers in conditioned space and it lowers than the fixed design ventilation flow rate. Hence,

energy consumption for the liquid desiccant dehumidification system and the fans can be reduced further. The simulation results show that the DCV strategy can save about 10.5% more overall energy consumption besides energy saved by adopting the supply air humidity ratio set point reset strategy.

Table 5.1 Breakdown of energy consumption of the system

Items	Basic strategy	Proposed strategy 1	Proposed strategy 2
Heater	44193.35	36112.97	30975.77
Total heating(MJ)	44193.35	36112.97	30975.77
<i>Saving (%)</i>	--	18.28%	29.91%
Cooler	26266.11	24015.70	20894.91
Dry coil	11036.57	11993.52	9721.82
Chilled ceiling	14527.06	14704.22	15654.75
Total cooling(MJ)	51829.75	50712.44	46271.49
<i>Saving (%)</i>	--	2.16%	10.72%
Supply fan	4864.80	4864.80	3944.16
Return fan	1945.92	1945.92	1577.64
Regeneration fan	1339.20	1339.20	1339.20
Total fan energy (MJ)	8149.92	8149.92	6861.00
<i>Saving (%)</i>	--	0%	15.82%
Overall energy(MJ)	104173.02	94976.33	84108.26
<i>Saving (%)</i>	--	8.83%	19.26%

5.4 Summary

Dedicated outdoor air-chilled ceiling systems can realize independent controls of indoor temperature, humidity and ventilation rate for multi-zone spaces with less energy consumption. In this chapter, a DOAS-CC system using liquid desiccant dehumidification is proposed. The fresh air flow rate and the supply air humidity ratio of DOAS are two crucial variables for the integrated system, which directly influence

indoor thermal comfort, indoor air quality and energy consumption. In this study, two control strategies are proposed to optimize these two variables and improve the system energy performance. Simulation tests show that the supply air humidity ratio set point reset strategy is effective to control indoor air relative humidity in the comfortable range. It can save about 8.8% of overall energy consumption in the tested case. The results also illustrate that the adopted liquid desiccant dehumidification system is feasible and reliable to control the supply air humidity in the DOAS subsystem. In addition, the DCV-based ventilation control method demonstrates obvious strength in energy saving, which can further save about 10.5% of overall energy consumption during the summer period.

The proposed optimization strategies in this chapter can also be applied in other kinds of independent temperature and humidity control air-conditioning systems.

CHAPTER 6 SIMPLIFIED MODELS OF MAJOR COMPONENTS FOR ONLINE APPLICATIONS

This chapter mainly presents the simplified models of major components of the dedicated outdoor air-chilled ceiling system for online optimal control strategy. The validation results of these models are also presented. Section 6.1 presents the importance of simplified models for online control applications. Section 6.2 presents the simplified models of major components of the integrated system, such as total heat exchanger, liquid dehumidifier, liquid desiccant regenerator, cooling coil, chilled ceiling, etc. The simplified models are validated in Section 6.3.

6.1 Importance of Simplified Model

For researches on the optimal control of building air-conditioning systems, development or selection of mathematic model for the HVAC systems is crucial, which is related to the performance prediction of a system. For online control applications, detailed physical models and purely data-driven models are not the proper choice. Many of the parameters in detailed physical models always require detailed information on the system and very high computational power and memory space may be required. This seriously limits their applications and makes the use of these models in online control unfeasible. The purely data-driven models are simple, but they cannot always ensure the stable performance prediction. The accuracy of these models depends on the size of data used to train the models. Compared with physical models, the reliability of these models

could be a problem when the models work in the range from where the training data sets lack information.

For online application, the models applied in the control system should preferably have simplified structures with certain physical significance to ensure the stable performance prediction and acceptable accuracy over a wide range of operation conditions. The models should also require less training or calibration efforts with readily or easily available operation data, less operation costs and memory demands. According to these criteria, simplified models might be the proper choice for online control applications. These simplified models allow the structure to be reasonable simple based on the online identification techniques. Therefore, the development or selection of the effective simplified models for major components in the dedicated outdoor air-chilled ceiling system is important and needed in order to develop the online optimal control strategy for the integrated system.

6.2 Simplified Model of Major Components

A model-based predictor is developed to predict the indoor environmental and energy performance for the optimal control. The model-based predictor of the dedicated outdoor air-chilled ceiling system mainly consists of a total heat exchanger model, a liquid dehumidifier model, a solution regenerator model, a dry cooling coil model, a chilled ceiling model and fan/pump models, etc. These simplified models are presented as follows.

6.2.1 Simplified Membrane-based Total Heat Exchanger Model

In the total heat recovery process, both heat and moisture are transferred between the fresh air and the exhaust air in the membrane-based heat exchanger. Since the air states and flow rates of the two air streams barely changes in a short prediction interval which is equivalent to control time step, the sensible effectiveness (ε_S) and the latent effectiveness (ε_L) as defined by Equations (6.1) and (6.2) can be assumed to be constant (Zhang 2006, Liang 2010).

$$\varepsilon_S = \frac{T_{f,in} - T_{f,out}}{T_{f,in} - T_{ex,in}} \quad (6.1)$$

$$\varepsilon_L = \frac{w_{f,in} - w_{f,out}}{w_{f,in} - w_{ex,in}} \quad (6.2)$$

where T and w are temperature and moisture content of air, respectively. The subscript f , ex , in and out represents fresh air, exhaust air, inlet and outlet, respectively. Since the fresh air and return air states can be measured in the real process, these two parameters can be estimated directly and updated at each sampling instant.

6.2.2 Simplified Dehumidifier Model

Given the air inlet temperature and humidity, air outlet humidity, air flow rate, strong solution inlet concentration and flow rate, the dehumidifier model predicts the required solution inlet temperature and the air temperature at the dehumidifier outlet. Analogous to the heat exchanger effectiveness used in heat transfer studies, the concept of effectiveness can be applied to the packed bed dehumidification process which

involves simultaneous heat and mass transfer. Two characteristic parameters (i.e. α_{deh} and β_{deh}) relating to the heat and mass transfer as dimensionless ratios, one for the difference in moisture content and the other for the temperature difference, can be computed by Equations (6.3) and (6.4) (Gandhidasan 2004).

$$\alpha_{deh} = \frac{w_{a,in} - w_{a,out}}{w_{a,in} - w_{min}} = \frac{P_{a,in} - P_{a,out}}{P_{a,in} - P_{s,in}} \quad (6.3)$$

$$\beta_{deh} = \frac{T_{a,in} - T_{a,out}}{T_{a,in} - T_{s,in}} \quad (6.4)$$

where $P_{a,in}$, $P_{a,out}$ and $P_{s,in}$ are the partial pressures of water vapor in the inlet air, outlet air and inlet solution, respectively; $T_{s,in}$ is the strong solution inlet temperature.

In the dehumidification process, when the variations of inlet air states, inlet solution states and the require outlet air humidity are small in a prediction period, the two dimensionless difference ratios (model parameters) can be assumed to be constant. They can be calculated by the inlet and outlet measurements of dehumidifier in the real process. Combining with the overall energy and mass balance equations for the dehumidifier as shown in Equations (6.5) and (6.6), the outlet conditions of air and the solution can be predicted.

$$m_a \cdot h_{a,in} + m_s \cdot h_{s,in} = m_a \cdot h_{a,out} + m_s \cdot h_{s,out} \quad (6.5)$$

$$m_s \cdot C_{s,in} = [m_s + m_a \cdot (w_{a,in} - w_{a,out})] \cdot C_{s,out} \quad (6.6)$$

where m is mass flowrate, h is enthalpy of air or solution, C is the solution concentration. The subscript a represents air, s represents solution.

6.2.3 Simplified Regenerator Model

Given the regeneration air inlet temperature and humidity, airflow rate, weak solution inlet concentration and flow rate, and the solution outlet concentration, the regenerator model predicts the required solution inlet temperature and the air states at the regenerator outlet. Similar to the dehumidifier model, two characteristic parameters (i.e. α_{rgn} and β_{rgn}) relating to the heat and mass transfer can be computed by Equations (6.7) and (6.8) (Gandhidasan 2005).

$$\alpha_{rgn} = \frac{W_{a,out} - W_{a,in}}{W_{max} - W_{a,in}} = \frac{P_{a,out} - P_{a,in}}{P_{s,in} - P_{a,in}} \quad (6.7)$$

$$\beta_{rgn} = \frac{T_{a,out} - T_{a,in}}{T_{s,in} - T_{a,in}} \quad (6.8)$$

In the regeneration process, when the variations of inlet air states, inlet solution states and the require outlet solution concentration are small in a prediction period, the two model parameters can be assumed to be constant. They can be calculated by the inlet and outlet measurements of regenerator in the real process. Combining with the overall energy and mass balance equations for the regenerator as shown in Equations (6.9) and (6.10), the outlet conditions of air and the solution can be predicted.

$$m_a \cdot h_{a,in} + m_s \cdot h_{s,in} = m_a \cdot h_{a,out} + m_s \cdot h_{s,out} \quad (6.9)$$

$$m_s \cdot C_{s,in} = [m_s + m_a \cdot (w_{a,in} - w_{a,out})] \cdot C_{s,out} \quad (6.10)$$

6.2.4 Simplified Cooling Coil Model

The cooling coil model is used to predict the required chilled water flow rate and the heat transfer rate since the cooling coil works under dry conditions in this study. The total heat transfer rates on the water side and air side are calculated by Equations (6.11) and (6.12), respectively. The heat transfer coefficients at the water side and the air side are assumed to be related only with the water flow rate and air flow rate, and the relations are invariable within a small working range. They can be computed by Equations (6.13) and (6.14), respectively (Xu 2009).

$$Q_{tot} = UA_w (T_b - T_{w,in}) \quad (6.11)$$

$$Q_{tot} = UA_a (h_{a,in} - h_b) \quad (6.12)$$

$$UA_w = \varphi_w (m_w)^{\gamma_w} \quad (6.13)$$

$$UA_a = \varphi_a (m_a)^{\gamma_a} \quad (6.14)$$

where UA is the heat transfer coefficient, m is the flow rate, Q is the heat transfer rate, T_b is the equivalent coil surface temperature, h_b is the saturated air enthalpy at the temperature T_b , φ and γ are the model parameters to be identified, and subscripts w and a indicate water and air, respectively.

To identify the model parameters of φ and γ , both heat transfer coefficients in the water side and air side need to be calculated based on the inlet and outlet air and water states of the coil. The model parameters are considered to be slowly-varying, and be constant within a limited working range. Using the heat transfer coefficients calculated at the current and former sampling instants, the recursive least-squares (RLS) estimation is used to estimate and update the parameters of the coil model.

6.2.5 Simplified Fan/pump Model

The power inputs of fans and pumps can be modeled to be approximately proportional to their flow rate cubed as Equation (6.15) when the changes of the flow rates are in a small range. Since the power input (W) and flow rate (V) are measured, the parameter (λ) can be learnt and estimated directly as Equation (6.16) and updated at each sampling instant.

$$W = \lambda V^3 \quad (6.15)$$

$$\lambda^{k+1} = W^k / (V^k)^3 \quad (6.16)$$

6.2.6 Simplified Chilled Ceiling Model

When the changes of the supply water states (i.e. temperature and flowrate) and the indoor air temperature are small in a prediction period, the UA value of the chilled ceiling can be regarded as constant. From the thermal balances of a test room, the UA value of chilled ceiling can be calculated as function of the water flow rate (m_w) and of

the log mean temperautre difference ($\Delta T_{Ln,system}$), as shown in Equations (6.17)-(6.19) (Diaz 2010).

$$UA_{CC} = \frac{Q_{CC}}{\Delta T_{Ln,system}} \quad (6.17)$$

$$Q_{CC} = m_w \cdot c_{pw} \cdot (T_{w,in} - T_{w,out}) \quad (6.18)$$

$$\Delta T_{Ln,system} = \left| \frac{(T_{w,in} - T_{w,out})}{\ln\left[\frac{T_{w,in} - T_{a,room}}{T_{w,out} - T_{a,room}}\right]} \right| \quad (6.19)$$

where Q_{CC} is the heat flow extracted by the chilled ceiling panel, c_{pw} is the specific heat of water.

In the operation period of the chilled ceiling, the model parameter can be estimated by the measurements and updated at each sampling instant. In terms of known inlet temperature and flow rate of supply water as well as the indoor air temperature, the outlet water temperature and cooling output of the chilled ceiling can be predicted by the simplified model.

6.2.7 Simplified Building Model

In conditioned space, the energy balance, moisture balance and pollutant balance for each zone can be expressed as Equations (6.20)-(6.22).

$$M_i c_p \frac{dT_i}{dt} = m_{a,i} c_{pa} (T_{a,s} - T_i) + Q_{CC,i} + Q_{sen,i} \quad (6.20)$$

$$M_i \frac{dw_i}{dt} = m_{a,i}(w_{a,s} - w_i) + D_i \quad (6.21)$$

$$V_i \frac{dC_i}{dt} = v_{a,i}(C_{a,s} - C_i) + S_i \quad (6.22)$$

In the study, sensible heat load ($Q_{sen,i}$), moisture load (D_i) and pollutant load (S_i) are called source terms since they are the driving forces in these equations. In a prediction period, these three source terms can be considered to be constant, and can be computed during a sampling step as Equations (6.23)-(6.25).

$$Q_{sen,i}^k = M_i c_p \frac{T_i^k - T_i^{k-1}}{\Delta t_{smp}} - m_{a,i}^k c_p (T_{a,s}^k - T_i^k) - Q_{CC,i}^k \quad (6.23)$$

$$D_i^k = M_i \frac{w_i^k - w_i^{k-1}}{\Delta t_{smp}} - m_{a,i}^k (w_{a,s}^k - w_i^k) \quad (6.24)$$

$$S_i^k = V_i \frac{C_i^k - C_i^{k-1}}{\Delta t_{smp}} - v_{a,i}^k (C_{a,s}^k - C_i^k) \quad (6.25)$$

where M is the air mass of one space, T is temperature, w is the moisture content, D is the moisture generation rates, Q_{CC} is the cooling output of chilled ceiling, c_{pa} is air specific heat, Δt_{smp} is the sampling interval. Additionally, k and $k-1$ represent the current and previous sampling instans respectively.

6.2.8 System Performance Prediction Model

System performance prediction includes the prediction of the indoor air states (i.e., temperature, moisture content and pollutant) of all the zones, the outlet air states of the

liquid dehumidifier and the cooling coil, the energy consumption of the liquid dehumidification system, the cooling coil, and the chilled ceiling system, the power consumption of fans etc. in one prediction period. To accurately predict the dynamic process responses at the end of one prediction period (Δt_{pred}) and within this prediction period, the prediction period is simulated by dividing this period into N simulation steps of the time step Δt_{sim} as Equation (6.26). For the performance prediction of the components, detailed descriptions have been given previously. During a small simulation time, supply air flow rate and conditions are assumed to be constant. Because sensible heat load ($Q_{sen,i}$), moisture load (D_i), and pollutant (S_i) are slowly-varying variables, they are assumed to be constant during a prediction period. Therefore, Equations (6.20)-(6.22) can be expressed approximately by replacing the derivative terms with finite difference terms as Equations (6.27)-(6.29) respectively.

$$\Delta t_{sim} = \frac{\Delta t_{pred}}{N} \quad (6.26)$$

$$T_i^{k+1} = T_i^k + \left[\frac{m_{a,i}^k}{M_i} (T_{a,s}^k - T_i^k) + \frac{Q_{CC,i} + Q_{sen,i}}{M_i c_p} \right] \Delta t_{sim} \quad (6.27)$$

$$w_i^{k+1} = w_i^k + \left[\frac{m_{a,i}^k}{M_i} (w_{a,s}^k - w_i^k) + \frac{D_i}{M_i} \right] \Delta t_{sim} \quad (6.28)$$

$$C_i^{k+1} = C_i^k + \left[\frac{V_{a,i}^k}{V_i} (C_{a,s}^k - C_i^k) + \frac{S_i}{V_i} \right] \Delta t_{sim} \quad (6.29)$$

where the subscripts k and $k+1$ represent the current and the next simulation time steps respectively, subscripts sim indicates simulation.

These models for the prediction of state variables (i.e., T_i , w_i , C_i) are needed to be tuned further for increasing accuracy since there may be derivations between the predictions and the real processes. The tuning model as Equation (6.30) is employed to correct the model predictions. At a sampling instant (t^{k-1}), the required measurement data are collected to estimate the source terms as Equations (6.23)-(6.25). These source terms are used by these models as Equations (6.27)-(6.29) to estimate the state variables at the next sampling instant (t^k) by the simulation of a few time steps. At the next sampling instant, these state variables are available and the model prediction error (e_{meas}^k) can be measured. To reduce the effects of the measurement uncertainty and model uncertainty, a filter using forgetting factor is used to stabilize the error estimation (e_{est}^k) as Equation (6.31). This error is used to correct the model output at the future next sampling instant (t^{k+1}).

$$\hat{Y} = Y + e \quad (6.30)$$

$$e_{est}^{k+1} = \lambda e_{est}^k + (1 - \lambda)e_{meas}^k \quad (6.31)$$

where Y is the output of the model (i.e., state variables T_i , w_i , C_i), \hat{Y} is the output of the model after correction, e is the correction factor representing the estimated error between model prediction and real process. e_{est} is the model error estimation, e_{meas} is the measured model error, λ is a forgetting factor.

6.3 Validation of Simplified Models

In the optimal control strategy, the developed or selected models are used for system performance prediction and optimization. The performance of these models directly impacts the performance of the strategy. The main models of concern are the liquid dehumidifier model for supply air dehumidification, the regenerator model for desiccant solution regeneration, the cooling coil model, the chilled ceiling model, the models of source terms of building and the models for estimating the indoor air states of each zone. The performances of these models are tested in a summer day. The weather data of the tested day is shown in Figure 6.1. The evaluations show these models have good performance. The performance evaluations of these simplified models are presented as follows.

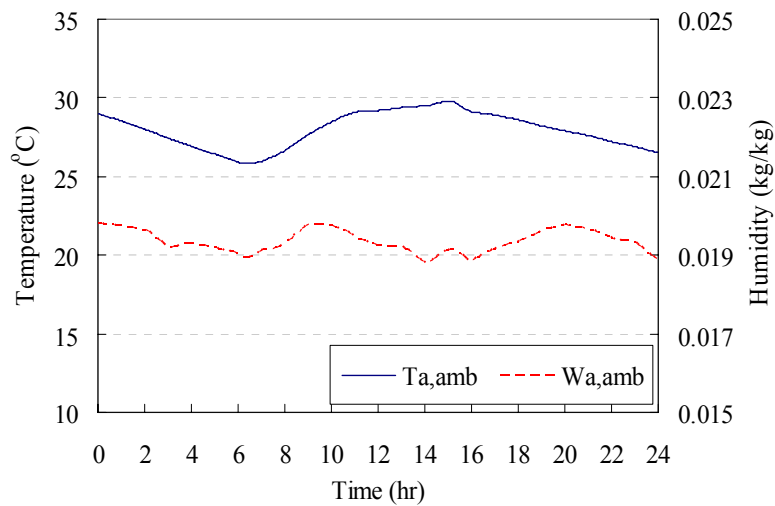


Figure 6.1 Outdoor air temperature and humidity on the summer day

Figure 6.2 presents the ‘measured’ and predicted strong solution temperature of dehumidifier inlet, respectively from 9:00 to 18:00 when the optimal control strategy

was used. The ‘measured’ inlet solution temperature was obtained from the measurements in the real process. The predicted inlet solution temperature was calculated using Equations (6.3)-(6.6) while the parameters were identified in advance. The predicted inlet solution temperature well matches the ‘measured’ data except for some steps, which is mainly caused by the changing supply air flow rate and supply air humidity set-point in the dedicated outdoor air subsystem. The inlet solution temperature is higher in noon period since the latent load in this period is lower, which is caused by less occupants in the space and lower outdoor air humidity ratio, as shown in Figure 6.1. The ‘measured’ and predicted outlet air temperatures after the dehumidifier were not presented since their values were very close to those of inlet solution temperatures.

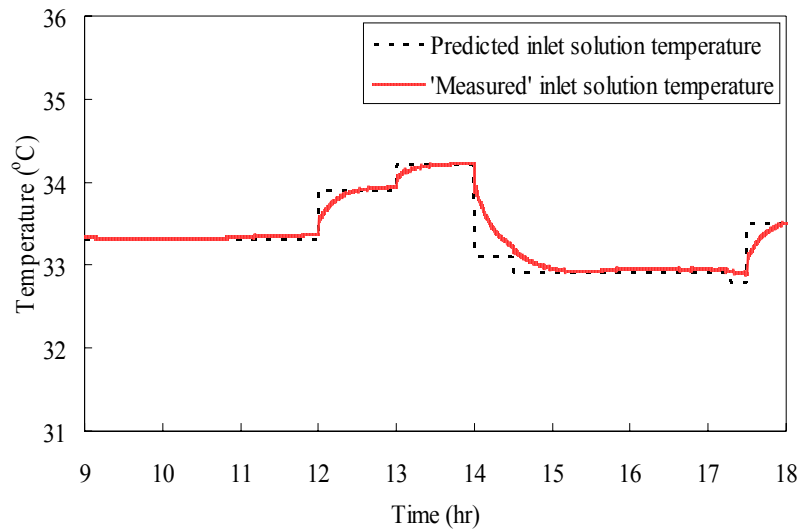


Figure 6.2 Validation of the simplified dehumidifier model

Figure 6.3 presents the ‘measured’ and predicted weak solution inlet temperature of regenerator as well as the outlet air state, respectively from 9:00 to 18:00 when the optimal control strategy was used. The ‘measured’ weak solution inlet temperature was

obtained from the measurements in the real process. The predicted inlet solution temperature was calculated using Equations (6.7)-(6.10) while the parameters were identified in advance. The predicted inlet solution temperature agrees well with the ‘measured’ data except for the noon period. The inlet solution temperature is lower in noon period since the latent load needed to treat is lower in this period, which is caused by fewer occupants in the space and lower outdoor air humidity ratio. The ‘measured’ and predicted outlet air humidity ratios after the dehumidifier are also presented in the figure. The predicted results by the simplified model well match the ‘measured’ results from the real process. The outlet air temperatures are not presented here, since their values are close to the solution inlet temperatures.

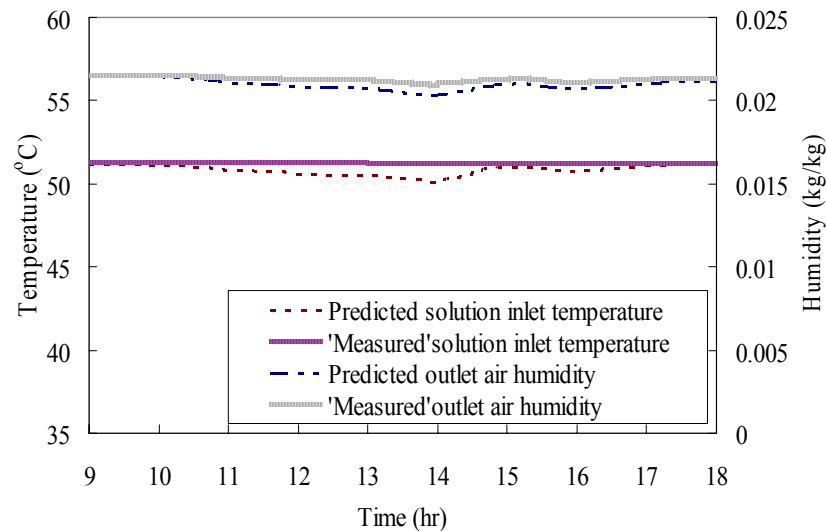


Figure 6.3 Validation of the simplified regenerator model

Figure 6.4 presents the ‘measured’ and predicted cooling outputs and outlet water temperatures of chilled ceiling in zone 5, respectively from 9:00 to 18:00 when the optimal control strategy was used. The ‘measured’ cooling output was calculated based on the measurements in the real process, while the predicted cooling output was

calculated using Equations (6.17)-(6.19). It can be found that the predicted results agree well with the ‘measured’ results. The heat flow extracted by the chilled ceiling panel is smaller in the noon and later afternoon period.

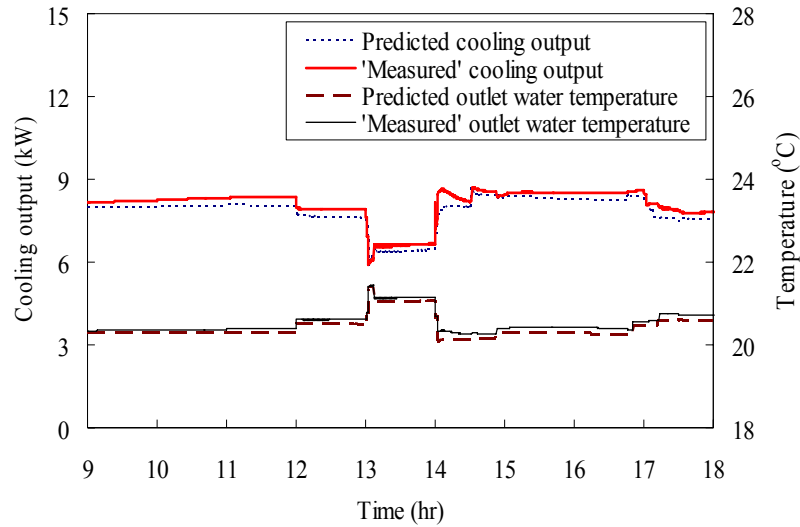


Figure 6.4 Validation of the simplified chilled ceiling model

For the source terms, i.e., sensible cooling load, latent load and pollutant load, the pollutant load (represented by CO₂ concentration) is easier to calculate based on the number of occupants than the sensible load and latent load. Therefore, the CO₂ generation rate is presented for validating the performance of models for source term identification. Figure 6.5 presents the ‘measured’ CO₂ generation rate and the predicted CO₂ generation rate of zone 5. The ‘measured’ rate was calculated based on the actual occupants. The predicted rate was estimated using the model as Equation (6.25) based on the measurements. The results show that the predicted CO₂ generation rate matched the ‘measured’ generation rate very well.

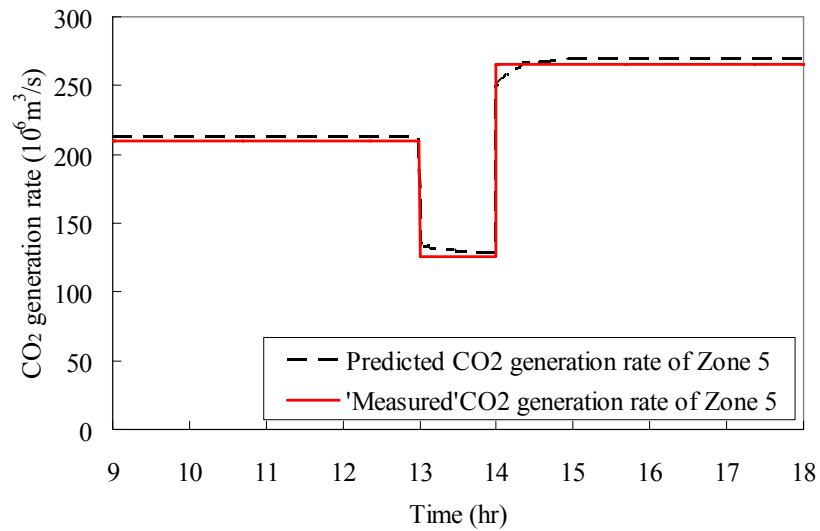


Figure 6.5 Comparison of measured and predicted CO₂ generation rates of zone 5

For the estimation of zonal air states, only the indoor temperature of zone 5 is presented for performance evaluation as shown in Figure 6.6. The results show that the predicted temperature using the model as Equation (6.27) basically agreed with the measured indoor air temperature. The prediction results slightly deviated from the actual measurement in some periods. The tests for the prediction of the zonal moisture content and CO₂ concentration also show the model prediction matched the coincident measurement very well.

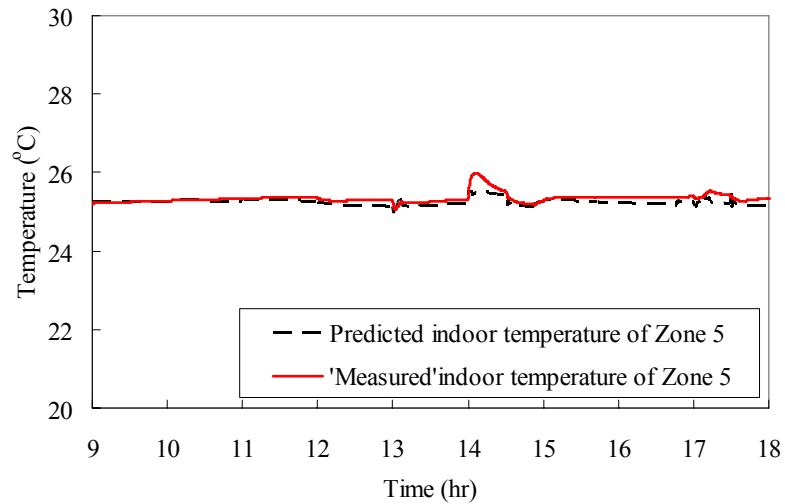


Figure 6.6 Comparison of measured and predicted air temperature of zone 5

6.4 Summary

This chapter presents simplified models of major components of the integrated dedicated outdoor-air chilled ceiling system, such as liquid dehumidifier model, liquid desiccant regenerator model, chilled ceiling model, building model, system performance prediction model, etc., for optimal control applications. These simplified models are also validated in this chapter. The validation results show that good agreement between the prediction values by the simplified models and the actual measured data from the real process was observed in the comparison studies. These tests illustrate that the simplified models can ensure the accuracy of the models and allow the models to be used conveniently in practical applications by identifying and updating the parameters online.

The models developed or selected in this chapter will be used to develop the online optimal control strategy presented in Chapter 7 for online applications of the dedicated outdoor air-chilled ceiling system.

CHAPTER 7 MODEL-BASED ONLINE OPTIMAL CONTROL OF DEDICATED OUTDOOR AIR-CHILLED CEILING SYSTEMS

This chapter mainly presents the optimal control strategy for the dedicated outdoor air-chilled ceiling system, including the principle of optimal control strategy, construction of cost function, etc., and the performance evaluation of the optimal strategy. Section 7.1 introduces the development of the optimal control strategy for DOAS-CC system. Section 7.2 presents the performance analysis of the optimal control strategy.

7.1 Development of the Optimal Control Strategy

A setting of a local optimization control may be optimal when concerning certain sub-system or certain system performance criteria only, but may not be optimal when the entire air-conditioning system and overall performance of the system are of concern. Therefore, the overall performance of the entire system should be concerned when optimizing the setting of the sub-processes. The strategy presented below aims at optimizing the setting of supply air temperature and supply air humidity ratio of the dedicated outdoor air subsystem as well as supply chilled water temperature of the integrated system which optimize the overall performance of the integrated system under dynamic conditions.

7.1.1 Outline of the Optimal Control Strategy

The optimal control strategy is developed to optimize the overall performance of the integrated dedicated outdoor air-chilled ceiling system, i.e. minimize energy use while maintaining acceptable thermal comfort in terms of indoor air temperature and relative humidity. Figure 7.1 illustrates the structure of the optimization strategy.

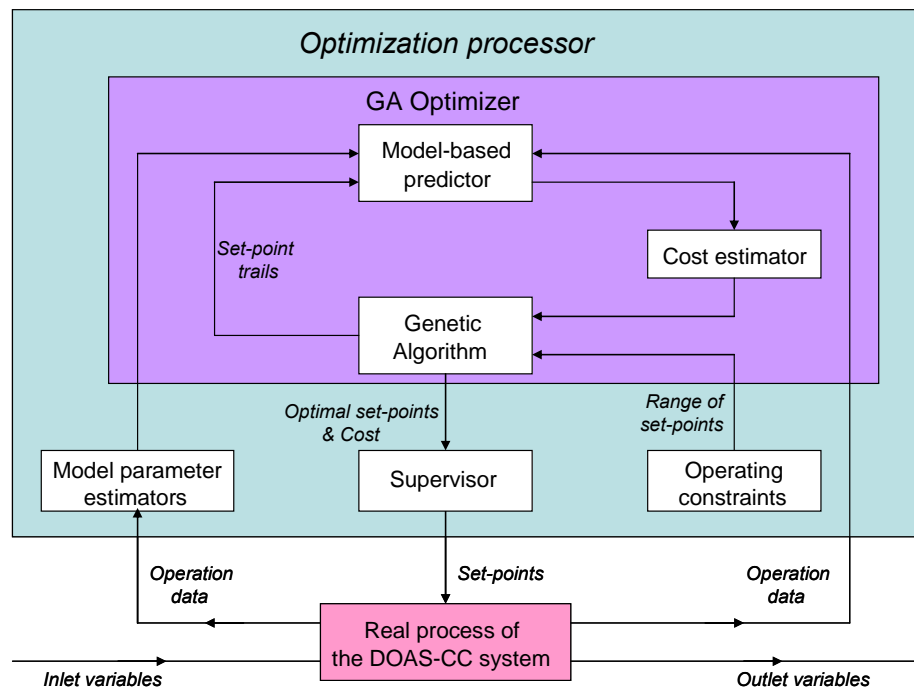


Figure 7.1 Illustration of the optimal control strategy

In this strategy, the model parameter estimators are used to identify and update the parameters of the models which are used in the model-based predictor using online measurements in the real process of the DOAS-CC system. The model-based predictor is used to predict system energy use and the indoor air states, i.e. indoor air temperature and relative humidity, under different operating conditions and with different control settings. A cost function is built in the cost estimator which calculates the overall cost of

the entire system considering both energy use and indoor thermal comfort. Genetic algorithm searches the optimal set-points of the three control variables by minimizing the overall cost. The operating constraints define the normal ranges (i.e. the upper and lower limits) of the control variables to be optimized, which can be determined according to the system design criteria. The supervisor makes decision on the actual set-points for the real process based on some rules. The logic of the optimal control strategy based on GA is described below in detail.

At a sampling instant, the optimization processor collects the real-time measurements required by the strategy. The allowed ranges of set-points in the following time step are provided to the GA optimizer by the operating constraints of the system. Then the GA optimizer starts with group of random set-point trails within their allowed ranges at its first generation. At the computation of each generation, each set-points trail of the group is given to the model-based predictor. The predictor simulates the responses of the system within a prediction period (Δt_{pred}), which is used by the cost estimator to compute the overall cost using the cost function. The GA optimizer produces the next generation (a group of set-points trails) according to its rules and the costs at current generation. Through many generations of computation, the GA optimizer finds the optimal set-point trail which minimizes the overall cost over the entire prediction period. Compromising the indoor environment and energy consumption, the optimal set-points obtained by the GA optimizer are further checked by the rule-based supervisor according to cost of the optimal set-points given by the GA optimizer and the cost of the current set-points in the next prediction period. When the cost saving is significant (i.e.

1% in the study), the optimal set-points will be used to update the current set-points. Otherwise, the set-points keep unchanged.

7.1.2 Formulation of the Cost Function

Based on the simplified models of major components as presented in Chapter 6, the responses of the integrated dedicated outdoor air-chilled ceiling system, i.e. the indoor air temperature, indoor air humidity and the entire system power consumption, etc. to the changes of the control set-points in a prediction period can be predicted. In order to optimize the control set-points and evaluate the overall performance of the integrated system, a cost function is constructed.

The overall cost function of the DOAS-CC system consists of three elements, which account for indoor air temperature, indoor air relative humidity and energy use as shown in Equations (7.1)-(7.4).

$$J = \alpha_T J_T + \alpha_{RH} J_{RH} + \alpha_E J_E \quad (7.1)$$

$$J_T = \int_0^{t=\Delta t_{pred}} \sum_{i=1}^{N_z} (T_{zi} - T_{zset})^2 dt \quad (7.2)$$

$$J_{RH} = \int_0^{t=\Delta t_{pred}} \sum_{i=1}^{N_z} [\coth(\frac{RH_{max}}{RH_{zi}}) - 1] dt \quad (7.3)$$

$$J_E = \int_0^{t=\Delta t_{pred}} (W_{fan} + W_{pump} + W_{chiller} + W_{heater}) dt \quad (7.4)$$

where J is the overall cost of the entire system, α_T , α_{RH} and α_E in the cost function are the weighting factors of the three costs. J_T is the cost concerning the indoor air temperature of all zones, J_{RH} is the cost concerning the indoor air relative humidity of all zones, J_E is the cost of total energy consumption. T_{zset} is the expected indoor air temperature (25°C was used), RH_{max} is the allowed maximum indoor air relative humidity (60% was used). Each cost represents the quantitative penalty when an index moves away from the relevant expectation up to certain threshold or close to an unacceptable range. Since the values of the costs are of very different orders, the order of amplitude of the factors should be determined first according to the actual range of each cost. It means that the selected factors should allow each cost to have significant contribution in cost function when an index moves away significantly from its expectation or close to an unacceptable range. Minimization of the overall cost function results in the optimal control of the entire air-conditioning system.

7.2 Performance Analysis of the Optimal Control Strategy

To evaluate the model-based optimal control strategy using the GA optimization method, two control strategies (including the optimal strategy) were tested on the DOAS-CC system. The second control strategy is a conventional strategy used for performance comparison. In the conventional strategy, the supply air temperature and humidity of the DOAS subsystem as well as the supply water temperature are constant. They are 19°C, 0.0093kg/kg and 17°C, respectively. In the tests using the optimal strategy, the ranges of supply air temperature and humidity set-points are between 19°C, 0.008kg/kg and 25°C, 0.012kg/kg, respectively. The supply water temperature set-point

is constrained between 17°C and 22°C. The weighting factors of the cost function are given in Table 7.1. The sampling interval for this strategy was 60 s. The prediction period was 300 s while the simulation time step of the optimal strategy was 60 s.

Table 7.1 Control settings of the cost function of the optimizer

Weighting factors of cost function	α_T	α_{RH}	α_E
Setting I	5	2	0.1
Setting II	0.5	2	0.1
Setting III	5	0.4	0.1
Setting IV	5	2	0.01

In the study, two different days, a summer day and a spring day, are selected to test and evaluate performance of the optimal control strategy. Figure 7.2 shows the outdoor air dry-bulb temperature and humidity in both test days.

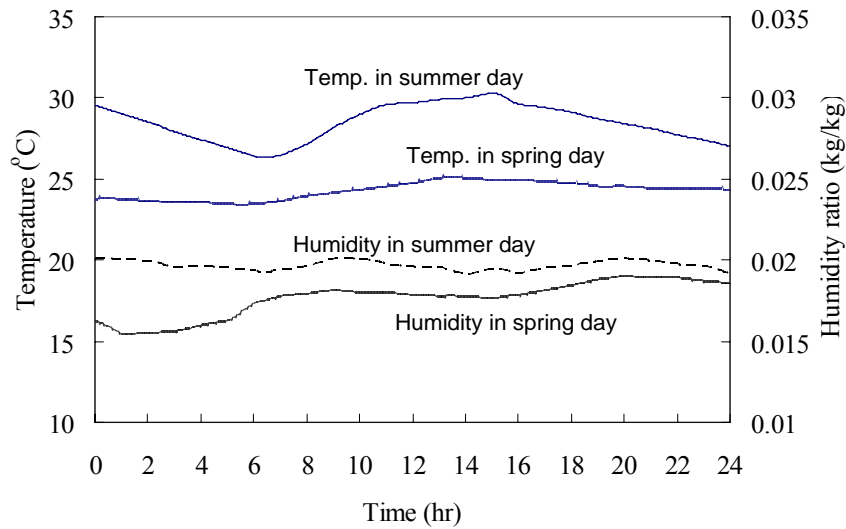


Figure 7.2 Temperature and humidity profiles of test days

7.2.1 Performance of the Optimal Control Strategy

The performance of the model-based optimal control strategy was evaluated by comparing with the conventional strategy. The results are presented as follows. Figure 7.3 shows the optimized set-points of the supply air temperature and humidity of the dedicated outdoor air subsystem as well as the supply water temperature on the summer test day when the weighting factors of Setting I were used. The supply water temperature is raised in the noon and later afternoon since the cooling load is lower in these periods. It is needed to point out that the sensible cooling load of the building in the study is mainly impacted by indoor load variations (i.e. occupant numbers and interior equipments) rather than outside weather conditions (i.e. outdoor air temperature, solar radiation, etc.). The supply air temperature is regulated to maintain the indoor air temperature. The supply air humidity ratio is lower in the noon period, since the supply air flow rate is lowest which is determined by the demanded control ventilation strategy and some other moisture sources except from occupants (i.e. moisture disturbance in this study) need to be removed. In the figure, it can be seen that the control variables almost keep constant in the morning and afternoon, which is different from the results presented in previous literature (Wang 2000, Xu 2009) that the optimized variables changed from time to time. The reason is that the indoor air temperature and relative humidity are allowed to vary in a range or have a small offset in the study as shown in Figure 7.4, but not a set of fixed values.

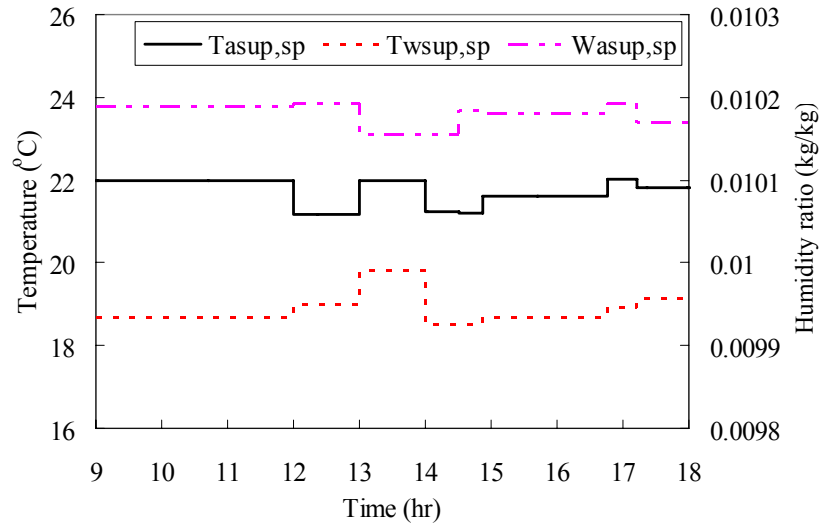


Figure 7.3 Set-points under optimal control strategy on the summer day (Setting I)

Figure 7.4 shows the indoor air temperature and humidity responses in zone 5 when the conventional control strategy and the optimal strategy are used in the integrated system. The data is shown for zone 5 since it has the highest load variation and would be representative of the thermal and moisture responses of the system. Under the conventional strategy, the indoor air temperature is about 25°C and the relative humidity is about 57%. Under the optimal strategy, the indoor air temperature and relative humidity are a little higher than those of conventional strategy. They are about 25.3°C and 60%, respectively.

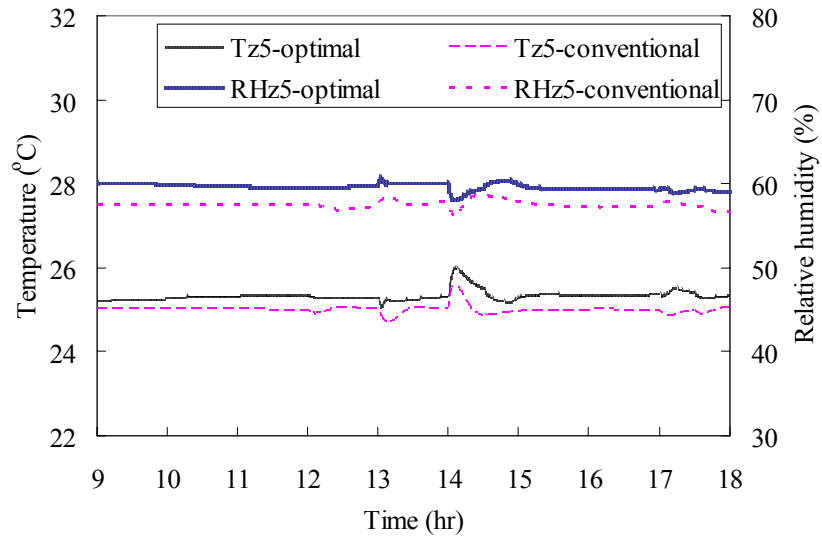


Figure 7.4 Temperature and RH of zone 5 using the optimal strategy (Setting I) and the conventional strategy

The costs related with the indoor air temperature, indoor air humidity and total energy consumption on the summer test day are presented in Table 7.2 when four different control settings of the weighting factors were used. These costs were integrated over the entire operation period. Comparing each item cost (i.e. temperature, humidity and energy) of four Settings, it can be found that the temperature cost of Setting II, humidity cost of Setting III and energy cost of Setting IV are the highest, respectively. It is caused by the lower weighting factor of the corresponding items compared with Setting I, as shown in Table 7.1. The effects of different control settings on the indoor environment and energy performance are described in the next section.

Table 7.2 Summary of the costs of the optimal strategy with different control settings on the summer test day

Cost	Control settings			
	Setting I	Setting II	Setting III	Setting IV
Cost of temperature	1811.48	4020.56	1814.86	1670.58
Cost of humidity	4205.22	4234.48	4363.79	2747.33
Cost of energy	84596.66	81667.46	83119.74	100013.95

The environmental and energy performance of the optimal strategy using different control settings on the summer day are presented in Table 7.3. The environmental and energy performance of the conventional strategy is also presented in the table as benchmark. In this section, only the performance of the optimal strategy using the control setting of Setting I is analyzed in detail.

In the summer day, the total cooling energy and heating energy of the optimal strategy with Setting I is about 15.9% and 8.0% less than those of conventional strategy, respectively, whereas the pump energy is about 26.0% larger under the optimal strategy. It is mainly caused by the higher supply water temperature (higher COP of chiller) and higher supply air humidity in the integrated system under the optimal strategy. Consequently, the total energy consumption of the optimal strategy is 7.8% less than that of the conventional strategy. In this case, the indoor air temperature and relative humidity under the optimal strategy are a little higher than those under the conventional strategy. The average surface temperature of ceiling panel is also shown in this table. The average surface temperature under the optimal strategy with Setting I is lower than that under conventional strategy since the optimized supply air temperature of DOAS is higher. When Setting II and III are adopted, the optimal control strategy can reduce

about 10.4% and 9.7% of energy consumption, respectively. While Setting IV is employed, the indoor air relative humidity is lower than the conventional strategy, but the system consumes about 8.5% more of energy.

Table 7.3 Summary of the environmental and energy performance of different strategies on the summer test day

Environmental and energy performance	Conventional strategy	Optimal strategy with different control settings			
		Setting I	Setting II	Setting III	Setting IV
<i>Environmental performance</i>					
Average return air temperature (°C)	24.97	25.30	25.64	25.29	25.25
Average return air RH (%)	56.89	59.88	59.50	60.83	51.61
Average ceiling temperature of Zone5 (°C)	21.40	20.85	21.34	20.82	20.69
<i>Energy performance</i>					
Total cooling energy (MJ)	889.06	747.36	705.13	732.24	897.05
Total heating energy (MJ)	1188.97	1094.04	1071.79	1077.95	1235.84
Total pump energy (MJ)	166.32	209.52	210.38	194.83	323.14
Total fan energy (MJ)	235.33	235.33	235.33	235.33	235.33
Overall energy consumption (MJ)	2479.68	2286.25	2222.63	2240.35	2691.36
Saving (%)	-	7.80	10.37	9.65	-8.54

The environmental and energy performance of the optimal strategy using different control settings on the spring day are also presented in Table 7.4. In the spring day, the total cooling energy and heating energy of the optimal strategy with Setting I is about 16.1% and 10.0% less than those of conventional strategy, respectively, whereas the pump energy is about twice of that under the conventional strategy. Totally, the optimal strategy with Setting I can save about 7.0% of energy compared the conventional strategy. The indoor air temperature and relative humidity under the optimal strategy are

a little higher than that under the conventional strategy, which is similar to the results in the summer day.

Table 7.4 Summary of the environmental and energy performance of different strategies on the spring test day

Environmental and energy performance	Conventional strategy	Optimal strategy with different control settings			
		Setting I	Setting II	Setting III	Setting IV
<i>Environmental performance</i>					
Average return air temperature (°C)	24.96	25.23	25.47	25.19	25.30
Average return air RH (%)	56.93	59.82	59.99	61.09	48.91
Average ceiling temperature of Zone5 (°C)	21.88	20.93	21.28	20.85	21.10
<i>Energy performance</i>					
Total cooling energy (MJ)	765.94	642.92	594.86	625.64	815.29
Total heating energy (MJ)	932.26	838.62	805.46	750.17	1100.84
Total pump energy (MJ)	75.60	152.06	137.38	146.88	278.21
Total fan energy (MJ)	235.33	235.33	235.33	235.33	235.33
Overall energy consumption (MJ)	2009.13	1868.93	1773.03	1758.02	2429.67
Saving (%)	-	6.98	11.75	12.50	-20.93

7.2.2 Impacts of the Weighting Factors

The weighting factors have significant impacts on the performance of the optimal strategy. Different settings give different weights to the three indices, i.e. indoor temperature, indoor humidity and energy consumption, and achieve different trade-off between thermal comfort and energy consumption. The weighting factors of Setting I in Table 7.1 are obtained using the trial-and-error method, which enable each cost term corresponding to temperature, humidity and energy consumption respectively have significant weight in the cost function when one of the three indices deviates significantly from its expectation.

In order to evaluate the influences of weighting factors, different values are used in Setting II to IV. Only one factor is changed in each case, while the other factors keep the same as those of Setting I. Setting II give less weight on indoor air temperature. Table 7.3 and 7.4 show that the indoor air temperatures increase obviously, from 25.3°C to about 25.6°C, comparing with those using Setting I. In this case, the total cooling energy is decreased because the supply water temperature and supply air temperature are higher. In Setting III, the cost function term related to indoor air humidity has less influence. In this situation, the average return air relative humidity changes from 59.9% to 60.8% as presented in Table 7.3, which is caused by the higher supply air humidity using this setting. When the cost of the total power consumption is less considered (i.e. Setting IV), the supply air humidity is lower. As a result, the indoor air relative humidity is lower than that of Setting I, varying from 59.9% to 51.6% as shown in Table 7.3, which can improve the indoor thermal comfort. However, the energy consumption of the integrated system in this case is much higher.

In practical applications, the proper weighting factors can be obtained by testing the systems and tuning the factors. The operators can select these weighting factors according to their preferences on different aspects, i.e. thermal comfort and energy consumption. Usually, a considerate choice of these weighting factors in the cost function requires more tests and rich experiences on the operation of the air conditioning system.

7.3 Summary

In this study, a model-based optimal control strategy is developed and validated for the dedicated outdoor air-chilled ceiling system incorporating liquid desiccant dehumidification and membrane-based total heat recovery technologies. The optimal strategy is based on the system performance prediction using adaptive simplified models and the genetic algorithm for optimizing the supply air temperature and humidity of the dedicated outdoor air subsystem and the supply water temperature. The testing results in a simulated multi-zone space served by the proposed system, which is built on the platform of TRNSYS, show that the optimal control strategy can reduce energy consumption while maintaining satisfactory indoor thermal comfort.

The results illustrate the optimal strategy can provide comfort indoor environment and achieve significant energy saving, i.e. save about 7.8% and 7.0% energy in the tested summer and spring days, respectively as compared with the conventional control strategy, in which set points of local controllers are fixed. The energy saving mainly comes from higher supply chilled water temperature, higher supply air humidity in the dedicated outdoor air subsystem and higher indoor air temperature and relative humidity in the conditioned space. The results also demonstrate that optimized and varying control set points are beneficial for the overall performance of air-conditioning systems under dynamic outdoor and indoor conditions.

In the study, the widely used thermal comfort indices, i.e. PMV and PPD, are not adopted to in the cost function. Since the PMV and PPD values are functions of some environmental variables and individual parameters, such as indoor air temperature, relative humidity, mean radiant temperature, air velocity, clothing level, etc. However, it is infeasible to get the real-time measurements of some variables, such as mean radiant

temperature, especially for on-line control. In addition, in humid regions, dehumidification of outdoor air for indoor humidity control significantly influences energy consumption of air conditioning systems, while the PMV and PPD values are rarely affected by indoor humidity (ISO 2005, Chow et al. 2010). If the PMV-PPD model is adopted for optimal control in this study, the indoor humidity will be severely sacrificed in order to achieve more energy saving. Therefore, indoor temperature and indoor humidity are considered in the cost function in this study.

CHAPTER 8 CONDENSATION CONTROL OF DEDICATED OUTDOOR AIR-CHILLED CEILING SYSTEMS

This chapter mainly presents a neural network based predictive condensation control strategy for the dedicated outdoor air-chilled ceiling system which can predict and prevent the condensation occurrence on the surface of chilled ceiling panels in the system start-up period. Section 8.1 introduces the risk of condensation on the chilled ceiling panels. Section 8.2 briefly introduces the neural network method. The developed neural network based predictive condensation control models and their performance are presented in Section 8.3.

8.1 Introduction of Condensation Risks

Chilled ceiling combining with dedicated outdoor air system as an alternative air conditioning manner has been investigated and successfully utilized in north-west Europe for about 20 years in public buildings, such as hospitals, office buildings, libraries, museums, schools, nursing homes and many more (Wilkins 1992). There are increased interests of this integrated system in North America (Stetiun 1999) and Asian countries (Imanari 1999, Matsuki 1999) in recent years. The dedicated outdoor air system integrated with chilled ceiling systems can realize independent temperature and humidity controls. It is believed that DOAS-CC systems can improve indoor thermal

comfort, and decrease air-conditioning energy consumption compared with conventional air-conditioning schemes, such as variable air volume systems and constant air volume systems. However, applications of chilled ceiling in hot and humid regions are much more challenging because of the risk of condensation on the surface of chilled ceiling panels, which limits the popularity of chilled ceiling.

Condensation on the surface of chilled ceiling most likely occurs in two situations. In situation 1, condensation occurs during operation period due to undesired opening windows or increasing occupancy (off-design conditions) in spaces served by DOAS-CC systems (Mumma 2002, 2003). In this situation, to prevent condensation, it is critical to control the panel surface temperature higher than the indoor air dew point temperature (DPT). For multi-zone DOAS-CC systems, two approaches are commonly adopted, i.e. regulate supply chilled water flow rate to chilled ceiling while keeping the supply water temperature constant and switch off the chilled water supply as soon as the relative humidity reaches the dangerous level. The former approach is more popular. Conroy and Mumma (2001) suggested a central dew-point temperature control. The supply chilled water flow rate to chilled ceiling panels decreases when the room air dew point temperature is close to the supply water temperature.

In situation 2, condensation occurs at the start-up moment of chilled ceiling systems, because the indoor air moisture level is the highest after one night's accumulation due to infiltration and the temperature of inlet chilled water to ceiling panels is low. An effective solution to prevent condensation occurrence is to operate a ventilation and dehumidification system (i.e. dedicated outdoor air system) prior to the operation of chilled ceiling systems. The dry supply air from DOAS can remove part of the moisture

in the space and therefore decrease the space dew point temperature. Zhang and Niu (2003) investigated indoor humidity behaviors associated with decoupled cooling in hot and humid climates. Their analysis results indicated that dehumidification and ventilation prior to cooling panels operation can reduce condensation risks. The larger the air infiltration rate is at night, the earlier it requires for air dehumidification to prevent condensation, and one hour in advance dehumidification and ventilation in summer in Hong Kong can completely eliminate condensation.

Due to changeable weather conditions and diverse building types, the required start time of DOAS prior to the operation of chilled ceiling systems is different. However, the prior time is critical which impacts both energy consumption and effect of condensation prevention. It is not easy to develop a physical model based method to predict the prior time because modeling of the moisture accumulation process and the surface temperature of the chilled ceiling panels at the start-up moment considering weather conditions and building types is quite difficult. An artificial neural network models based dynamic predictive condensation control strategy is developed in this study.

8.2 Brief of Artificial Neural Network

Artificial neural network (ANN), usually called neural network (NN), is one of the two major branches of artificial intelligence. The other one is expert systems. During the last ten years there has been a substantial increase in the interest on artificial neural networks.

The ANNs are good for some tasks involving incomplete data sets, fuzzy or incomplete information and for highly complex and ill-defined problems, where humans usually decide on an intuitional basis. They can learn from examples and are able to deal with non-linear problems. Furthermore, they exhibit robustness and fault tolerance (Irwin et al. 1995, Kalogirou 1999).

According to Haykin (1994), a neural network is a massively parallel distributed processor that has a natural propensity for storing experiential knowledge and making it available for use. It resembles the human brain in two respects; the knowledge is acquired by the network through a learning process, and inter-neuron connection strengths known as synaptic weights are used to store the knowledge.

Artificial neural network models may be used as an alternative method in engineering analysis and prediction. ANNs mimic somewhat the learning process of a human brain. They operate like a 'black box' model, requiring no detailed information about the system. Instead, they learn the relationship between the input parameters and the controlled and uncontrolled variables by studying previous recorded data, similar to the way of a non-linear regression might perform. Another advantage of using ANNs is their ability to handle large and complex systems with many interrelated parameters. They seem simple to ignore excess data that are of minimal significance and concentrated instead on the more important inputs.

A schematic diagram of typical multilayer feed forward neural network architecture is shown in Figure 8.1. The network usually consists of an input layer, some hidden layers and an output layer. In its simple form, each single neuron is connected to other

neurons of a previous layer through adaptable weights. Knowledge is usually stored as a set of connection weights. Training is the process of modifying the connection weights in some orderly fashion using a suitable learning method. The network uses a learning mode, in which an input is presented to the network along with the desired output. The weights after training contain meaningful information, whereas before training, they are random and have no meaning.

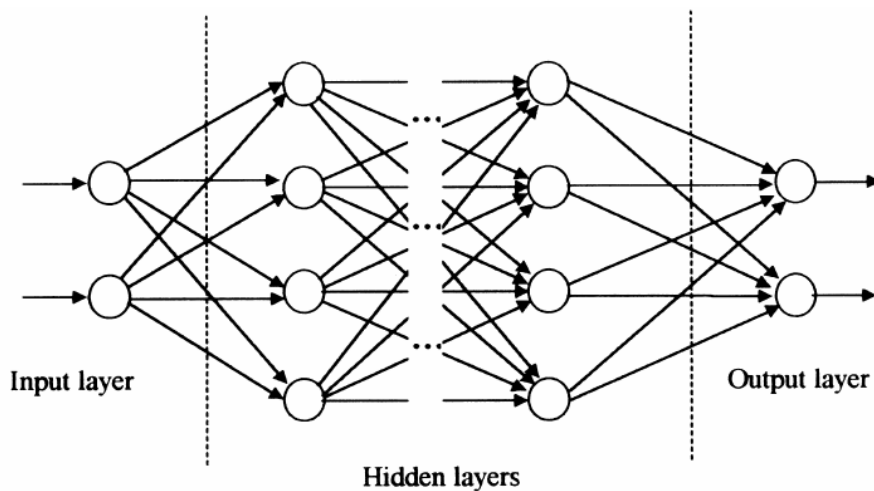


Figure 8.1 Schematic diagram of a multilayer feed forward neural network

Figure 8.2 illustrates how information is processed through a single node. The node receives weighted activation of other nodes through its incoming connections. First, these are added. Then the result is passed through an activation function, the outcome being activation of the node. For each of the outgoing connections, this activation value is multiplied with the specific weight and transferred to the next node.

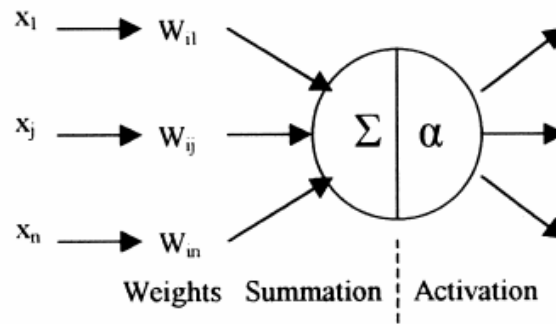


Figure 8.2 Information processing in a neural network unit

A training set is a group of matched input and output patterns used for training the network, usually by suitable adaptation of the weights. The outputs are the dependent variables that the network produces for the corresponding input. It is important that all the information the network needs to learn is supplied to the network as a data set. When each pattern is read, the network uses the input data to produce an output, which is then compared to the training pattern, i.e. the correct or desired output. If there is a difference, the connection weights are altered in such a direction that the error is decreased. After the network has run through all the input patterns, if the error is still greater than the maximum desired tolerance, the ANN runs again through all the input patterns repeatedly until all the errors are within the required tolerance. When the training reaches a satisfactory level, the network holds the weights constant and uses the trained network to make decisions, identify patterns, or define associations in new input data sets not used to train it.

The most popular learning algorithms are the back-propagation and its variants. The back-propagation (BP) algorithm is one of the most powerful learning algorithms in neural networks (Gurney 1997, Kalogirou 1999). The training of all patterns of a

training data set is called an epoch. The training set has to be representative collection of input-output examples. Back-propagation training is a gradient descent algorithm. It tries to improve the performance of the neural network by reducing the total error by changing the weights along its gradient. The error is expressed by the root-mean-square (RMS) value, which can be calculated by:

$$E = \frac{1}{2} \left[\sum_p \sum_i |t_{ip} - o_{ip}|^2 \right]^{1/2} \quad (8.1)$$

where E is the RMS error, t the network output and o the desired output vectors over all pattern. An error of zero would indicate that all the output patterns computed by the ANN perfectly match the expected values, and the network is well trained. In brief, back-propagation training is performed by initially assigning random values to the weight term in all nodes. Each time a training pattern is presented to the ANN, the activation for each node, α_{pi} , is computed. After the output of the layer is computed the error term, δ_{pi} , for each node is computed backwards through the network. This error term is the product of the error function, E , and the derivative of the activation function and, hence, is a measure of the change in the network output produced by an incremental change in the node weight values. For the output layer nodes and for the case of the logistic-sigmoid activation, the error term is computed as:

$$\delta_{pi} = (t_{pi} - \alpha_{pi}) \alpha_{pi} (1 - \alpha_{pi}) \quad (8.2)$$

For a node in a hidden layer:

$$\delta_{pi} = \alpha_{pi}(1 - \alpha_{pi}) \sum_k \delta_{pk} w_{ki} \quad (8.3)$$

where the k subscript indicates a summation over all nodes in the downstream layer. The j subscript indicates the weight position in each node. Finally, the δ and α terms for each node are used to compute an incremental change to each weight term via:

$$\Delta w_{ij} = \varepsilon(\delta_{pi} \alpha_{pi}) + m w_{ij}(old) \quad (8.4)$$

The term ε is referred to as the learning rate and determines the size of the weight adjustments during each training iteration. The term m is called momentum factor. It is applied to the weight change used in the previous training iteration, $w_{ij}(old)$. Both of these constant terms are specified at the start of the training cycle and determine the speed and stability of the network.

Neural network has been used by a number of researchers for modeling and prediction in the field of building energy systems. Ruano et.al (2006) discussed the use of neural networks for inside air temperature prediction in a building, which is used for predictive control of air-conditioned systems. Ben-Nakhi and Mahmoud (2004) adopts general regression neural networks to predict the building cooling load and optimize thermal energy storage in buildings. Yang and Kim (2003, 2004) developed optimized artificial neural network models to predict the time of room air temperature descending for heating systems in buildings and to determine the optimal start time for a heating system. The results showed that the ANN approach is effective and can provide high accuracy and reliability. Argiriou et al. (2004) presented an ANN-based controller for hydronic heating plants for buildings. Ben-Nakhi and Mahmoud (2003) investigated the

feasibility of using NNs for optimizing air conditioning setback scheduling in public buildings to achieve best performance. In the above-mentioned applications of NNs, the modeled objects include air conditioning processes and building envelopes, which are typically dynamic, multidimensional and nonlinear. It is not easy to build up physical models to map the quantitative relations that exist among the variables. However, NNs are quite suitable for modeling these processes and systems, because the NN requires less expertise, knowledge and experimentation to determine the relationships between the inputs and outputs of nonlinear systems. Moreover, building automation systems are widely used in modern buildings which make huge numbers of data available for training and validating NNs.

8.3 NN-based Predictive Condensation Control for DOAS-CC System

Condensation is prone to occur at the start-up moment of chilled ceiling systems in hot and humid regions, due to the infiltration moisture through building envelopes at night. In this study, the infiltration rate of the building envelope is assumed to be constant. In this case, condensation occurrence is significantly affected by ambient weather conditions, mainly the outdoor air temperature and humidity ratio. The schematic of the DOAS-CC system and the condensation prediction strategy for the integrated system at start-up moment are shown in Figure 8.3 and Figure 8.4, respectively. At the start moment, the cooling load due to occupants and equipment can be ignored and the sensible cooling load is largely determined by the outdoor air temperature. In DOAS-CC systems, the supply chilled water flow rate to the chilled ceiling panels is usually regulated to meet the sensible load demand. The change of the supply water flow rate

will subsequently affects the surface temperature of ceiling panels (T_{panel}). Therefore, the outdoor air temperature is used to predict the surface temperature of chilled ceiling. Outdoor air humidity ratio will affect the dew point temperature of indoor air ($DPT_{a,in}$) at the beginning moment of system operation when the infiltration is considered. When the temperature of ceiling panel is higher than dew point temperature of indoor air, no condensation will occur and dehumidification in advance is not needed. While the T_{panel} is lower than $DPT_{a,in}$, which means condensation will occur at startup period. The prior dehumidification is required for the DOAS to prevent the condensation occurring on the surface of chilled ceiling panels. In this case, the supply air state is fixed, i.e. 9.5g/kg.da and 25°C, and the supply air flow rate at the period is constant.

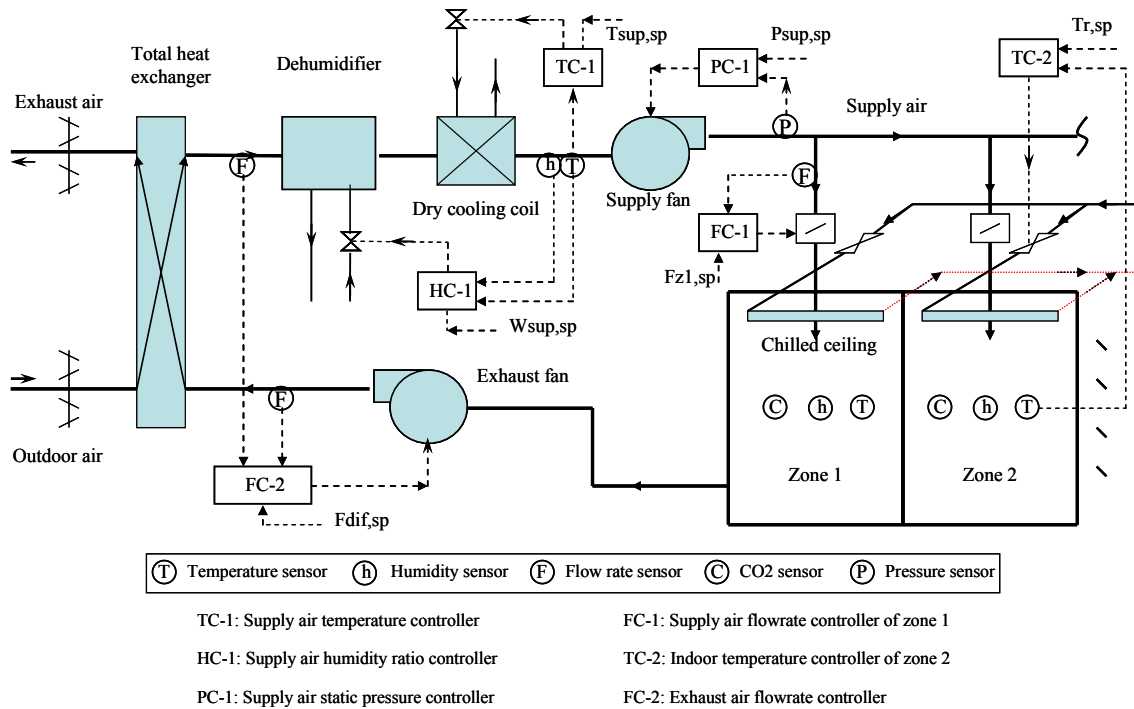


Figure 8.3 Schematic of DOAS-CC systems and its control system

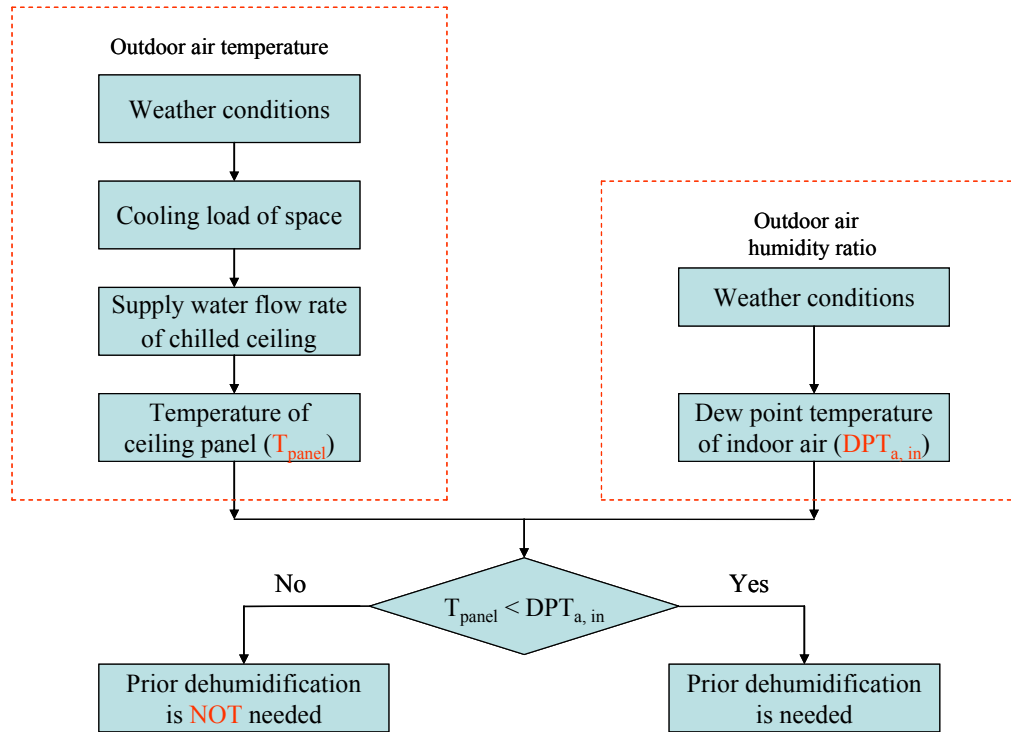


Figure 8.4 The flowchart of condensation prediction at startup moment

Three neural network models will be developed for the condensation prediction and the optimal prior time prediction. One is used for chilled ceiling surface temperature prediction; the second one is used for the prediction of indoor air dew-point temperature at the startup moment of the integrated system; and the third one for the optimal prior time prediction for DOAS to prevent condensation.

In this study, three-layer neural network will be adopted, which is widely applied in the field of prediction. The standard three-layer network topological structure is made up of input layer, hidden layer and output layer. The nonlinear mapping from input layer to output layer is realized by using connective weight matrixes from input layer to hidden layer and from hidden layer to output layer. Back propagation learning algorithm is adopted for the learning procedure. In learning, the neural network autonomously adjusts

the connection weights among the processing units according to imposed learning rules and obtains unique knowledge from the training data. After the neural network is trained with samples, the connective weight values among neural nodes are adjusted constantly according to errors between expectation and actual output. Eventually, the output of network comes close to the expectation in desired precision. The node number in hidden layer can directly influence the network nonlinear capacity. It can be increased to improve the network training precision. In this study, the neural network uses experiential formula as follows to determine the node number in hidden layer.

$$p = \begin{cases} n + 0.618(n - m) & n \geq m \\ m - 0.618(m - n) & n < m \end{cases} \quad (8.5)$$

Where n is the input node number, m is the output node number, and p is the hidden node number. Additionally, in the training and prediction processes, the input and output data must be normalized. The normalization makes the inputs and outputs distribute between 0 and 1. This can improve the training speed of neural network and prevent certain a factor dominating the learning. In the built neural network models, the activation function of hidden layer nodes is ‘Tansig’, and the activation function of output layer nodes is ‘Purelin’. The training algorithm function is ‘Traingdm’.

8.3.1 NN Models for Condensation Control

The architecture of neural network for chilled ceiling surface temperature prediction is schematically illustrated in Figure 8.5. The structure of the neural network model is $3 \times 5 \times 1$. In the input layer, three input nodes, $T_{a,in}$, $T_{a,out,1}$ and $T_{a,out,2}$, are the indoor air temperature at an earlier moment, say 7:30am, and the outdoor air temperatures at

7:30am and 9:00am, respectively. It should be noted that only the outdoor air dry bulb temperature is used to predict the building cooling load. In addition, the initial indoor air temperature ($T_{a,in}$) is important for the cooling load prediction. The output of the neural network is the predicted ceiling panel temperature at 9:05am. Because the response time of chilled ceiling is about 3-5mins (Jeong and Mumma 2004). The weather data can use the data on previous day or the weather data predicted by a dynamic grey model (Zhou et al. 2008).

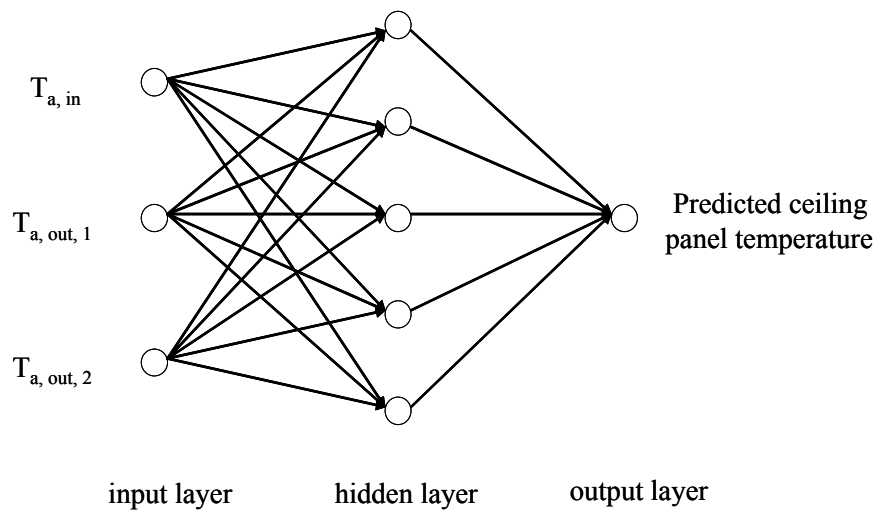


Figure 8.5 The structure of neural network for T_{panel} prediction

The architecture of neural network for indoor air dew-point temperature prediction is illustrated in Figure 8.6. The structure of neural network model is $3 \times 5 \times 1$. In the NN model, three inputs, $DPT_{a,in,1}$, $W_{a,out,1}$ and $W_{a,out,2}$, represent the indoor air dew-point temperature at 7:30am and the outdoor air humidity ratios at 7:30am and 9:00am, respectively. In the prediction process, the indoor air dew point temperature is majorly affected by the initial condition ($DPT_{a,in,1}$) and the outdoor air moisture content, when

the occupancy schedule of space is assumed to be the same on each day. The output of the neural network is the predicted indoor air dew-point temperature at 9:05am.

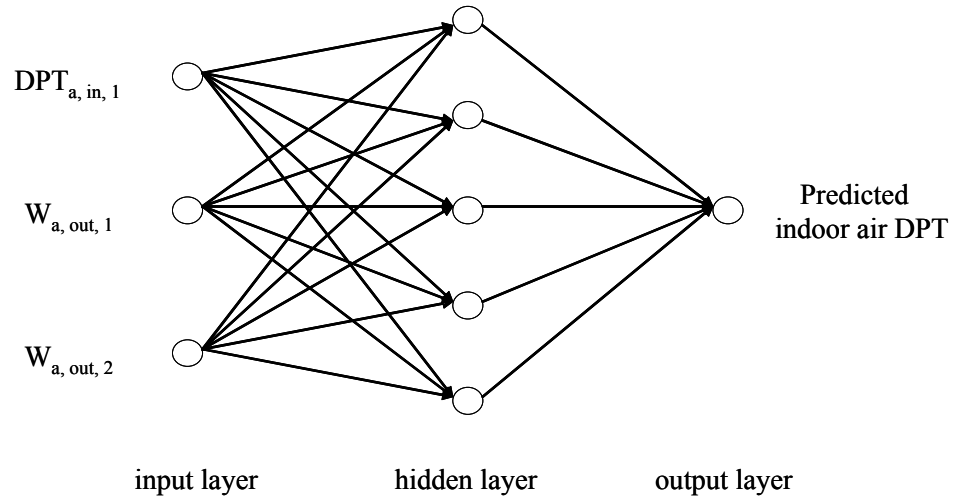


Figure 8.6 The structure of neural network for indoor air DPT prediction

The architecture of neural network for optimal prior time prediction is shown in Figure 8.7. The structure of neural network model is $4 \times 6 \times 1$. In the input layer, the input nodes, $DPT_{a,in,1}$, $W_{a,out,1}$, $W_{a,out,2}$ and $DPT_{a,in,2}$, are the indoor air dew-point temperature at 7:30am, the outdoor air humidity ratios at 7:30am and 9:00am, and the expected indoor air dew-point temperature at 9:05am, respectively. The expected indoor air dew-point temperature ($DPT_{a,in,2}$) should be equal or lower than the predicted T_{panel} value as shown in Figure 8.5 to prevent condensation. The output of the neural network is the predicted start time of DOAS prior to the operation of chilled ceiling systems for condensation prevention.

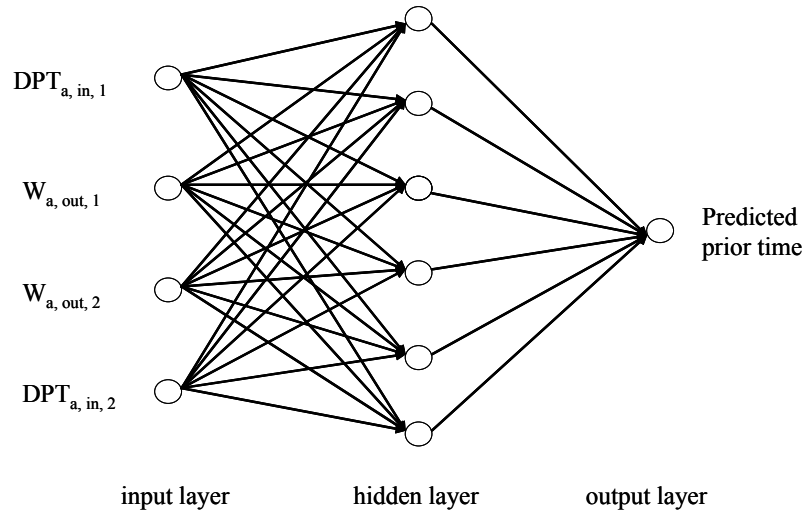


Figure 8.7 The structure of neural network for prior time prediction of DOAS

In the process of applying the neural network approach for the predictive condensation control in DOAS-CC systems, it can be divided in two stages. The first stage is the training and validation of the above-mentioned neural network models. The second stage is to use these neural network models to predict whether condensation will occur on the chilled ceiling panels or not, then to predict the optimal prior time for the DOAS to prevent the condensation occurrence.

In the present study, the training and validation data are mainly collected from simulation results in zone 5 during June and July, because zone 5 is the most likely to condense at the startup moment in this study. The trained neural network models are used for the condensation predictive control of the DOAS-CC system in early August, i.e. from Aug.1st to Aug.8th.

8.3.2 Training and Validation of the NN Models

43 groups of data (T1-01—T1-43), which are mainly collected from simulation results during June and July in two years, are used to train the neural network model for chilled ceiling surface temperature prediction in zone 5, and another 15 groups of data (V1-01—V1-15) are used to validate the model. Table 8.1 shows parts of the training data (T1-01—T1-15) and validation data (V1-01—V1-08) for the neural network model. The validation results are shown in Figure 8.8. The maximum model prediction bias between the prediction values and the simulation results is less than 0.2°C, and the maximum relative error is about 1.0%. The result shows that neural network approach is effective and accurate to predict the ceiling panel temperature at the startup moment.

Table 8.1 Training and validation data for T_{panel} prediction in zone 5

	$T_{a, \text{in}}(7:30\text{am})$ (°C)	$T_{a, \text{out}, 1}(7:30\text{am})$ (°C)	$T_{a, \text{out}, 2}(9:00\text{am})$ (°C)	$T_{\text{panel}}(9:05\text{am})$ (°C)
T1-01	30.8	26.4	27.2	19.5
T1-02	28.6	26.6	27.5	19.4
T1-03	30.7	26.1	27.3	19.5
T1-04	29.5	24.4	25.6	19.5
T1-05	27.6	22.8	24.7	19.6
T1-06	28.5	25.7	27.0	19.6
T1-07	28.5	27.5	28.6	19.4
T1-08	27.5	25.1	25.9	19.0
T1-09	28.8	27.1	28.0	19.4
T1-10	29.0	28.3	28.9	19.2
T1-11	27.9	27.7	27.9	18.9
T1-12	28.0	25.2	26.9	19.6
T1-13	31.0	26.4	28.0	19.9
T1-14	30.5	25.4	26.9	20.0
T1-15	30.1	29.0	29.7	19.6
V1-01	30.4	28.0	29.0	19.5
V1-02	29.7	26.1	27.6	19.7
V1-03	28.5	28.3	29.2	19.3
V1-04	29.4	28.2	29.5	19.7

V1-05	28.6	25.8	27.3	19.8
V1-06	27.8	26.7	27.1	19.1
V1-07	29.1	29.4	29.4	19.0
V1-08	30.1	28.2	29.3	19.4

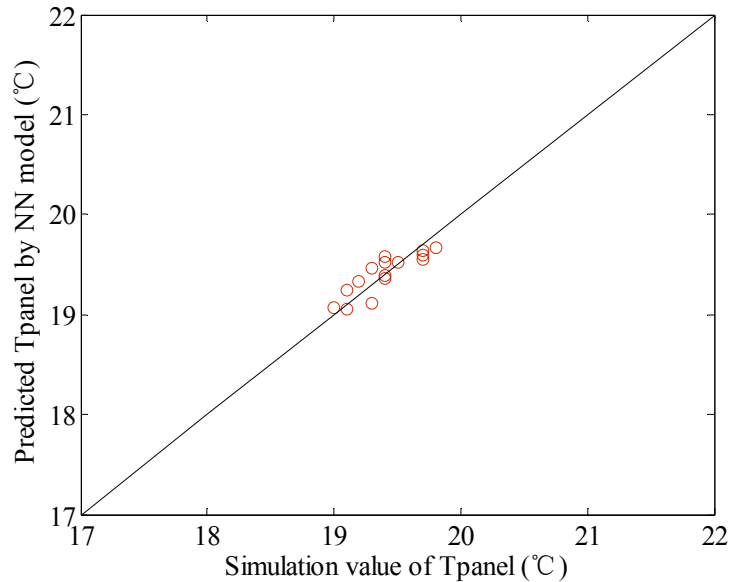


Figure 8.8 The validation result for NN-based T_{panel} prediction

Table 8.2 shows the training and validation data of neural network model for indoor air dew-point temperature prediction. 43 groups data (T2-01—T2-43), which is also collected from simulation results during June and July in two years, are used to train the neural network model, and the latter 15 groups of data (V2-01—V2-15) are used to validate the model. Parts of the training data (T2-01—T2-15) and validation data (V2-01—V2-08) are shown in Table 8.2. The validation results are shown in Figure 8.9. The maximum prediction bias is less than 0.3°C compared with the simulation results, and the maximum relative error is about 1.0%. According to the comparison analysis, it is illustrated that the neural network-based indoor air dew-point temperature prediction is reliable.

Table 8.2 Training and validation data for indoor air DPT prediction in zone 5

	DPT _{a, in, 1} (7:30am) (°C)	W _{a, out, 1} (7:30am) (g/kg.da)	W _{a, out, 2} (9:00am) (g/kg.da)	DPT _{a, in, 2} (9:05am) (°C)
T2-01	21.9	19.1	19.4	22.0
T2-02	23.5	20.4	20.5	23.1
T2-03	21.2	17.8	18.1	21.4
T2-04	21.0	17.0	17.0	21.1
T2-05	20.0	16.1	16.7	20.4
T2-06	22.6	19.8	20.1	22.5
T2-07	23.2	20.7	20.9	23.0
T2-08	21.7	17.9	18.4	21.7
T2-09	23.2	20.2	20.4	22.9
T2-10	22.9	20.9	21.0	22.8
T2-11	24.2	22.5	22.5	23.8
T2-12	23.0	19.2	19.5	22.7
T2-13	22.8	19.8	20.1	22.7
T2-14	22.0	18.6	18.8	22.0
T2-15	24.0	22.4	22.6	23.7
V2-01	22.9	19.8	19.8	22.6
V2-02	22.4	19.2	19.7	22.4
V2-03	23.4	21.9	22.2	23.2
V2-04	24.3	21.9	22.0	23.8
V2-05	22.2	18.5	18.8	22.1
V2-06	22.7	20.1	20.2	22.6
V2-07	25.3	24.7	24.6	24.8
V2-08	25.5	23.6	23.7	24.8

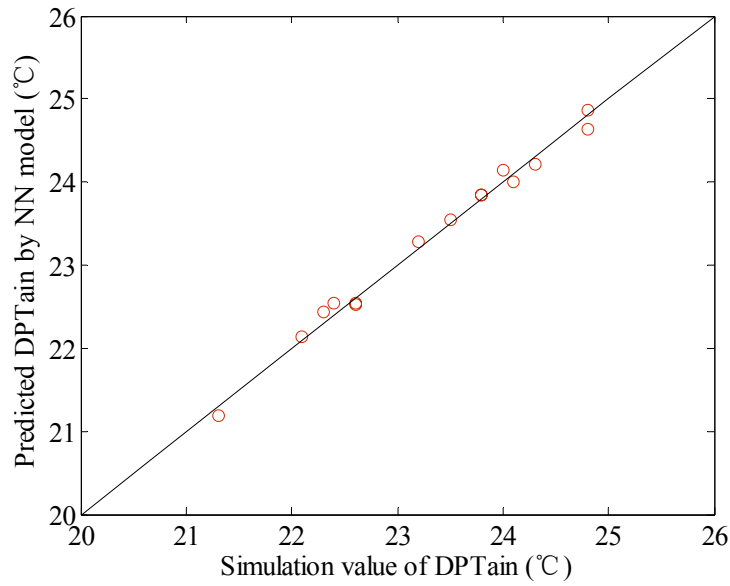


Figure 8.9 The validation result for NN-based indoor air DPT prediction

46 groups of data (T3-01—T3-46) are used to train the neural network model for the optimal earlier time prediction of DOAS, and another 15 group data (V3-01—V3-15) are used to validate the model. Table 8.3 shows parts of the training data (T3-01—T3-15) and validation data (V3-01—V3-08) of the optimal earlier time prediction neural network model. The validation results are shown in Figure 8.10. The maximum prediction bias compared with the simulation results is about 4.5mins.

Table 8.3 Training and validation data for prior time prediction

	DPT _{a,in,1} (7:30am) (°C)	W _{a,out,1} (7:30am) (g/kg.da)	W _{a,out,2} (9:00am) (g/kg.da)	DPT _{a,in,2} (9:05am) (°C)	Prior time (min)
T3-01	21.9	19.1	19.4	22.0	0
T3-02	23.3	20.9	20.8	20.0	20
T3-03	21.3	16.7	17.0	17.3	40
T3-04	23.1	20.5	20.7	17.1	60
T3-05	21.0	17.0	17.0	21.1	0
T3-06	20.1	15.6	15.8	18.1	20
T3-07	21.4	18.3	18.5	17.4	40

T3-08	23.4	20.1	20.5	17.1	60
T3-09	23.2	20.7	20.9	23.0	0
T3-10	23.0	19.8	19.9	19.8	20
T3-11	21.9	17.9	18.3	17.5	40
T3-12	22.7	20.2	20.8	17.0	60
T3-13	22.9	19.8	19.8	22.6	0
T3-14	22.0	17.9	17.8	19.2	20
T3-15	21.8	19.3	19.4	17.6	40
V3-01	22.9	20.9	21.0	22.8	0
V3-02	23.2	20.2	20.3	19.9	20
V3-03	24.3	21.8	22.1	18.5	40
V3-04	22.4	18.9	19.3	16.8	60
V3-05	24.0	21.8	21.6	23.6	0
V3-06	22.1	18.0	18.3	19.2	20
V3-07	21.3	17.1	17.5	17.3	40
V3-08	23.6	20.8	20.8	17.2	60

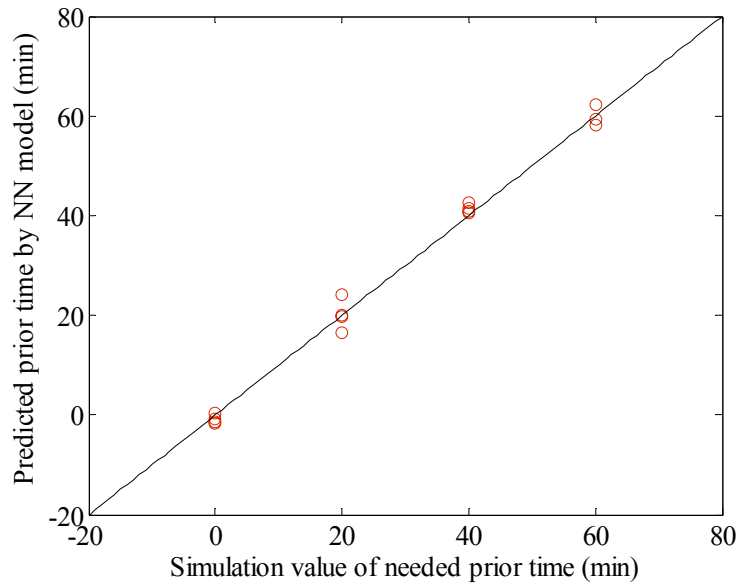


Figure 8.10 The validation result for NN-based optimal prior time prediction

In the training and validation process, those data for the prediction control models can also be acquired from the site measurements in practical applications. The data for T_{panel} prediction model and $DPT_{a,\text{in}}$ prediction model is easier to collect from the

building Energy Management and Control System (EMCS), but the data for optimal prior time prediction is a little difficult. Because additional manual control operations are required to collect these data.

8.3.3 Condensation Control Performance

8.3.3.1 Prior time prediction by NN models

After the training and validation process, the validated neural network models can be applied to predict the chilled ceiling panel temperature and indoor air dew-point temperature at the beginning moment of the operation of the DOAS-CC system in other periods. The predictive results, T_{panel} and $DPT_{\text{a,in}}$ of Aug.1st to Aug.8th, are shown in Table 8.4 and Table 8.5, respectively. It can be found that there is condensation occurrence at the morning on each day in the period, because the predicted panel temperatures are lower than the predicted indoor air dew-point temperature at the beginning period. Hence, the dehumidification of the DOAS in advance is necessary to prevent condensation. The needed optimal prior time for DOAS operation can be predicted by NN-based optimal prior time model.

Table 8.4 T_{panel} prediction of each day during Aug.1st-8th

	$T_{\text{a, in}}(7:30\text{am})$ (°C)	$T_{\text{a, out, 1}}(7:30\text{am})$ (°C)	$T_{\text{a, out, 2}}(9:00\text{am})$ (°C)	Predicted $T_{\text{panel}}(9:05\text{am})$ (°C)
G1-01	29.2	26.3	27.7	19.57
G1-02	28.0	25.4	26.8	19.52
G1-03	26.9	24.1	24.8	18.88
G1-04	26.9	23.9	25.3	19.17
G1-05	26.8	25.9	25.9	18.46
G1-06	28.6	25.3	26.6	19.57
G1-07	28.5	24.9	26.0	19.47

G1-08	28.8	26.5	27.2	19.25
-------	------	------	------	-------

Table 8.5 Indoor air DPT prediction of each day during Aug.1st-8th

	DPT _{a, in,1} (7:30am) (°C)	W _{a, out, 1} (7:30am) (g/kg.da)	W _{a, out, 2} (9:00am) (g/kg.da)	Predicted DPT _{a, in, 2} (9:05am) (°C)
G2-01	23.1	19.2	19.8	23.10
G2-02	22.5	19.1	19.4	22.43
G2-03	21.8	17.7	18.0	21.79
G2-04	21.4	17.6	18.1	21.60
G2-05	22.8	20.5	20.3	22.39
G2-06	22.8	19.4	19.6	22.59
G2-07	21.9	18.2	18.5	21.89
G2-08	22.8	20.3	20.1	22.38

The predicted prior time of the DOAS system to dehumidification on each day is presented in the sixth column of Table 8.6, to avoid the condensation occurring on the surface of chilled ceiling panels. When the infiltration rate of the building envelopes is assumed to be 0.1ACH, the needed maximum prior time is about 32mins.

Table 8.6 Optimal prior time prediction of each day during Aug.1st-8th

	DPT _{a,in,1} (7:30am) (°C)	W _{a,out,1} (7:30am) (g/kg.da)	W _{a,out,2} (9:00am) (g/kg.da)	DPT _{a,in,2} (9:05am) (°C)	Predicted prior time (min)	Simulated prior time (min)
G3-01	23.1	19.2	19.8	19.57	20.6	23
G3-02	22.5	19.1	19.4	19.52	18.3	21
G3-03	21.8	17.7	18.0	18.88	22.2	25
G3-04	21.4	17.6	18.1	19.17	18.3	21
G3-05	22.8	20.5	20.3	18.46	31.8	30
G3-06	22.8	19.4	19.6	19.57	18.6	23
G3-07	21.9	18.2	18.5	19.47	16.5	20
G3-08	22.8	20.3	20.1	19.25	21.4	24

The optimal prior time for DOAS operation can be also obtained by simulation on TRNSYS through trial and error, as shown in the last column in Table 8.6. According to the comparison, the maximum bias between the predicted prior time by neural network models and the simulated prior time is about 4.4mins. It indicates that the NN-based prior time prediction is feasible and acceptable.

8.3.3.2 Effect of infiltration rate on the prior time of DOAS

When the infiltration rate of the building envelopes is different, the required prior dehumidification time of the dedicated outdoor air system will be various. The effect of infiltration rate on the prior time of the DOAS is investigated. Air infiltration rates ranging from 0.1 to 0.3ACH are simulated and compared. The results are illustrated in Figure 8.11. It can be found that the higher the air infiltration rate of building envelopes, the earlier it requires for air dehumidification of DOAS to prevent condensation. When the infiltration rate of the building envelopes is assumed to be 0.3ACH, the maximum needed prior time for condensation prevention is less than 1hr.

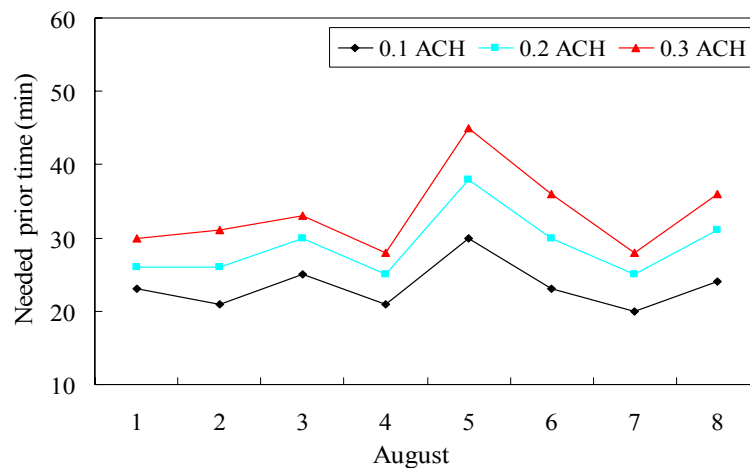


Figure 8.11 The needed prior time of DOAS at different infiltration rates

8.4 Summary

Condensation is prone to occur at the startup moment of dedicated outdoor air-chilled ceiling systems in hot and humid regions, due to the infiltration air through building envelopes. In the present study, neural network approach is proposed for the condensation prediction in DOAS-CC systems and to determine the optimal start time of DOAS prior to the operation of chilled ceiling systems for condensation prevention. Simulation tests shows that the neural network method is convenient and accurate to predict the temperature of chilled ceiling panel (T_{panel}) and indoor air dew-point temperature ($DPT_{\text{a,in}}$) at the startup moment of DOAS-CC systems, hence to predict whether condensation will occur or not on the surface of chilled ceiling. Moreover, the neural network model is reliable for the prior start time prediction for DOAS, and the prediction results show that the maximum bias between predicted values and simulation values is about 4.4mins. In addition, the simulation results demonstrate that the larger the air infiltration rate of building envelopes, the earlier it requires for air dehumidification of DOAS to prevent condensation.

In the study, simulation results from the DOAS-CC system simulator on platform of TRNSYS are utilized to train and validate the neural network models. However, it is noteworthy to point out that one set of the prediction models, say three NN models, are not suitable for the year-round prediction, because the ambient weather condition is various in different months. One set of the prediction models can be trained and validated by two or three months data, which means the applicable period of each set of

prediction models is two or three months. For different periods, the parameters of the NN models are different and necessary to regulate correspondingly.

In addition, the effect of prior dehumidification of DOAS for condensation prevention on the energy performance of the DOAS-CC integrated system is not investigated in the study. However, in the further research and practical applications, the recirculation air from conditioned space can be considered to utilize in the prior dehumidification period of DOAS. It is beneficial to cut out the ventilation load of the system in this period, consequently reduce the energy consumption for air dehumidification.

CHAPTER 9 CONCLUSIONS AND RECOMMENDATIONS

Dedicated outdoor air-chilled ceiling (DOAS-CC) system is a promising air conditioning scheme, which can achieve independent controls of indoor temperature and humidity, provide more effective ventilation, reduce the risk of virus and bacteria transmission among different zones through air ducts, enhance COP of chillers etc. Therefore, it can improve indoor thermal comfort and indoor air quality with higher energy efficiency. By incorporating total heat recovery and liquid desiccant dehumidification technologies in the DOAS-CC system, the energy performance of the integrated system can be further improved. This system has attracted world-wide interests and is more and more popular in modern buildings in recent years. However, studies on the control issues of the integrated system are quite few so far. Reliable control strategies are necessary for this integrated air conditioning system to realize normal operation and achieve the benefits. In addition, proper control and operation have significant impacts on energy efficiency of air conditioning systems. It is therefore highly desirable to develop reliable and cost-effective control strategies for this kind of air conditioning system. The present thesis has addressed this need through making the following contributions.

Conclusions on Main Contributions

- i. The main contribution of this thesis is the development of reliable local control methods and systematic optimal control strategy for the dedicated outdoor

air-chilled ceiling system integrated with novel membrane-based total heat recovery and liquid desiccant dehumidification technologies. Adaptive simplified models of major system components were used to construct the cost function. Genetic algorithm was adopted to solve the multiple-variable optimization problem. Compared with previous optimization method used in air conditioning systems which usually only attempted to minimize energy consumption or improve thermal comfort, the GA-based multiple-variable optimization method can achieve optimal trade-off between indoor thermal comfort and system energy consumption. The implementation guidelines for applying the optimal control strategy have also been provided.

- ii. This thesis develops a simulation platform for the complex integrated DOAS-CC system, which can be used to test and analyze control, indoor environment and energy performances of different control strategies under varying working conditions.
- iii. A novel membrane-based total heat exchanger is firstly studied in an air conditioning system under changing working conditions. It is found that the use of total heat exchanger before liquid desiccant systems can obtain significant energy saving and improve the control robust for air dehumidification process.
- iv. Control strategies for a packing type counter-flow liquid desiccant system have been developed. The control performances of these strategies were tested in a simulated environment. The control characteristics of the liquid desiccant system were also evaluated in different working conditions.
- v. A neural-network based predictive condensation control method was developed for the DOAS-CC system to predict and prevent from the occurrence of

condensation on the chilled ceiling panel surfaces at the beginning period of the system start-up.

Control Strategies and Characteristics of Liquid Desiccant Dehumidification System

Different control strategies for a counter-flow liquid desiccant system have been developed. They include : (1) variable strong solution inlet temperature method and variable strong solution flow rate method for supply air humidity control in the dehumidifier side; (2) variable weak solution inlet temperature method and variable regeneration air flow rate method for desiccant solution regeneration control in the regenerator side.

In the air dehumidification process, the variable strong solution inlet temperature control method is found to be more effective. The dehumidification capacity of the liquid desiccant system is more sensitive to variation of the strong solution inlet temperature than variation of the strong solution flow rate. In the desiccant solution regeneration process, the performance of the variable diluted solution inlet temperature method is found to be better than that of the variable regeneration air flow rate method under part latent load conditions. Simulation tests demonstrate that it consumes about 3.3% less energy on a tested summer day.

The simulation results also show that the proposed liquid desiccant system is more suitable for hot and humid climates, a higher supply air flow rate, and higher supply air humidity ratio conditions. In addition, a lower solution flow rate and a higher regeneration air flow rate are preferable in this hybrid dehumidification system for improving its energy performance.

When liquid desiccant dehumidification is utilized in air-conditioning systems, more outdoor air flow rate can be taken into conditioned space to improve indoor air quality, considering the energy savings potential and control characteristics of the dehumidification system.

Independent Temperature and Humidity Control in Multi-zone Dedicated Outdoor Air System

Control strategies for multi-zone dedicated outdoor air system have been developed. The local control loops include: (1) indoor air temperature control; (2) indoor air humidity control; (3) outdoor air ventilation flow rate control. The performance tests and evaluation of the local control methods show that they are reliable and can maintain satisfactory indoor air quality and provide acceptable indoor thermal comfort.

For optimization control, the fresh air flow rate and the supply air humidity ratio of dedicated outdoor air system are two crucial variables for the DOAS system, which directly influence indoor thermal comfort, indoor air quality and energy consumption. In the study, two control strategies i.e. demand controlled ventilation strategy and the supply air humidity ratio set point reset strategy, are proposed to optimize these two variables and improve the system energy performance. Simulation tests show that the supply air humidity ratio set point reset strategy is effective to control indoor air relative humidity in the comfortable range. It can save about 8.8% of overall energy consumption in the tested case. Moreover, the DCV-based ventilation control method demonstrates obvious strength in energy saving, which can further save about 10.5% of overall energy consumption during the summer period.

Optimal Control Strategy for the Integrated DOAS-CC System

In order to improve the overall performance of the dedicated outdoor air-chilled ceiling system, a model-based optimal control strategy is developed in this study. The optimal strategy is based on the system performance prediction using adaptive simplified models and the genetic algorithm for optimizing the supply air temperature and humidity of the dedicated outdoor air subsystem and the supply water temperature. The testing results in a simulated multi-zone space served by the proposed system show that the optimal control strategy can reduce energy consumption while maintaining satisfactory indoor thermal comfort.

The simulation results illustrate that the optimal strategy can provide comfort indoor environment and achieve significant energy saving, i.e. save about 7.8% and 7.0% energy in the tested summer and spring days, respectively as compared with a conventional control strategy, in which set points of local controllers are fixed at design values. The energy saving mainly comes from higher supply chilled water temperature, higher supply air humidity in the dedicated outdoor air subsystem and higher indoor air temperature and relative humidity in the conditioned space. The results also demonstrate that optimized and varying control set points are beneficial for the overall performance of air-conditioning systems under dynamic outdoor and indoor conditions.

Neural Network Based Predictive Condensation Control Strategy

Condensation is prone to occur at the start-up moment of chilled ceiling systems in hot and humid regions, due to the infiltration air through building envelopes and accumulation of moisture during system-off period. The risk of condensation on ceiling

panels seriously limits the popularity of chilled ceiling systems. To prevent condensation, an effective solution is to operate dedicated outdoor air system prior to the operation of chilled ceiling. The prior operation time of DOAS is critical, which influences the energy consumption and effect of condensation prevention. In this study, neural network method is proposed for predicting condensation on chilled ceiling and the optimal start time of DOAS prior to the operation of chilled ceiling systems. Two neural network models are developed to predict the temperature on the surface of chilled ceiling and the indoor air dew-point temperature at the startup period of DOAS-CC systems, hence to predict whether condensation will occur or not on ceiling panels. The third neural network model is employed to predict the optimal prior operation time for DOAS to prevent condensation. Simulation tests shows that the neural network method is convenient and accurate to predict the temperature of chilled ceiling panel and indoor air dew-point temperature at the startup moment of DOAS-CC systems. Moreover, the neural network model is reliable for the prior start time prediction for DOAS. The prediction results show that the maximum bias between predicted values and simulation values is about 4.4mins. In addition, the simulation results demonstrate that the larger the air infiltration rate of building envelopes, the earlier it requires for air dehumidification of DOAS to prevent condensation.

It is noteworthy to point out that the sensitivity of neural network models are affected by training data. The sensitivity will be degraded if training data in a longer period, i.e. three months, are used due to large variations in weather data. Therefore, it is suggested that one or two months' data be used to train the NN models. For year-round applications, six sets of NN models are proper.

Recommendations for Future Work

The proposed dedicated outdoor air-chilled ceiling system incorporating liquid desiccant dehumidification and membrane-based total heat recovery technologies is a novel and complicated air conditioning system. Major efforts of this thesis are made on the development of the local control methods and optimal control strategy for the integrated DOAS-CC system. The performances of these strategies are mainly tested and evaluated in a simulated environment. Although each component in the simulator is validated by experimental data, the simulator as a whole is not validated by experimental data or field data due to the shortage of those data. It would be very desirable and valuable to make further efforts on in-situ implementations and validation of the local control methods and the optimal control strategy developed in this thesis on the complex integrated DOAS-CC system.

REFERENCES

- Abe, O.O., C.J. Simonson, R.W. Besant, and W. Shang. 2006. Effectiveness of energy wheels from transient measurements: Part II. Results and verification. *International Journal of Heat and Mass Transfer* 49(1-2): 63-77.
- Ardehali, M.M. and T.F. Smith. 1997. Evaluation of HVAC system operational strategies for commercial buildings. *Energy Conversion and Management* 38(3): 225-236.
- Argiriou, A.A., I. Bellas-Velidis, M. Kummert, and P. Andre. 2004. A neural network controller for hydronic heating systems of solar buildings. *Neural Networks* 17(3): 427-440.
- ASHARE. 2001. ANSI/ASHARE Standard 62.1-2001, Ventilation for Acceptable Indoor Air Quality. American Society of Heating, Refrigerating and Air-Conditioning Engineers, Inc., Atlanta, GA.
- ASHARE. 2007. ANSI/ASHARE Standard 62.1-2007, Ventilation for Acceptable Indoor Air Quality. American Society of Heating, Refrigerating and Air-Conditioning Engineers, Inc., Atlanta, GA.
- ASHRAE. 2007b. ANSI/ASHRAE/IESNA Standard 90.1-2007, Energy Standard for Buildings Except Low-Rise Residential Buildings. American Society of Heating, Refrigerating, and Air-Conditioning Engineers, Inc.
- ASHRAE. 2008. ASHRAE Handbook-HVAC systems and equipment. American Society of Heating, Refrigerating, and Air-Conditioning Engineers, Inc.
- Babakhani, D. and M. Soleymani. 2009. An analytical solution for air dehumidification by liquid desiccant in a packed column. *International Communications in Heat and Mass Transfer* 36(9): 969-977.
- Bassily, A.M and G.M. Colver. 2005. Cost optimization of a conical electric heater. *International Journal of Energy Research* 29(4): 359-376.

- Ben-Nakhi, A.E. and M.A. Mahmoud. 2004. Cooling load prediction for buildings using general regression neural networks. *Energy Conversion and Management* 45(13-14): 2127-2141.
- Beyer, H. 2001. *The Theory of Evolution Strategies*, Springer-Verlag, Berlin Heidelberg.
- Capozzoli, A., P. Mazzei, F. Minichiello, and D. Palma. 2006. Hybrid HVAC systems with chemical dehumidification for supermarket applications. *Applied Thermal Engineering* 26(8-9):795-805.
- Chang, Y.C. 2004. A novel energy conservation method--Optimal chiller loading. *Electric Power Systems Research* 69(2): 221-26.
- Chang, Y.C. 2005. Genetic algorithm based optimal chiller loading for energy conservation. *Applied Thermal Engineering* 25(17-18): 2800-2815.
- Chen, X.Y., Z. Li, Y. Jiang, and K.Y. Qu. 2006. Analytical solution of adiabatic heat and mass transfer process in packed-type liquid desiccant equipment and its application. *Solar Energy* 80(11): 1509-1516.
- Chowdhury, A.A., M.G. Rasul, and M.M.K. Khan. 2008. Thermal-comfort analysis and simulation for various low-energy cooling-technologies applied to an office building in a subtropical climate. *Applied Energy* 85(6): 449-462.
- Chow, T.T., G.Q. Zhang, Z. Lin, and C.L. Song. 2002. Global optimization of absorption chiller system by genetic algorithm and neural network. *Energy and Buildings* 34(1): 103-109.
- Chow, T.T., K.F. Fong, B. Givoni, Z. Lin, and A.L.S. Chan. 2010. Thermal sensation of Hong Kong people with increased air speed, temperature and humidity in air-conditioned environment. *Building and Environment* 45(10): 2177-2183.
- Chow, T.T., L.S. Chan, and C.L. Song. 2004. Building-mix optimization in district-cooling system implementation. *Applied Energy* 77(1):1-13.
- Conroy, C.L. and S.A. Mumma. 2001. Ceiling radiant cooling panels as a viable distributed parallel sensible cooling technology integrated with dedicated outdoor air systems. *ASHRAE Transactions* 107(1): 578-585.

- Dai, Y.J. and H.F. Zhang. 2004. Numerical simulation and theoretical analysis of heat and mass transfer in a cross flow liquid desiccant air dehumidifier packed with honeycomb paper. *Energy Conversion and Management* 45(9-10): 1343-1356.
- Dai, Y.J., R.Z. Wang, H.F. Zhang, and J.D. Yu. 2001. Use of liquid desiccant cooling to improve the performance of vapor compression air conditioning. *Applied Thermal Engineering* 21(12): 1185-1202.
- Daou, K., R.Z. Wang, and Z.Z. Xia. 2006. Desiccant cooling air conditioning: a review. *Renewable and Sustainable Energy Reviews* 10(2): 55-77.
- Dedanco. 2001. Active Chilled Beam Documentation/FAQ. Available at: www.dadanco.com.au.
- Diaz, N.F. 2011. Modeling of a hydronic ceiling system and its environment as energetic auditing tool. *Applied Energy* 88(3): 636-649.
- Diaz, N.F., J. Lebrun, and P. Andre. 2010. Experimental study and modeling of cooling ceiling systems using steady-state analysis. *International Journal of Refrigeration* 33(4): 793-805.
- EMSD. 2010. Hong Kong Energy End-use Data. The Energy Efficiency Office, Electrical & Mechanical Services Department, Hong Kong.
- Energy Design Resources. 2001. Design Brief: Radiant Cooling. Final Draft, prepared by Financial Times Energy, Inc.
- Environmental Protection Department, The Government of the Hong Kong Special Administrative Region, 2010. <http://www.info.gov.hk/epd>.
- Factor, H.M. and G. Grossman. 1980. A packed bed dehumidifier/regenerator for solar air-conditioning with liquid desiccant. *Solar Energy* 24(6): 541-550.
- Fisk, W.J. 2002. How IEQ affects health, productivity. *ASHRAE Journal* 2002(May): 56-58.
- Fumo, N. and D.Y. Goswami. 2002. Study of an aqueous lithium chloride desiccant system: air dehumidification and desiccant regeneration. *Solar Energy* 72(4): 351-361.

- Gandhidasan, P. 2004. A simplified model for air dehumidification with liquid desiccant. *Solar Energy* 76(4): 409-416.
- Gandhidasan, P. 2005. Quick performance prediction of liquid desiccant regenerator in a packed bed. *Solar Energy* 79(1): 47-55.
- Gurney, K. 1997. An introduction to neural networks. UCL Press Limited, Taylor & Francis Group, London.
- Hao, X.L., G.Q. Zhang, Y.M. Chen, S.H. Zou, and D.J. Moschandreas. 2007. A combined system of chilled ceiling, displacement ventilation and desiccant dehumidification. *Building and Environment* 42(9): 3298-3308.
- Haykin, S. 1994. Neural networks: a comprehensive foundation. New York: Macmillan.
- IEA. 2010. Energy Balances of OECD Countries-2010 edition, Paris.
- Imanari, T., T. Omori, and K. Bogaki. 1999. Thermal comfort and energy consumption of the radiant ceiling panel system: comparison with the conventional all-air system. *Energy and Buildings* 30(2): 167-175.
- Irwin, G.W., K. Warwick, and K.J. Hunt. 1995. Neural network applications in control. The Institution of Electrical Engineers, London, United Kingdom.
- ISO 7730. 2005. Ergonomics of the thermal environment--analytical determination and interpretation of thermal comfort using calculation of the PMV and PPD indices and local thermal comfort criteria. Third edition.
- Jeong, J. and S.A. Mumma. 2003. Ceiling radiant cooling panel capacity enhanced by mixed convection in mechanically ventilated spaces. *Applied Thermal Engineering* 23(18): 2293-2306.
- Jeong, J. and S.A. Mumma. 2004. Simplified cooling capacity estimation model for top insulated metal ceiling radiant cooling panels, *Applied Thermal Engineering* 24 (14-15): 2055-2072.
- Kalogirou, S.A. 1999. Applications of artificial neural networks in energy systems: a review. *Energy Conversion and Management* 40(10): 1073-1087.
- Kettle, J.P. 1998. Controlling Minimum Ventilation Volume in VAV systems. *ASHRAE Journal* 1998(May): 45-50.

- Kinsara, A.A., M.M. Elsayed, and O.M. Al-Rabghi. 1996. Proposed energy-efficient air conditioning system using liquid desiccant. *Applied Thermal Engineering* 16(10): 791-806.
- Kinsara, A.A., O.M. Al-Rabghi, and M.M. Elsayed. 1997. Parametric study of an energy efficient air conditioning system using liquid desiccant. *Applied Thermal Engineering* 18(5): 327-335.
- Kittler, R. 1996. Mechanical dehumidification control strategies and psychrometrics. *ASHRAE Transactions* 102(2): 613-617.
- Klein, S.A., W.A. Beckman, and J.W. Mitchell et al. 2006. TRNSYS, a Transient Simulation Program. University of Wisconsin-Madison, USA: Solar Energy Laboratory, Version 16.1.
- Labs21. Chilled beams in laboratories: key strategies to ensure effective design, construction, and operation. *Labs for the 21st Century*. Available online at: http://www.epa.gov/labs21century/pdf/bp_chilled-beam_508.pdf.
- Lazzarin, R.M. and A. Gasparella. 1998. Technical and economical analysis of heat recovery in building ventilation systems. *Applied Thermal Engineering* 18(1-2): 47-67.
- Liang, C.H., L.Z. Zhang, and L.X. Pei. 2010. Independent air dehumidification with membrane-based total heat recovery: modeling and experimental validation. *International Journal of Refrigeration* 33(2): 398-408.
- Lim, J.H., J.H. Jo, Y.Y. Kim, M.S. Yeo, and K.W. Kim. 2006. Application of the control methods for radiant floor cooling system in residential buildings. *Building and Environment* 41(1): 60-73.
- Liu, X.H., K.C. Geng, B.R. Lin, and Y. Jiang. 2004. Combined cogeneration and liquid-desiccant system applied in a demonstration building. *Energy and Buildings* 36(9): 945-953.
- Liu, X.H., X.M. Chang, J.J. Xia, and Y. Jiang. 2009. Performance analysis on the internally cooled dehumidifier using liquid desiccant. *Building and Environment* 44(2): 299-308.

- Liu, X.H., Y. Jiang, and K.Y. Qu. 2007. Heat and mass transfer model of cross flow liquid desiccant air dehumidifier/regenerator. *Energy Conversion and Management* 48(2): 546-554.
- Liu, X.H., Z. Li, Y. Jiang, and B.R. Lin. 2006. Annual performance of liquid desiccant based independent humidity control HVAC system. *Applied Thermal Engineering* 26(11-12): 1198-1207.
- Ma, Z.J. and S.W. Wang. 2011. Supervisory and optimal control of central chiller plants using simplified adaptive models and genetic algorithm. *Applied Energy* 88(1): 198-211.
- Mahmoud, M.A. and A.E. Ben-Nakhi. 2003. Architecture and performance of neural networks for efficient A/C control in buildings. *Energy Conversion and Management* 44(20): 3207-3226.
- Mathews, E.H., C.P. Botha, D.C. Arndt, and A. Malan. 2001. HVAC control strategies to enhance comfort and minimize energy usage. *Energy and Buildings* 33(8): 853-863.
- Matsuki, N., Y. Nakano, T. Miyanaga, N. Yokoo, and T. Oka. 1999. Performance of radiant cooling system integrated with ice storage. *Energy and Buildings* 30(2): 177-183.
- Mossolly, M., K. Ghali, N. Ghaddar, and L. Jensen. 2008. Optimized operation of combined chilled ceiling displacement ventilation system using genetic algorithm. *ASHRAE Transactions* 143(2): 541-554.
- Mumma, S.A. 2001a. Fresh Thinking: Dedicated Outdoor Air Systems. *Engineered Systems* 2001(May): 54-60.
- Mumma, S.A. 2001b. Ceiling Panel Cooling Systems. *ASHRAE Journal*. 2001(November): 28-32.
- Mumma, S.A. 2002. Chilled ceilings in parallel with dedicated outdoor air system: addressing the concerns of condensation, capacity, and cost. *ASHRAE Transactions* 108(2): 220-231.
- Mumma, S.A. 2003. Chilled ceiling condensation control. *ASHRAE IAQ Applications* 2003(Fall): 22-23.

- Mumma, S.A. and J. Jeong. 2005a. Direct digital temperature, humidity and condensate control for a dedicated outdoor air-ceiling radiant cooling panel system. *ASHRAE Transactions* 111(1):547-558.
- Mumma, S.A. and J. Jeong. 2005b. Field experience controlling a dedicated outdoor air system. *ASHRAE Transactions* 111(2):433-442.
- Nelles, O. 2001. Nonlinear system identification: from classical approaches to neural networks and fuzzy models. Berlin: Springer-Verlag, Inc.
- Ning, M. and M. Zaheeruddin. 2010. Neuro-optimal operation of a variable air volume HVAC&R system. *Applied Thermal Engineering* 30(5): 385-399.
- Niu, J.L., J.V.D. Kooi, and H.V.D. Rhee. 1995. Energy saving possibilities with cooled-ceiling systems. *Energy and Buildings* 23(2): 147-158.
- Niu, J.L., L.Z. Zhang, and H.G. Zuo. 2002. Energy savings potential of chilled ceiling combined with desiccant cooling in hot and humid climates. *Energy and Buildings* 34(5): 487-495.
- Nizet, J., L. Lecomte, and F. Litt. 1984. Optimal control applied to air conditioning in building. *ASHRAE Transactions* 90(1B): 587-600.
- Perez-Lombard, L., J. Ortiz, and C. Pout. 2008. A review on buildings energy consumption informantion. *Energy and Buildings* 40(3): 394-398.
- Roth, K. W., D. Westphalen, J. Dieckmann, S. D. Hamilton, and W. Goetzler. 2002. Energy consumption characteristics of commercial building HVAC systems volume III: Energy savings potential. Building Technologies Program, Department of Energy, United States.
- Ruano, A.E., E.M. Crispim, E.Z.E. Conceicao, and M.M.J.R. Lucio. 2006. Prediction of building's temperature using neural networks models. *Energy and Buildings* 38(6): 682-694.
- Sekhar, S.C., U. Maheswaran, K.W. Tham, and K.W. Cheong. 2004. Development of energy efficient single coil twin fan air-conditioning system with zonal ventilation control. *ASHRAE Transactions* 110(2): 204-217.

- Shelquist, P. and R. Amborn. 2001. Ventilation control strategies. *ASHRAE Journal* 2001(Sept.): 30-35.
- Spears, J.W. and J. Judge. 1997. Gas-fired desiccant system for retail super center. *ASHRAE Journal* 1997(Oct): 65-69.
- Springer, D. 2001. Personal Communication, Davis Energy Group.
- Stetiu, C. 1999. Energy and peak power savings potential of radiant cooling systems in US commercial buildings. *Energy and Buildings* 30(2): 127-138.
- Sun, J. and A. Reddy. 2005. Optimal control of building HVAC&R systems using complete simulation-based sequential quadratic programming (CSB-SQP). *Building and Environment* 40(5): 657-69.
- Sun, Z.W. 2010. Ventilation control and ventilation performance of multi-zone air conditioning systems. PhD thesis, The Hong Kong Polytechnic University.
- Tu, M., C.Q. Ren, L.A. Zhang, and J.W. Shao. 2009. Simulation and analysis of a novel liquid desiccant air-conditioning system. *Applied Thermal Engineering* 29(11-12): 2417-2425.
- Wang, S.W. 1999. Dynamic simulation of building VAV air-conditioning system and evaluation of EMCS on-line control strategies. *Building and Environment* 34(6): 681-705.
- Wang, S.W. 2010. Intelligent buildings and building automation. Spon Press.
- Wang, S.W. and X.H. Xu. 2002. A robust control strategy for combining DCV control with economizer control. *Energy Conversion and Management* 43(18): 2569-2588.
- Wang, S.W. and X.H. Xu. 2004. Optimal and robust control of outdoor ventilation airflow rate for improving energy efficiency and IAQ. *Building and Environment* 39(7): 763-773.
- Wang, S.W. and X.Q. Jin. 2000. Model-based optimal control of VAV air-conditioning system using genetic algorithm. *Building and Environment* 35(6): 471- 487.
- Wilkins, C.K. and R. Kosonen. 1992. Cool ceiling system: a European air-conditioning alternative. *ASHRAE Journal* 1992(August): 41-45.

- Xiao, F., G.M. Ge, and X.F. Niu. 2011. Control performance of a dedicated outdoor air system adopting liquid desiccant dehumidification. *Applied Energy* 88(1): 143-149.
- Xiong, Z.Q., Y.J. Dai, and R.Z. Wang. 2010. Development of a novel two-stage liquid desiccant dehumidification system assisted by CaCl₂ solution using exergy analysis method. *Applied Energy* 87(5): 1495-1504.
- Xu, X.H. and S.W. Wang. 2007. An adaptive demand-controlled ventilation strategy with zone temperature reset for multi-zone air-conditioning systems. *Indoor and Built Environment* 16(5): 426-437.
- Xu, X.H. and S.W. Wang. 2007b. Optimal Simplified Thermal Models of Building Envelope Based on Frequency Domain Regression Using Genetic Algorithm. *Energy and Building* 39(5): 525-536.
- Xu, X.H., S.W. Wang, Z.W. Sun, and F. Xiao. 2009. A model-based optimal ventilation control strategy of multi-zone VAV air-conditioning systems. *Applied Thermal Engineering* 29(1): 91-104.
- Yang, I.H. and K.W. Kim. 2004. Prediction of the time of room air temperature descending for heating systems in buildings. *Building and Environment* 39(1): 19-29.
- Yang, I.H., M.S. Yeo, and K.W. Kim. 2003. Application of artificial neural network to predict the optimal start time for heating system in building. *Energy Conversion and Management* 44(17): 2791-2809.
- Yin, Y.G., X.S. Zhang, G. Wang, and L. Luo. 2008. Experimental study on a new internally cooled/heated dehumidifier/regenerator of liquid desiccant systems. *International Journal of Refrigeration* 31(5): 857-866.
- Yin, Y.G., X.S. Zhang, and Z.Q. Chen. 2007. Experimental study on dehumidifier and regenerator of liquid desiccant cooling air conditioning system. *Building and Environment* 42(7): 2505-2511.
- Zhang, L.Z. 2006. Energy performance of independent air dehumidification systems with energy recovery measures. *Energy* 31(8-9): 1228-1242.

- Zhang, L.Z., C.H. Liang, and L.X. Pei. 2008. Heat and moisture transfer in application scale parallel-plates enthalpy exchangers with novel membrane materials. *Journal of Membrane Science* 325(2): 672-682.
- Zhang, L.Z. and F. Xiao. 2008. Simultaneous heat and moisture transfer through a composite supported liquid membrane. *International Journal of Heat and Mass Transfer* 51(9-10): 2179-2189.
- Zhang, L.Z. and J.L. Niu. 2001. Energy requirements for conditioning fresh air and the long-term savings with a membrane-based energy recovery ventilator in Hong Kong. *Energy* 26(2):119-135.
- Zhang, L.Z. and J.L. Niu. 2002. Performance comparisons of desiccant wheels for air dehumidification and enthalpy recovery. *Applied Thermal Engineering* 22(12): 1347-1367.
- Zhang, L.Z. and J.L. Niu. 2003. Indoor humidity behaviors associated with decoupled cooling in hot and humid climates. *Building and Environment* 38(1): 99-107.
- Zhang, L.Z. and J.L. Niu. 2003b. A pre-cooling munters environmental control desiccant cooling cycle in combination with chilled ceiling panels. *Energy* 28(3): 275-292.
- Zhang, Y.P., Y. Jiang, L.Z. Zhang, Y.C. Deng, and Z.F. Jin. 2000. Analysis of thermal performance and energy savings of membrane based heat recovery ventilator. *Energy* 25(6): 515-527.
- Zhong, K. and Y.M. Kang. 2009. Applicability of air-to-air heat recovery ventilators in China. *Applied Thermal Engineering* 29(5-6): 830-840.
- Zhou, Q., S.W. Wang, X.H. Xu, and F. Xiao. 2008. A grey-box model of next-day building thermal load prediction for energy-efficient control. *International Journal of Energy Research* 32(15): 1418-1431.